Universidade de Aveiro Departamento de Ambiente e Ordenamento
2018

CARLA MARIA DOS SANTOS GAMA DA SILVA

CONTRIBUIÇÃO DAS POEIRAS DO DESERTO PARA O AEROSSOL ATMOSFÉRICO EM CABO VERDE E EM PORTUGAL

DESERT DUST CONTRIBUTION TO THE ATMOSPHERIC AEROSOL IN CAPE VERDE AND IN PORTUGAL

Universidade de Aveiro Departamento de Ambiente e Ordenamento
2018

CARLA MARIA DOS SANTOS GAMA DA SILVA

CONTRIBUIÇÃO DAS POEIRAS DO DESERTO PARA O AEROSSOL ATMOSFÉRICO EM CABO VERDE E EM PORTUGAL

DESERT DUST CONTRIBUTION TO THE ATMOSPHERIC AEROSOL IN CAPE VERDE AND IN PORTUGAL

Tese apresentada à Universidade de Aveiro para cumprimento dos requisitos necessários à obtenção do grau de Doutor em Ciências e Engenharia do Ambiente, realizada sob a orientação científica da Doutora Oxana Tchepel, Professora Auxiliar da Faculdade de Ciências e Tecnologia da Universidade de Coimbra, e coorientação científica do Doutor Casimiro Pio, Professor Catedrático do Departamento de Ambiente e Ordenamento da Universidade de Aveiro, e do Doutor José María Baldasano, Professor Catedrático da Universitat Politècnica de Catalunya.

Governo da República Portuguesa
UNIÃO EUROPEIA Fundo Social Europeu

Apoio financeiro do FEDER através do COMPETE e por Fundos Nacionais através da FCT e POCTI no âmbito do III Quadro Comunitário de Apoio, no âmbito dos Projetos CV-DUST (PTDC/AAC-CLI/100331/2008) e AIRSHIP (PTDC/AAG-MAA/1581/2014).

Apoio financeiro da FCT e do FSE no âmbito do III Quadro Comunitário de Apoio, através da Bolsa de Doutoramento com a referência SFRH/BD/87468/2012.

Apoio financeiro através do protocolo estabelecido pela APA com o IDAD, no âmbito de “Desenvolvimento e aplicação de modelos matemáticos na avaliação da qualidade do ar e no apoio à gestão e monitorização dos planos de melhoria de qualidade do ar”.

o júri

presidente

Prof. Doutor Carlos Alberto Diogo Soares Borrego
professor catedrático do Departamento de Ambiente e Ordenamento da Universidade de Aveiro

Prof. Doutora Ana Isabel Couto Neto da Silva Miranda
professora catedrática do Departamento de Ambiente e Ordenamento da Universidade de Aveiro

Doutor Francisco Manuel Freire Cardoso Ferreira
professor auxiliar da Faculdade de Ciências e Tecnologia da Universidade Nova de Lisboa

Doutora Oxana Anatolievna Tchepel
professora auxiliar da Faculdade de Ciências e Tecnologia da Universidade de Coimbra
(orientadora)

Doutora Susana Marta Almeida
investigadora auxiliar da Universidade Técnica de Lisboa

agradecimentos

Agradeço, antes de mais, aos meus orientadores: Oxana Tchepel, José María Baldasano, Casimiro Pio. Em primeiro lugar, pela paciência: esta tese foi um processo moroso e eu nem sempre (ou nunca!) cumpri prazos. Em segundo lugar, pelo rigor científico que sempre mostraram e exigiram. Pelo desafio. Por me terem acolhido tão bem, na UA e no BSC-CNS. Pela inspiração.

Ao GEMAC, que me acolheu, e de onde nunca saí. Que sempre confiou no meu trabalho, que tantos desafios me proporcionou. Obrigada Professores Carlos Borrego e Ana Isabel Miranda. Obrigada Alexandra (a principal responsável por ter saído da ilha): por todos os momentos juntas, por tantos trabalhos onde me envolveste! Ao Michael, que teve sempre paciência para as minhas dúvidas de inglês. Obrigada a todos os colegas, que fazem deste grupo um grupo onde é tão bom trabalhar. E também ao Eduardo e à Luz, amigos do andar de cima: o DAO é tão melhor com vocês por aqui! Ao Luís Carvalheiro, por todo o apoio técnico com o WRF e CHIMERE no ARGUS, e também por me ter convertido ao Linux :)

À equipa do BSC-CNS, especialmente à Sara. Dear Sara, thank you so much for your support: with the paper (my very first paper!); with the presentation in the 7th dust workshop (my very first international presentation!); with everything! You rock and I look forward to keep working with you!

À mana, a pessoa no mundo que melhor compreende, e que tantas tardes passou com a miss O., sem questionar.

Aos meus pais. Que fizeram ao longo da vida um esforço gigantesco para que os cinco filhos conseguissem estudar. Que sempre souberam respeitar e apoiar as minhas decisões.

Ao Rubi, por me chatear tanto por nunca mais parir esta criatura chamada Tese (*não te estou realmente grata por isso, mas... :)*). E à Olívia, a cria mais bonita deste mundo, que nasceu no meio deste percurso chamado doutoramento, o tornou mais difícil, mas tão mais bonito.

Obrigada a todos.

palavras-chave

poeiras do deserto, qualidade do ar, modelos de poeiras do deserto, aerossol atmosférico, PM10, PM2.5, Cabo Verde, Portugal

resumo

Através de processos de erosão são introduzidas na atmosfera grandes quantidades de partículas com origem no solo e transportadas a longa distância, afetando a qualidade do ar e o balanço radiativo da Terra. Este estudo, que se desenvolve no âmbito da interação entre os sistemas terra-atmosfera, tem como objetivo principal caracterizar o transporte de poeiras dos desertos de África, focando a análise em Cabo Verde e Portugal.

Para atingir este objetivo, recorre-se à modelação de poeiras do deserto, conjugada com observações, incluindo concentrações distribuídas por tamanho de partículas e características óticas das poeiras. Ao longo da Tese, utilizam-se três sistemas de modelos: BSC-DREAM8b, NMMB/BSC-Dust e WRF-CHIMERE, considerando diferentes modelos de produção de poeiras do deserto. Para melhorar a modelação da distribuição por tamanhos das partículas, é implementada e testada uma nova parametrização nas emissões, conduzindo a uma diminuição da fração fina e a um aumento da fração grosseira das emissões. Esta alteração tem impacte nas concentrações e parâmetros óticos modelados a jusante das emissões. Os ciclos temporais dos aerossóis são caracterizados neste trabalho, e são implementados e avaliados diferentes métodos para estimar a contribuição das poeiras do Sahara para os níveis regionais de matéria particulada.

Durante o inverno, várias intrusões significativas de poeiras com origem no Noroeste de África influenciam as concentrações de matéria particulada à superfície em Cabo Verde. Durante o verão, as poeiras são transportadas a elevadas altitudes, dando origem a elevados valores de espessura ótica do aerossol. Em termos médios anuais, e de acordo com a metodologia aplicada, cerca de 42% da massa de PM10 observada em Cabo Verde está relacionada com o transporte das poeiras do deserto. Embora os episódios de poeiras do deserto sejam menos severos em Portugal, durante 2016, verificaram-se pelo menos duas situações de transporte de poeiras do deserto, que ocorreram em Fevereiro e em Outubro, responsáveis por excedências regionais ao valor limite diário definido para PM10 na Diretiva Quadro da Qualidade do Ar.

Este estudo contribui para a caracterização dos processos e fontes responsáveis pela intrusão de poeiras minerais na atmosfera e apresenta novas abordagens e informação importante para transmitir aos agentes envolvidos em processos de tomada de decisão.

keywords

desert dust, air quality, dust models, atmospheric aerosol, PM10, PM2.5, Cape Verde, Portugal

abstract

Due to erosion processes, huge quantities of soil-derived particles are entrained into the atmosphere and transported away from the source, impacting air quality and affecting the Earth's radiative budget. This Thesis addresses those land-atmosphere interactions, dealing with atmospheric mineral aerosol, with a main objective of improving the assessment of long-range transport of African dust focusing on Cape Verde and Portugal.
To achieve the objective, dust modelling is employed and combined with observations, including size distributed particle concentrations and optical properties. Three different modelling systems are used, namely BSC-DREAM8b, the NMMB/BSC-Dust model and WRF-CHIMERE, with distinct dust production models. In order to improve characterization of the dust size distribution at emission, a new parametrization is tested in this work, leading to a decrease in the emission fine fractions and an increase in the coarser ones, which has an impact in modelled downwind concentrations and optical parameters. Aerosol cycles are characterized and different methods to estimate the contribution of Saharan dust to regional PM levels are implemented and assessed.
Significant dust intrusions from North West Africa severely affect Cape Verde PM surface concentrations during winter. In the summer dust is transported towards the region at higher altitudes, yielding high aerosol optical depths. On a yearly basis, and according to the methodology employed, roughly 42% of the PM10 mass observed in Cape Verde is associated with dust transported from North African deserts. Desert dust outbreaks are less severe in Portugal. Nevertheless, during 2016, at least two dust episodes, occurring in February and October, are responsible for regional exceedances of the PM10 daily limit value defined in the Air Quality Directive.
This study intends to improve the scientific knowledge on processes and sources responsible for mineral dust loading into the atmosphere and to provide new means and valuable information for science-based decision making.

Publications related to this Thesis

International Journals included in the Science Citation Index (SCI)

1. **Gama, C.**, Monteiro, A., Borrego, C., Pio, C., Baldasano, J.M., Tchepel, O. Comparison of different methodologies for assessing desert dust contribution to regional PM10 and PM2.5 levels: a one-year study over Portugal. submitted to Aeolian Research [in review].

2. **Gama, C.**, Monteiro, A., Pio, C., Miranda, A.I., Baldasano, J.M., Tchepel, O. (2018) Temporal patterns and trends of particulate matter over Portugal: a long-term analysis of background concentrations. Air Quality, Atmosphere and Health. doi:10.1007/s11869-018-0546-8

3. **Gama, C.**, Tchepel, O., Baldasano, J.M., Basart, S., Ferreira, J., Pio, C., Cardoso, J., Borrego, C. (2015) Seasonal patterns of Saharan dust over Cape Verde – a combined approach using observations and modelling. Tellus B 67, 24410. doi:10.3402/tellusb.v67.24410.

4. Monteiro, A., Fernandes, A.P., **Gama, C.**, Borrego, C., Tchepel, O. (2015) Assessing the mineral dust from North Africa over Portugal region using BSC-DREAM8b model. Atmospheric Pollution Research 6, 70-81. doi:10.5094/APR.2015.009.

International Congresses and Workshops

1. **Gama, C.**, Monteiro, A., Fernandes, A.P., Vieira, M., Pio, C., Miranda, A.I., Tchepel, O. (2016) Forecasting Saharan dust events over Portugal: analysis of the CHIMERE Dust module performance. 4th Iberian Meeting on Aerosol Science and Technology (RICTA 2016), 29 Jun.-01 Jul. 2016, Aveiro, Portugal.

2. **Gama, C.**, Basart, S., Baldasano, J.M., Pio, C., Borrego, C., Tchepel, O. (2016) Assessing the size distribution of dust in the NMMB/BSC-Dust model. 8th International Workshop on Sand/Duststorms and Associated Dustfall, 1-4 May 2016, Lisbon, Portugal.

3. **Gama, C.**, Basart, S., Cardoso, J., Ferreira, J., Baldasano, J.M., Pio, C., Borrego, C., Tchepel, O. (2015) Contribuição das poeiras do deserto para a degradação da qualidade do ar em Cabo Verde. XVII Encontro da Rede de Estudos Ambientais dos Países de Língua Portuguesa, 7-12 Sep., Praia, Santiago, Cape Verde.

4. Basart, S., **Gama, C.**, Jorba, O., Spada, M., Pérez, C., Baldasano, J.M., Tchepel, O., Pio, C. (2013) Desert dust and sea-salt evaluation of the NMMB/BSC-CTM model for North Africa. 7th International Workshop on Sand/Duststorms and Associated Dustfall, 2-4 Dec., Frascati, Italy.

5. Pio, C.A., Cardoso, J., Nunes, T., Cerqueira, M., Tchepel, O., Rocha, F., Fialho, P., Alves, C., Gonçalves, C., **Gama, C.**, Ferreira, J., Almeida, S.M., Almeida-Silva, M., Reis, M., Freitas, M.C., Baldasano, J. (2013) Seasonal variability of atmospheric aerosol composition in Cape Verde islands under the influence of Sahara dust intrusions: results of the CV-Dust campaign. 1st Iberian Meeting on Aerosol Science and Technology (RICTA 2013), 1-3 Jul., Évora, Portugal.

6. Tchepel, O., Ferreira, J., Fernandes, A.P., **Gama, C.**, Baldasano, J.M., Borrego, C., Cardoso, J., Almeida, S.M., Pio, C. (2012) Modelling of long-range transport of mineral dust to Cape Verde. European Aerosol Conference. 2-7 Sep., Granada, Spain.

National Conferences

1. **Gama, C.**, Basart, S., Cardoso, J., Tchepel, O., Baldasano, J.M., Pio, C., Borrego, C. (2015) One year of aerosol measurements and modelling of dust over Cape Verde. Research Day, 20 Maio, Aveiro, Portugal.

2. **Gama, C.**, Tchepel, O., Ferreira, J., Baldasano, J.M., Pio, C. (2013) Modelação das poeiras atmosféricas provenientes do deserto: aplicação à região de Cabo Verde. 10a Conferência Nacional do Ambiente. Repensar o ambiente: Luxo ou inevitabilidade? 6-8 Nov., Aveiro, Portugal.

Contents

List of acronyms

AEMET	Spanish Meteorological Agency
AERONET	AErosol RObotic NETwork
AOD	Aerosol Optical Depth
AQMs	Air Quality Models
BSC-CNS	Barcelona Supercomputing Center - Centro Nacional de Supercomputación
BSC-DREAM8b	Barcelona Supercomputing Center Dust REgional Atmosphere Model 8 bins
CHIMERE	Eulerian off-line chemistry-transport model
CV-DUST	Atmospheric aerosol in Cape Verde region: seasonal evaluation of composition, sources and transport
EMEP	European Monitoring and Evaluation Programme
HYSPLIT	HYbrid Single-Particle Lagrangian Integrated Trajectory model
LIDAR	LIght Detection And Ranging
NCAR	(United States) National Center for Atmospheric Research
NCEP	(United States) National Centers for Environmental Prediction
NMMB	Nonhydrostatic Multiscale Meteorological Model on de B grid
PM	Particulate Matter
PM2.5	Particulate Matter with an aerodynamic diameter smaller than 2.5 μm
PM10	Particulate Matter with an aerodynamic diameter smaller than 10 μm
PMc	Particulate Matter with an aerodynamic diameter between 2.5 and 10 μm
SNAP	Selected Nomenclature for reporting of Air Pollutants
USGS	United States Geological Survey
WMO	World Meteorological Organization
WRF	Weather Research and Forecasting model

List of Figures

List of Tables

Part One. Introduction

Chapter 1

Introduction

1.1 Background

The Earth's atmosphere surrounds our planet and protects life as we know it. It is characterized by variations of pressure and temperature with height – the latter is the basis for the classification of the layers of the atmosphere. This Thesis addresses processes that occur in the lowest layer of the atmosphere, the troposphere.

We live in the troposphere; everyday of our lives we breathe its air. We release pollutants into the troposphere. We change our lands' use, which has an impact on the interactions between the Earth's surface and the atmosphere. We modify the troposphere composition and affect the natural equilibrium of our planet. To understand the environment and the physical laws that govern it, and to explore the beauty of atmospheric processes, are the motivations behind this Thesis, which deals with aerosols.

Aerosols are particles suspended in the atmosphere. They arise from direct emissions (primary aerosols) and from gas-to-particle conversion in the atmosphere (secondary aerosols). They can have a natural origin or be the result of human activities. Anthropogenic sources are mostly related to the burning of fuels. Examples of natural sources include volcanic activity or the entrainment of soil-derived particles which occurs mainly in deserts and other bare lands.

At elevated concentrations, aerosols inhibit visibility and are a human health hazard. There is a growing body of epidemiological evidence that increasing levels of aerosols may cause a significant

increase in human mortality (Seinfeld and Pandis, 1998). Moreover, aerosols interact with climate, directly by scattering and absorption of shortwave and thermal radiation (Liao and Seinfeld, 1998), and indirectly by modification of cloud properties (Posfai et al., 2013).

The focus of this Thesis is the mineral dust aerosol which is entrained from the soil into the atmosphere. Although, at global level, this aerosol has primarily a natural origin, various human activities can extend the geographical area of dust sources and increase the dust loading into the atmosphere. Ginoux et al. (2012) attribute 75 % of the global dust emissions to natural origin, while 25 % are related to anthropogenic (primarily agricultural) emissions.

The mineral dust cycle

Due to erosion processes, huge quantities of soil-derived mineral dust particles are entrained into the atmosphere, being transported over large distances downwind from the source. The process of dust emission is a complex function of surface (soil) conditions and air turbulence. Dust emission occurs when wind speed exceed a threshold, strong enough to break soil cohesion. The threshold friction velocity significantly varies in space and time, in response to soil moisture variability, surface roughness heterogeneity, and vegetation phenology (Xi and Sokolik, 2015).

The main natural dust sources are associated with topographic depressions where alluvium has been accumulated (Prospero et al., 2002). Dust emission may occur by aerodynamic lift, saltation bombardment (also known as sandblasting) and aggregate disintegration (Figure 1.1). Saltation refers to a layer of soil moving with the wind just above the surface. Sandblasting, or saltation bombardment, refers to the release of dust aerosol during impacts by saltating particles. Saltation and sandblasting have been recognized as the most important mechanisms for producing small dust aerosols (Shao et al., 1993), since the importance of gravity and aerodynamic forces (involved in the direct aerodynamic lift) diminishes for smaller particles. The dust aerosol may be remnants of disintegrating aggregate saltators or surface particles ejected by the saltator impact.

Globally, the largest and most persistent sources are located in the Northern Hemisphere, mainly across a broad "dust belt" that extends from the west coast of North Africa, over the Middle East, Central and South Asia, to China (Prospero et al., 2002). Every year, large plumes of dust are transported from the sources in North Africa across the Atlantic Ocean, reaching the Caribbean Basin and South America (Prospero et al., 2014), as well as across the Mediterranean into Europe

(Israelevich et al., 2012). Large quantities of dust, originating in Central Asia, are regularly carried out over the North Pacific to the West Coast of the United States (Fischer et al., 2009).

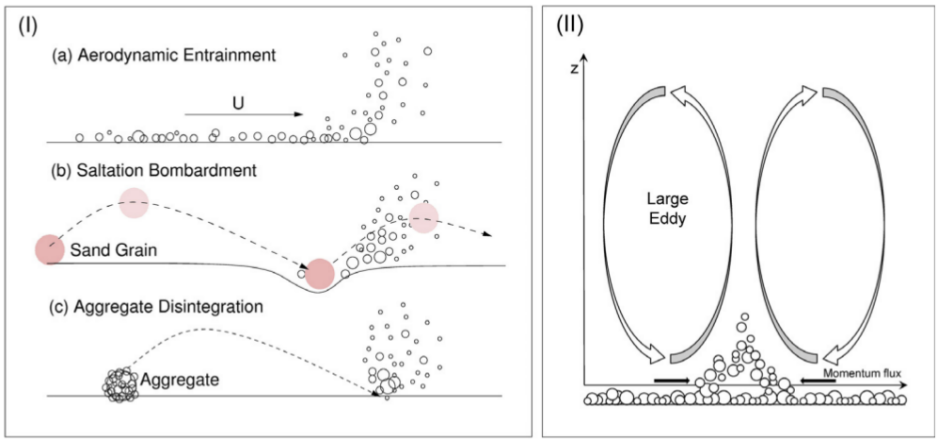

Figure 1.1: Mechanisms for dust emission. (I) Dust emission by (a) aerodynamic lift, (b) saltation bombardment and (c) aggregate disintegration. Traditionally, these processes are considered to be driven by mean wind shear, but large eddies can also cause intermittent sand drift and dust emission. (II) Illustration of particle lifting caused by the momentum intermittently transported to the surface by turbulent eddies. Saltation may be involved but does not need to be. source: Shao et al. (2015)

The atmospheric lifetime of dust depends on particle size; large particles are quickly removed from the atmosphere by gravitational settling, while sub-micron sized particles can have atmospheric lifetimes of several weeks (Seinfeld and Pandis, 1998).

Dust is removed from the atmosphere by dry (including gravitational settling) and wet deposition (i.e. scavenging through precipitation in the water or ice phase).

Dust impacts

While in the atmosphere, dust particles play an important role in the Earth system. Mineral dust from deserts contributes largely to the content of tropospheric aerosols and has impacts on air quality in several regions across the globe (Fairlie et al., 2007; Bouchlaghem et al., 2009; Pey et al., 2013; Salvador et al., 2013). Apart from air quality issues, airborne dust particles affect the Earth's radiative budget and modify cloud properties (Yin et al., 2002; Posfai et al., 2013) and photolysis rates (Jeong and Sokolik, 2007).

The effect of mineral dust aerosols on the Earth system depends on its physical and chemical properties, namely on its size, shape and composition. Dust aerosols affect the Earth's radiation balance by scattering (dust particles diffuse light in all directions but mostly forward) and absorbing

(dust plumes appear yellowish because they absorb mostly the blue wavelengths) solar radiation, and also by absorbing part of the terrestrial long-wave radiation (they trap, like Greenhouse gases, thermal radiation) (Liao and Seinfeld, 1998; Perez et al., 2006b).

Atmospheric aerosol particles serve as condensation nuclei for the formation of cloud droplets and atmospheric ice particles, affecting the formation of rain, snow and other forms of precipitation (Andreae and Rosenfeld, 2008). Dust is known for its important effect on precipitation formation particularly in mixed-phase clouds. For example, Fan et al. (2014) showed that two mixed-phase storms classified as "atmospheric rivers" with essentially identical meteorology and dynamics, one with clouds seeded with anthropogenic originated aerosols and the second seeded with dust, produced 40% more precipitation having dust as seeds. Creamean et al. (2013) demonstrated the importance of Saharan and Asian dust, and biological aerosols, in cloud ice and precipitation enhancement during a severe winter storm over the western United States.

Mineral dust is believed to play also an important role in marine and terrestrial biogeochemical processes. Trace metals in dust are important nutrients for the development of ecosystems. When deposited into the ocean, mineral dust acts as a nutrient supplier, which may increase the primary production of phytoplankton and eventual carbon export to the deep ocean (Mahowald et al., 2005; Moxim et al., 2011; Gallisai et al., 2014).

The focus of this Thesis is the impact of mineral aerosols on air quality. Dust concentrations can be very high during dust events, affecting air quality and public health (Zhang et al., 2016; Stafoggia et al., 2016). For example, it has been suggested that dust plays an important role in developing meningitis outbreaks in Sahel (Garcia-Pando et al., 2014).

Major dust storms are a frequent occurrence over Northwest Africa and the Sahara Desert. However, countries located in other regions may suffer the effect of desert dust injection into the atmosphere, since aerosols can be transported far-away from sources. In some regions, the transport of dust is so common that a specific word exists to describe this phenomenon, as happens in Cape Verde and in Spain. In Cape Verde, *bruma seca* (dry haze) refers to the dust storms blown off the Sahara Desert, which take place usually between October and April. In Spain, *calima* refers to the main winds which often carry dust toward the Canary Islands (Figure 1.2).

The Mediterranean basin is especially vulnerable to injections of desert dust because of its proximity to Sahara to the south and to the Arabian Peninsula to the east. Over the Mediterranean,

desert dust outbreaks are caused by specific meteorological scenarios, well characterized for western, central, and eastern sides of the basin (Salvador et al., 2014; Gkikas et al., 2013; Escudero et al., 2005). Several studies focus on the effect of these events in air quality over Spain (Pey et al., 2013; Querol et al., 2009; Rodriguez et al., 2001). However, few studies evaluate the contribution of outflows from North African deserts to the particulate matter levels over Portugal.

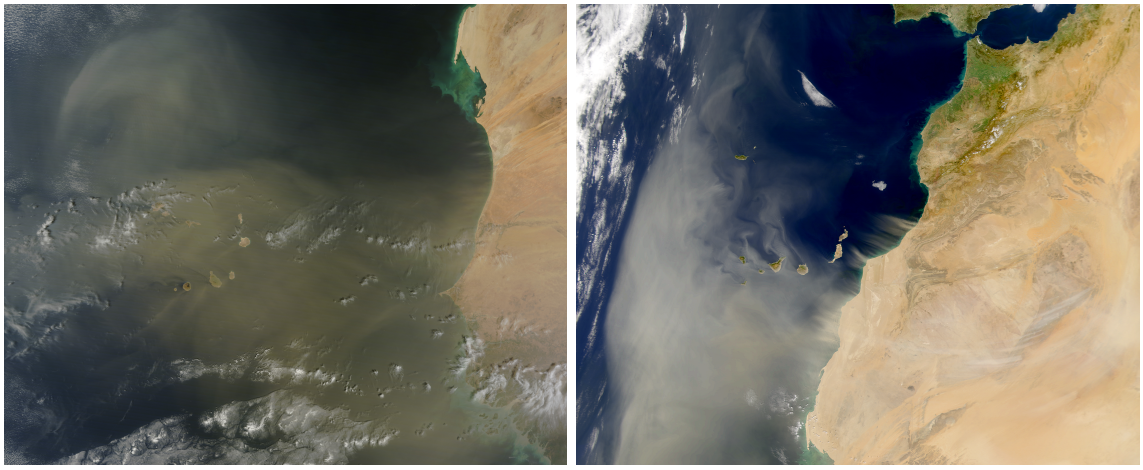

Figure 1.2: Dust storms. The left image was acquired on February 28, 2014 by the Moderate Resolution Imaging Spectroradiometer (MODIS) on NASA's Terra satellite; the yellow dust was concentrated largely over the Cape Verde Islands, where the mountain topography created swirling eddies and triangular wakes in the dust cloud. The right image was acquired on February 11, 2001 by the Sea-viewing Wide Field-of-view Sensor (SeaWiFS), and shows a massive dust storm affecting the Canary Islands, in Spain.

Dust modelling

The quantification of Earth's atmosphere characteristics is traditionally done based on observations. However, the assessment of desert dust atmospheric life cycle cannot be done based only on scarce measurements. Atmospheric modelling is an important tool to provide information on the spatial and temporal variability of dust emissions, transport and deposition, its composition and size distribution. In addition, dispersion models are used as valuable tools to establish a relationship between emission sources and observed pollution levels.

Schepanski et al. (2009) applied the regional dust model LM-MUSCAT (Heinold et al., 2007) to characterise Saharan dust transport and deposition towards the tropical North Atlantic, which was described in terms of horizontal and vertical distribution of dust concentration, optical thickness and dry and wet deposition rates over three typical months in different seasons. In SAMUM-2, the regional dust model COSMO-MUSCAT (Multi-Scale Chemistry Aerosol Transport Model Heinold et al., 2011) was used to study the mixed plume of Saharan dust and biomass-burning

aerosol transported off the West African coast towards the Cape Verde area during January and February 2008. Several other regional numerical models were developed to simulate the atmospheric desert dust cycle for operational purposes, such as SKIRON (Nickovic and Dobricic, 1996), BSC-DREAM8b (Nickovic et al., 2001; Perez et al., 2006b,a; Basart et al., 2012b), CHIMERE-DUST (Menut et al., 2009; Schmechtig et al., 2011), MOCAGE (Martet and Peuch, 2009) and NMMB/BSC-Dust (Perez et al., 2011; Haustein et al., 2012), among others. The main differences between models are related with the emission schemes, geographic-information databases, atmospheric drivers and land-surface schemes, spatio-temporal resolutions and meteorological input files.

In 2007, the World Meteorological Organization (WMO) established the Sand and Dust Storm Warning Advisory and Assessment System to enhance the ability of countries to deliver timely and quality sand and dust forecasts, observations, information, and knowledge to users. Within this program, the North Africa, Middle East and Europe Regional Center (http://sds-was.aemet.es/), hosted by the Spanish Meteorological Agency (AEMET) and the Barcelona Supercomputing Center - Centro Nacional de Supercomputación (BSC-CNS), aims to lead the development and implementation of a system for dust observation and forecast. Currently, this Regional Center distributes forecasts over North Africa from eight (regional and global) models that are evaluated in near-real-time.

1.2 Research questions and objectives

The main objective of this Thesis, which deals with mineral aerosols and addresses land-atmosphere interaction, is to improve the assessment of long-range transport of African dust. The work focus on two different case studies: Cape Verde, located in an area of massive transport of dust from land to ocean, and Portugal, located at Europe's South-Western border. In this context, the following research questions are formulated:

1. which are the processes and sources responsible for desert dust loading in the Cape Verde region?

2. how accurately dust models reproduce the dust cycle in a strategic site such as Cape Verde? can we improve models performance?

3. how do particulate matter concentrations vary through time over Portugal?

4. what is the contribution from the North African deserts to the atmospheric aerosol in Portugal?

5. how is the operational air quality forecasting system performing over Portugal? can we improve its performance?

To achieve the thesis main objective and to answer the research questions, the following specific goals should be accomplished:

1. to systematize, based on the available observations, detailed information about aerosol levels and their variability, both at surface level and using vertical column integrated data;

2. to apply dust modelling, in order to study the spatial and temporal variability of dust emissions and transport to specific areas;

3. to compare model outputs with available observations;

4. to characterize the processes and sources responsible for aerosol loading in the regions of Cape Verde and Portugal;

5. to contribute for dust models improvement.

1.3 Structure of the thesis

The present document is divided into four parts (see Figure 1.3). Each part consists of one or more chapters, grouped according their theme and/or geographical location of the study area. The chapters are consecutively numbered throughout the thesis; Part II, for example, begins with Chapter 2 since Chapter 1 belongs to part I.

Part I / **Chapter 1** has provided an overview of the desert dust cycle and its impacts.

Part II contains the work developed within the framework of the CV-DUST Project, a joint initiative of the University of Aveiro (UA) and the Technological and Nuclear Institute (ITN), together with the Cape Verde University (Uni-CV) and with support from the Cape Verde Atmospheric

Observatory (CVAO) and the Barcelona Supercomputing Center - Centro Nacional de Supercomputación (BSC-CNS). Part II contributes to the characterization of the processes and sources responsible for aerosol loading in the Cape Verde region. **Chapter 2** includes an evaluation exercise of two dust models widely used for operational forecasts that are used on the Sand and Dust Storms Warning Advisory and Assessment System (SDS-WAS) and for research (BSC-DREAM8b and NMMB/BSC-Dust), in a strategic site to study Saharan Atlantic transport.

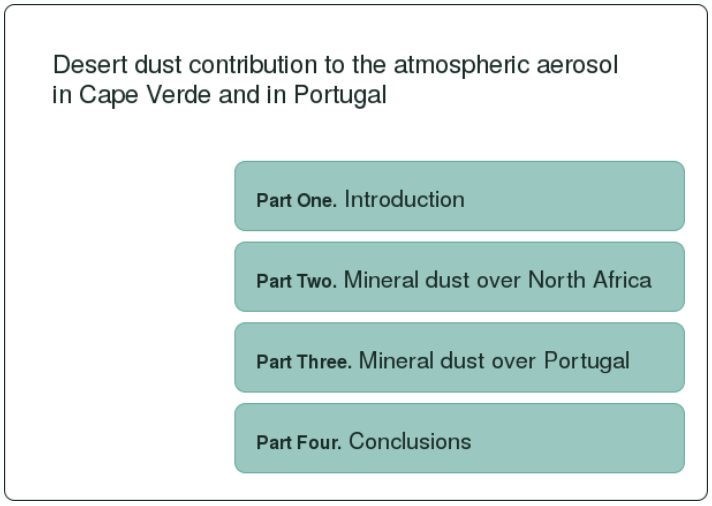

Figure 1.3: Structure of the thesis.

The work presented in Chapter 2 allows a comparison between the two dust models and identification of areas where further improvements are needed, such as in terms of model size distribution. In this context, **Chapter 3** focus on the dust size distribution considered by the NMMB/BSC-Dust model. In this Chapter, a new dust size distribution is prescribed at sources. Model results are then assessed against available observations.

The transport of dust from the Sahara desert and its margins does not affect North African latitudes only. The Mediterranean countries, including Portugal, are typically affected by the long-range transport of eroded mineral soils carried from the North Africa deserts. In this scope, Part III of this thesis focus on the desert dust carried north to Portugal.

Part III starts with **Chapter 4**, with the characterization of the particulate matter levels over Portugal based on the analysis of data from the national air quality monitoring network. Then, **Chapter 5** introduces the air quality modelling system in use in Portugal for forecast and assessment purposes. Based on the available observations, the performance of the system is evaluated and its limitations concerning the ability to forecast and/or reproduce particulate matter / dust events is discussed. In order to achieve a better model performance, different experimental set-

ups are tested and evaluated. By the end of Chapter 5, the best model set-up to reproduce the dust transport from North Africa to Portugal is selected. In **Chapter 6** this model set-up is used to study the impact of the dust on PM concentrations and the results of this assessment are compared with the common methodologies available for the same purpose.

Finally, the conclusions of this thesis and future work (Part IV) are presented in **Chapter 7**.

Chapters 2, 4 and 6 are presented in a similar form as they have been published or submitted to an international journal (some adjustments have been performed with respect to the journal version in order to avoid unnecessary repetitions or to increase the logical between chapters in this thesis). Chapter 3 has been presented in an international workshop. Chapter 5 is part of a report delivered to the Portuguese Environmental Agency.

Part Two. Mineral dust over North Africa

Chapter 2

Seasonal patterns in North Africa and Cape Verde

This chapter is based on: Gama, C., Tchepel, O., Baldasano, J.M., Basart, S., Ferreira, J., Pio, C., Cardoso, J., Borrego, C. (2015) Seasonal patterns of Saharan dust over Cape Verde – a combined approach using observations and modelling. Tellus 67B, 24410. doi:10.3402/tellusb.v67.24410.

2.1 Introduction

Mineral dust from deserts contributes largely to the content of tropospheric aerosols, being North Africa, specifically the Saharan desert and its margins, widely regarded as the Earth's largest source of dust (Prospero et al., 2002; Ginoux et al., 2012). Every year, millions of tons of eroded mineral soils are carried from the Sahara and Sahel regions, in North Africa, to the Americas (including the Caribbean and the Amazon basin), Europe and Middle East. Airborne dust particles have impact on air quality in several regions (e.g. Pey et al., 2013; Prospero, 1999), affect Earth's radiative budget by scattering and absorption of solar and infrared radiation (Nabat et al., 2012), and modify cloud properties and photolysis rates (Teller et al., 2012).

The Cape Verde Islands, located 570 km off the coast of Western Africa in an area of massive dust transport from land to ocean, are one of the best places to set up experimental campaigns to characterize and quantify the dust transported from North Africa through the tropical Eastern North Atlantic Ocean region. Examples of previous campaigns in Cape Verde worth mention within

the scope of this thesis are the Saharan Dust Experiment (SHADE) in September 2000 (Formenti et al., 2003; Tanre et al., 2003), the African Monsoon Multidisciplinary Analysis (AMMA) between August and September 2006 (Jeong et al., 2008; Chen et al., 2011), the Reactive Halogens in the Marine Boundary Layer (RHaMBLe) intensive study during summer 2007 (Mueller et al., 2010), the Saharan Mineral Dust Experiment (SAMUM-2) between January and February 2008 (Ansmann et al., 2011; Kandler et al., 2011; Knippertz et al., 2011) and, more recently, between January 2011 and January 2012, the CV-Dust Project (Pio et al., 2014). Moreover, the Cape Verde Atmospheric Observatory (CVAO) was established in 2006 and is undertaking long-term ground- and ocean-based atmospheric observations (Fomba et al., 2014).

In this Chapter, we aim to characterize a complete annual cycle of the aerosol over Cape Verde using ground-based observations and model outputs. Surface aerosol measurements performed within the scope of the CV-DUST Project and data from one AERONET station were used, together with two dust models, BSC-DREAM8b and the NMMB/BSC-Dust, as well as a trajectory model, in order to characterize dust particle size distribution, concentrations and optical properties for the whole year of 2011. This is the first attempt to test and compare dust models, for surface concentration and size distribution in Northern Africa across an annual cycle. Model results will contribute to a better characterization of the seasonality of the Saharan and Sahelian dust source regions and of the long-range transport of the desert dust through North and West Africa, and through the Eastern North Atlantic Ocean.

2.2 Data sources and methods

2.2.1 Measurement data

In-situ particulate matter observations

Aerosol concentrations were measured in Cape Verde for one year, from January 2011 to January 2012, in the scope of CV-DUST Project. The measuring instruments were installed at 98 m above sea level at the Cape Verde National Institute for Meteorology and Geophysics (INMG) located in the former Airport Francisco Mendes (14.92º N, 23.48º W), about 2 km away from central Praia (Cape Verde capital city) and 1700 m from the sea border. Measurements of particulate matter (PM) size distributed concentrations were based on the optical particle counter (OPC) method

and were carried out using a GRIMM EDM164 Environmental Dust Monitor. The equipment allowed the continuous counting of particles in real time (5 minute averages) with sizing from 0.25 up to 32 µm, using 31 size channels. A detailed description, with schematic diagrams of a similar instrument, can be found in Grimm and Eatough (2009). A density of 2.5 g cm^{-3} was used to convert the aerosol volume deduced from the particle number and size measurements to mass concentrations and mass size distribution. This density was adopted based on two main features: Cape Verde aerosol is composed predominantly of soil dust and sea salt (Mueller et al., 2010; Almeida-Silva et al., 2013); dust particles measured previously at Cape Verde and in Morocco showed a specific dry mass between 2.45 and 2.7 g cm^{-3} (Kaaden et al., 2009; Haywood et al., 2001) and dry density of sodium chloride which is the major constituent of sea salt is approximately 2.16 g cm^{-3} (Schladitz et al., 2011). In order to achieve a more correct estimate of concentrations and size distribution, the particle size bin diameters were recalculated from the original factory calibration of the equipment, taking into account the refractive index characteristic of sampled dust, 1.53-0.005i (see Pio et al. (2014) for more details). The recalculated diameter values give mass concentration estimations 11% below the gravimetric values. PM size distribution was also measured using a Tisch Environmental TE-236 High Volume Cascade Impactor with 6 collection stages ($<0.49 < Dp < 10$ µm).

AERONET observations

To complement the surface concentration observations obtained through the CV-DUST field campaign, column-integrated aerosol optical properties were used, routinely observed within the AErosol RObotic NETwork (AERONET; http://aeronet.gsfc.nasa.gov Holben et al., 1998; Smirnov et al., 2000). These instruments rely on extinction measurements of direct and scattered solar radiation at several nominal wavelengths (between 340 and 1020 nm). In the present work, quality-assured direct-sun data (Level 2.0) from the Capo Verde station (16.733°N, 22.935°W) in the 440-870 nm wavelength range was used, as these channels are highly accurate.

To allow a comparison with model results, as the aerosol optical depth (AOD) is simulated by the BSC-DREAM8b and NMMB/BSC-Dust models at 550 nm, data from AERONET station was extrapolated for a wavelength of 550 nm from data between 440 and 870 nm following Ångström's law. The Ångström exponent (AE), which is available in the same AERONET database, is a measure of the dependency of the aerosol optical properties on wavelength, being inversely

related to the average size of the particles in the aerosol. Large particles such as mineral dust and sea-salt have small AE (sometimes even < 0), since their optical properties do not change much with wavelength, while AE values above 1.5 indicate a significant presence of fine-mode particles (mainly smoke and urban aerosols) (e.g. O'Neill et al., 2003; Gobbi et al., 2007; Basart et al., 2009).

2.2.2 Numerical models

The BSC-DREAM8b dust model

The BSC-DREAM8b v1.0 model (Nickovic et al., 2001; Perez et al., 2006a,b; Basart et al., 2012b) solves the Euler-type partial differential non-linear equation for dust mass continuity, which is fully embedded as one of the governing prognosis equations in the Eta/NCEP atmospheric model. Thus, the model is able to simulate and predict the 3-dimensional field of dust concentration in the troposphere by taking into account all major processes of the dust life cycle, such as dust emission (Shao and Raupach, 1993) with an introduced viscous sub-layer (Janjic, 1994), horizontal and vertical diffusion and advection, turbulent and lateral diffusion (Janjic, 1994), dry deposition and gravitational settling (Giorgi, 1986) and a simple below-cloud wet scavenging scheme (Nickovic et al., 2001).

The main features of BSC-DREAM8b, described in detail by Perez et al. (2006b), include a source function based on the aridity categories of a 1 km USGS land use data set and the FAO 4 km global soil texture data set, a dust size distribution profile described by 8 size bins within a 0.1-10 μm radius range according to Tegen and Lacis (1996), a source distribution, derived from D'Almeida (1987), and dust radiative feedback Perez et al. (2006b). The emission scheme implemented in BSC-DREAM8b, described in detail by Basart et al. (2012b), directly entrains dust-sized particles into the atmosphere and includes the influence of soil structure and particle size distribution, as well as atmospheric conditions - where the near-surface wind speed must exceed the local threshold velocity to force dust mobilization.

In recent years, this model has been used for dust forecasting and as a research tool for dust in North Africa and Southern Europe (Jimenez-Guerrero et al., 2008; Amiridis et al., 2013, 2009; Klein et al., 2010; Pay et al., 2010; Alonso-Perez et al., 2011; Basart et al., 2012b; Kokkalis et al., 2012; Gallisai et al., 2014). The model has also been evaluated and tested for longer

time periods over Europe (Basart et al., 2012a; Pay et al., 2012; Tchepel et al., 2013) and against measurements at source regions (SAMUM I (Haustein et al., 2009) and BoDEx (Todd et al., 2008)). Moreover, the operational model predictions are near-real-time evaluated with satellites (MODIS and MSG) and AERONET data (http://www.bsc.es/earth-sciences/mineral-dust-forecast-system/bsc-dream8b-forecast/).

For the present analysis, the simulation domain (see Figure 2.1) covered North Africa, Middle East and Europe (NA-ME-E) with a resolution set to 1/3°, in the horizontal, and to 24 Eta-layers, extending up to approximately 15 km in the vertical. The simulated dust distributions consist of 365 daily runs, for the year 2011. The initial state of the dust concentration was defined by the 24-h forecast of the previous-day model run. Only in the "cold start" of the model, concentration is set to zero. The cold start of the model was initiated on 23 December 2010. The Final Analyses of the National Centers of Environmental Prediction (NCEP/FNL; at 1°x1°) at 0 UTC were used every 24 hours, as initial conditions, and boundary conditions were updated every 6 hours.

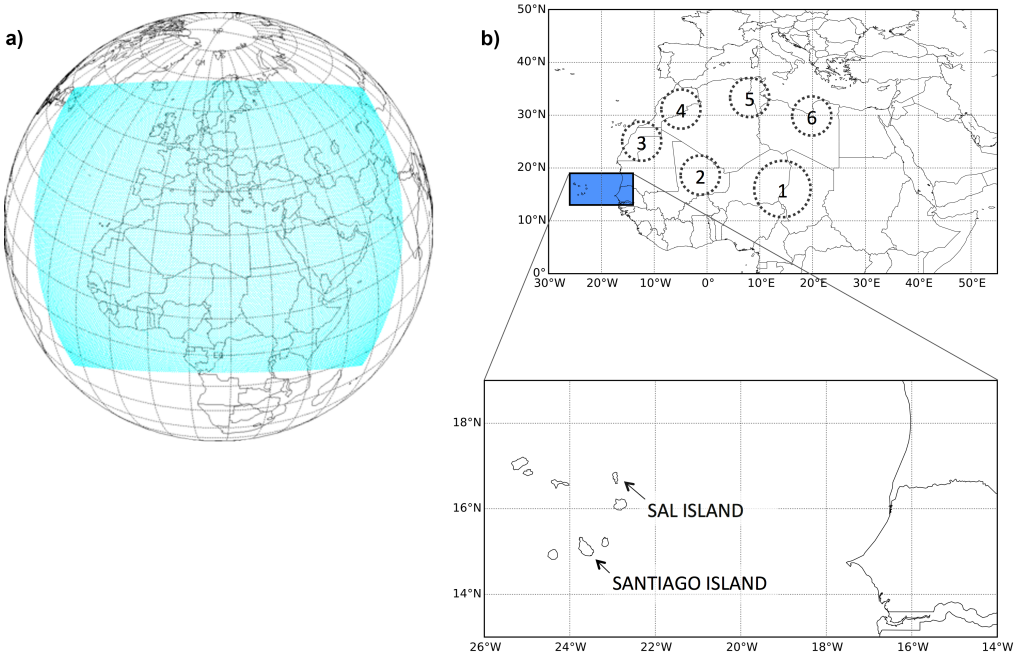

Figure 2.1: (a) Model simulation domain and (b) location of the measurement points Praia (Santiago Island) and Espargos (Sal Island) in Cape Verde. In the map, the dotted circles indicate dust emission source areas: (1) Bodélé, (2) Algeria-Mali, (3) West Sahara-Mauritania, (4) Algeria-Morocco, (5) Algeria-Tunisia and (6) Libya Desert.

The NMMB/BSC-Dust model

The NMMB/BSC-Dust model (Perez et al., 2011; Haustein et al., 2012) is the dust module of the NMMB/BSC-Chemical Transport Model (NMMB/BSC-CTM; Perez et al., 2011; Haustein et al., 2012; Jorba et al., 2012; Spada et al., 2013; Badia and Jorba, 2015) which is an online multi-scale atmospheric model designed and developed at BSC-CNS in collaboration with NOAA/NCEP, NASA Goddard Institute for Space Studies and the International Research Institute for Climate and Society (IRI). The dust model is fully embedded into the Non-hydrostatic Multiscale Model (NMMB) developed at NCEP and is intended to provide short to medium-range dust forecasts for both regional and global domains.

This model, which is described in detail in Perez et al. (2011), is a state-of-the-art dust model that includes a much more sophisticated meteorological driver than BSC-DREAM8b (NMMB meteorological model). The NMMB/BSC-Dust model solves the mass balance equation for dust by taking into account the following processes: (1) dust generation and uplift by surface wind and turbulence; (2) horizontal and vertical advection (Janjic et al., 2009); (3) horizontal diffusion and vertical transport by turbulence and convection (Janjic et al., 2009); (4) dry deposition and gravitational settling (Zhang et al., 2001); (5) wet removal that includes in-cloud and below-cloud scavenging from convective and stratiform clouds (Betts, 1986; Betts and Miller, 1986; Janjic, 1994; Ferrier et al., 2002). Furthermore, in order to take into account the effects of aerosols and mineral dust interactively, the rapid radiative transfer model (RRTM) (Mlawer et al., 1997) is implemented in the model.

The NMMB/BSC-Dust model includes a physically-based dust emission scheme which explicitly takes into account saltation and sandblasting processes (White, 1979; Marticorena and Bergametti, 1995; Marticorena et al., 1997) and assumes a viscous sublayer between the smooth desert surface and the lowest model layer (Janjic, 1994; Nickovic et al., 2001). To specify the soil size distribution we use the soil textures of the hybrid STATSGO-FAO soil map. In this database, the FAO two-layer 5-minute global soil texture is remapped into a global 30-second regular latitude-longitude grid. Four soil populations are used in the model, distinguishing fine-medium sand and coarse sand according to the criteria used in Tegen et al. (2002). The dust vertical flux is distributed according to D'Almeida (1987) and then distributed by 8 dust size transport bins with intervals taken from Tegen and Lacis (1996) and Perez et al. (2006a), as in the case of the BSC-DREAM8b model. For the source function, the model uses the topographic preferential

source approach, after Ginoux et al. (2001) and the National Environmental Satellite, Data, and Information Service (NESDIS) vegetation fraction climatology (Gutman and Ignatov, 1998).

The NMMB/BSC-Dust model has been evaluated at regional and global scales (Perez et al., 2011; Haustein et al., 2012). Perez et al. (2011) provides daily to annual evaluations of the model for its global and regional configurations. At the global scale, the model lies within the top range of AEROCOM dust models in terms of performance statistics for surface concentration, deposition and aerosol optical depth (AOD). At regional scale, the model reproduces significantly well the daily variability and seasonal spatial distribution of the dust optical depth over Northern Africa, the Middle East and Europe. In Haustein et al. (2012), the model was evaluated at the regional scale against measurements at source regions from the Saharan Mineral Dust experiment (SAMUM I) and the Bodélé Dust Experiment (BoDEx) campaigns.

For the present analysis, the regional domain covering North Africa, the Middle East and Europe (NA-ME-E) was selected, with a resolution set to 1/4°, in the horizontal, and to 40 σ-layers, in the vertical. As in the case of the BSC-DREAM8b model, the simulated dust distributions consisted of 365 daily runs for the year 2011. The initial state of the dust concentration was defined by the 24-h forecast of the previous-day model run. Only in the "cold start" of the model, concentration is set to zero. The cold start of the model was initiated on 23 December 2010. The Final Analyses of the National Centers of Environmental Prediction (NCEP/FNL; at 1°x1°) at 0UTC were used every 24 hours as initial conditions and boundary conditions were updated every 6 hours. In this contribution, simulations were carried with the operational GFDL radiation scheme, which does not allow feedback between dust and radiation.

2.3 Desert dust characterization in Cape Verde

2.3.1 Surface concentrations (Praia, Santiago Island)

Simulated desert dust concentrations at the surface level for Praia (Santiago Island), in 2011, were analysed and compared with OPC observations. It must be noted that both models take into account only aeolian mineral particles emitted from the deserts, whereas the measurement data set may also reflect non-dust aerosols like sea-salt or biomass burning particles, secondary pollutants and local sources. As can be observed in Figure 2.2, surface concentrations exhibit a strong

seasonal trend, which is in accordance with Chiapello et al. (1995) and Fomba et al. (2014), with maximum concentrations in winter and lower values during spring and summer. Between January and March, it is possible to highlight three episodes where observed concentrations reached hourly average values between 490 and 710 $\mu g\,m^{-3}$ of PM10, and between 160 and 240 $\mu g\,m^{-3}$ of PM2.5.

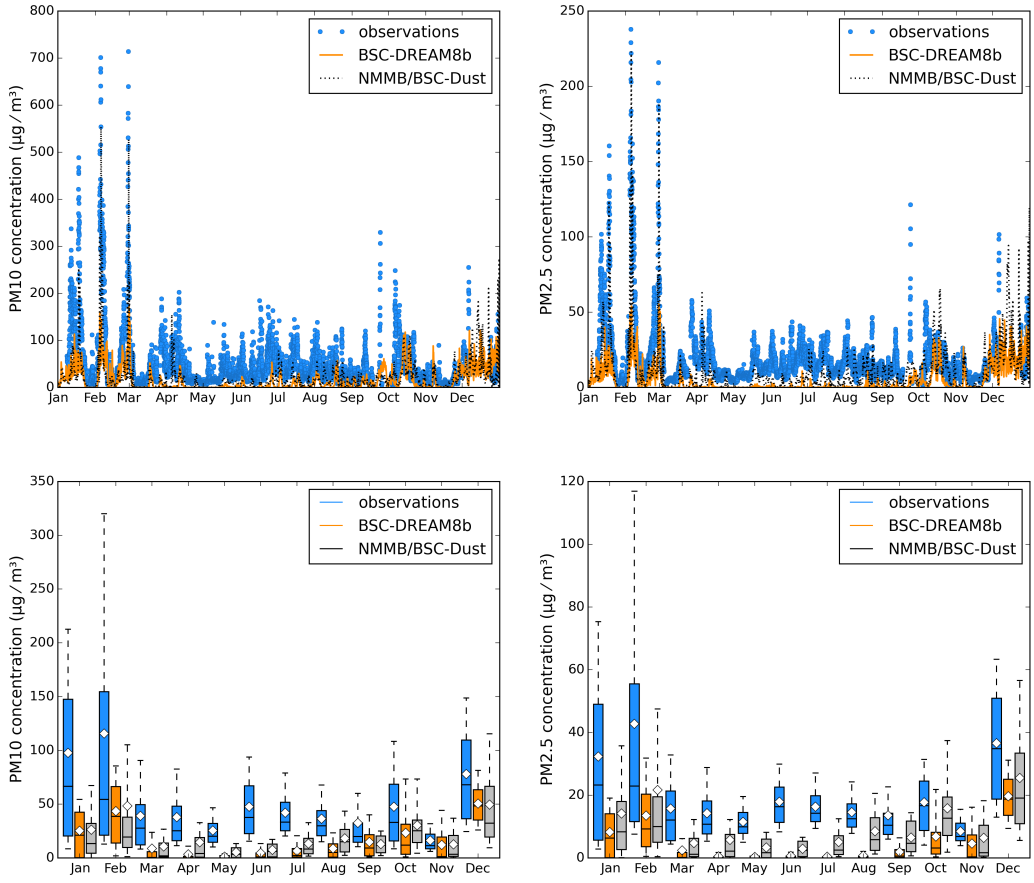

Figure 2.2: (top) Measured and modelled PM10 and PM2.5 hourly concentrations in Praia, Cape Verde, and (bottom) monthly analysis of the same datasets. The bottom and top of the box represent the first and third quartiles and the band inside the box represents the median. The ends of the whiskers represent the 10th and the 90th percentiles. White diamonds represent the mean value. Outliers are not shown.

Both models are able to reproduce those episodes, although the magnitude of the BSC-DREAM8b predicted concentrations is much lower than the observed, reaching maximum values of 170 $\mu g\,m^{-3}$ in the case of PM10, and 55 $\mu g\,m^{-3}$ for the PM2.5 fraction. NMMB/BSC-Dust estimates were much closer to the observations, reaching values up to 550 $\mu g\,m^{-3}$ of PM10 and up to 220 $\mu g\,m^{-3}$ of PM2.5. Table 2.1 presents the statistical parameters computed for model evaluation. A good agreement between observations and models results was found for PM10 daily average concentrations with correlation coefficients of 0.63 (BSC-DREAM8b) and 0.77 (NMMB/BSC-Dust) for the 1-year period, denoting the importance of mineral dust contribution for the total aerosol mass.

The average difference between measured bulk PM10 and model dust < 10 µm ("bias") was 32.9 µg m^{-3} for BSC-DREAM8b and 29.0 µg m^{-3} for NMMB/BSC-Dust (models under predict PM10 surface levels). The box-and-whisker plots of the PM10 and PM2.5 concentrations for every month (Figure 2.2, bottom) allow a quantitative view of the differences between model and experimental data.

Table 2.1: Statistical parameters computed for daily average surface concentrations.

Dust model	Specie	Observed mean (µg m^{-3})	Predicted mean (dust only) (µg m^{-3})	Correlation coefficient	Root mean square error (µg m^{-3})	Bias (µg m^{-3})
BSC-DREAM8b	PM10	49.7	16.8	0.63	56.8	32.9
NMMB/BSC-Dust			20.7	0.77	49.3	29.0
BSC-DREAM8b	PM2.5	19.5	5.0	0.64	21.1	14.5
NMMB/BSC-Dust			10.0	0.76	16.1	9.5

Annual average observed concentrations for PM10 and PM2.5 were 49.7 $\pm$ 62.3 and 19.5 $\pm$ 21.0 µg m^{-3}, respectively, whereas annual average model dust concentrations were, for the < 10 µm and < 2.5 µm fractions, respectively, 16.8 $\pm$ 24.7 and 5.0 $\pm$ 8.6 using BSC-DREAM8b and 20.7 $\pm$ 36.5 and 10.0 $\pm$ 16.3 using NMMB/BSC-Dust. These values were in good agreement with the five-year means found by Fomba et al. (2014) at CVAO on São Vicente Island, which had a PM10 mean of 47.1 $\pm$ 55.5 µg m^{-3} and mineral dust mean of 27.9 $\pm$ 48.7 µg m^{-3}. The SAMUM-2 intensive one-month (January 2008) field campaign in Praia revealed PM10 values on the order of 29 µg m^{-3} during transport of maritime air masses, and 223 µg m^{-3} during dust events with air masses transported directly from Africa (Kandler et al., 2011). Their mass ratio of between PM10 and PM2.5 did not present a significant variation during the field experiment, with an average of 2.67, which is not very different from our annual average measured ratio of 2.55.

Due to the location of the CV-DUST measurement station, observed aerosol concentrations were expected to be affected not only by the transport of dust from Africa, but also by local dust, anthropogenic emissions and sea salt spray. The results obtained with the NMMB/BSC-Dust model and observations gave an averaged modelled dust concentration < 10 µm equal to 20.7 µg m^{-3}; and averaged measured bulk PM10 equal to 49.7 µg m^{-3}. This allows a rough estimation that on a yearly basis, 42% of the PM10 mass observed in Cape Verde is associated with dust transported from North African deserts. Indeed, Almeida et al. (2013a) found on average for the same year 2011, a natural origin of 68% of the PM10 mass in Cape Verde, with 48% associated

with soil and 20% associated with the sea. These values were lower than the 80% coupled contribution of sea salt and mineral dust for the aerosol mass (being about 55% associated with mineral dust only) found by Fomba et al. (2014) for a five-year period (2007 to 2011) at the CVAO (in a less anthropogenically influenced region). Nunes et al. (2012) analysed the water-soluble inorganic species present in the Cape Verde atmosphere and found a high correlation (R $>$0.95) among chloride, sodium and magnesium ions, which denotes the importance of sea salt contribution to the local observed aerosol. From the CV-DUST elemental analysis, an average sea salt concentration of 12-14 $\mu g\, m^{-3}$ was observed during 2011 in PM10 particles, which represents nearly half of the unexplained PM10 bias. A sea salt five-year mean concentration of 11.1 $\pm$ 5.5 $\mu g\, m^{-3}$ was reported by Fomba et al. (2014). In addition, aerosols from the African continent carry not only Saharan dust, but also anthropogenic emissions from ship tracks near the African coast, African coastal cities and sometimes biomass burning aerosols (Kaufman et al., 2005; Ansmann et al., 2009; Dall'Osto et al., 2010; Rodriguez et al., 2011). The chemical analysis of size-segregated samples performed under CV-DUST studies in Praia show a less than 20% contribution of submicron PM mass from carbonaceous constituents (EC + OC) and secondary aerosols species (non-sea salt sulphate, nitrate and ammonium).

The size distribution of desert dust is crucial to understanding how far particles can travel from source regions. Moreover, the size distribution of mineral dust aerosols partially determines their interactions with clouds, radiation, ecosystems, and other components of the Earth system (Mahowald et al., 2014). It is also one of the key modelling factors in order to correctly incorporate dust-radiation and dust-cloud interactions into regional dust models (Perez et al., 2006a). Figure 2.3 shows the seasonal analysis of observed and modelled surface PM size distribution for Praia, Cape Verde. To plot this Figure, data from the 31 size channels by the OPC were converted into the 8-bins model size channels. Only the first seven size ranges are presented, including particles up to 12 μm in diameter.

Different behaviours were obtained for the four seasons. During the dust season in winter (corresponding to December, January and February), the experimental data showed that most of the dust mass occurs at between 2 and 12 µm. Similar results were found during RHaMBLe intensive campaign, when days influenced by mineral dust presented a maximum PM concentration in the size fraction of 1.2 - 3.5 µm, followed by a coarse mode fraction of 3.5 - 10 µm (Mueller et al., 2010). During spring and summer, particles within a range of 6 - 12 µm contribute the most to the aerosol mass. PM size distribution modelled with BSC-DREAM8b seems to be in greater

agreement with observations than NMMB/BSC-Dust, since the estimated contribution of the larger particles for the total dust mass is higher. With the NMMB/BSC-Dust model, particles between 2.0 and 3.6 µm contribute to the higher aerosol mass throughout the year.

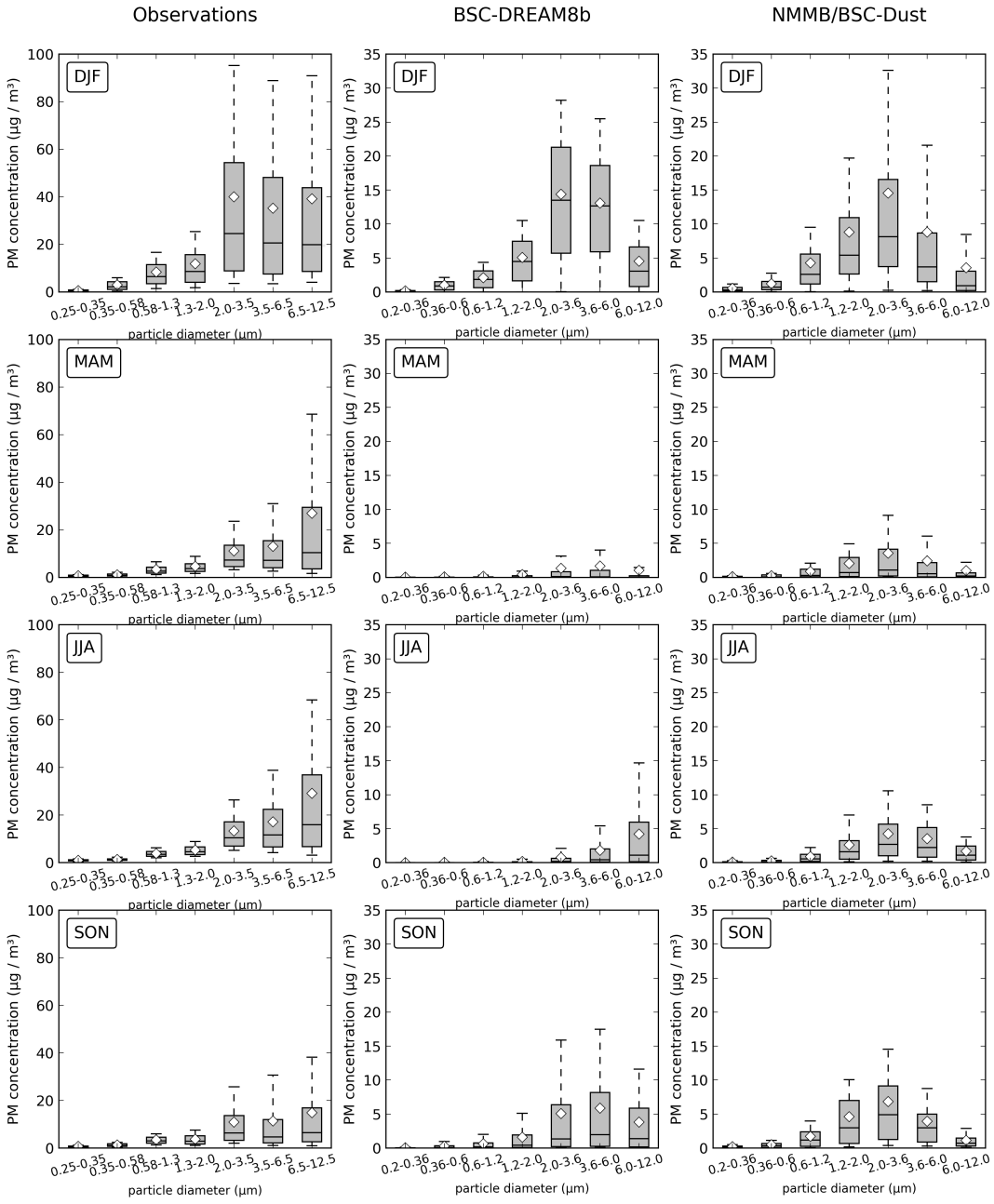

Figure 2.3: Seasonal analysis of the observed (left panels) and modelled (centre and right panels) size distribution surface PM concentrations, for Praia, Cape Verde, 2011. DJF corresponds to December, January and February, MAM to March, April and May, JJA to June, July and August and SON to September, October and November. The bottom and top of the box represent the first and third quartiles and the band inside the box represents the median. The ends of the whiskers represent the 10th and the 90th percentiles. White diamonds represent the mean value. Outliers are not shown.

In addition to OPC measurements, PM size distribution was measured with a high-volume cascade impactor with six collection stages ($<0.49 < Dp < 10$ µm). Figure 2.4 shows observations and BSC-DREAM8b and NMMB/BSC-Dust models results, for the periods between Jan 14 and 18 and between Feb 24 and 27. These two periods were selected amongst available samples, since they are associated with mineral dust episodes. Although none of the models display the bimodal shape obtained with gravimetric data (with maxima at 1-2 and 5-6 µm), observed PM size distribution was reproduced better by the BSC-DREAM8b, as it shows a mode at larger particle sizes (at 4-5 µm) than the one presented by NMMB/BSC-Dust (at 3 µm). Differences between both models are partly linked to the different dry deposition schemes implemented in each model. The origin of the first mode that is visible in the impactor results is unknown. However, this peak is as well exhibited by the Ca^{2+}, but not by the Cl^- analysis (not shown), which rejects the possibility of marine origin. This mode probably appears as a consequence of the rupture of dust agglomerates, as observed in Izana (Rodriguez et al., 2012). The modelled monomodal shape of an aerosol size distribution is related to the transport description in 8 size bins (Tegen and Lacis, 1996), with the source size distribution derived from D'Almeida (1987) – which yields 81% of the dust emissions at the 2.0-12.0 µm size bins – and along with the fact that there was no consideration of exchange between size bins.

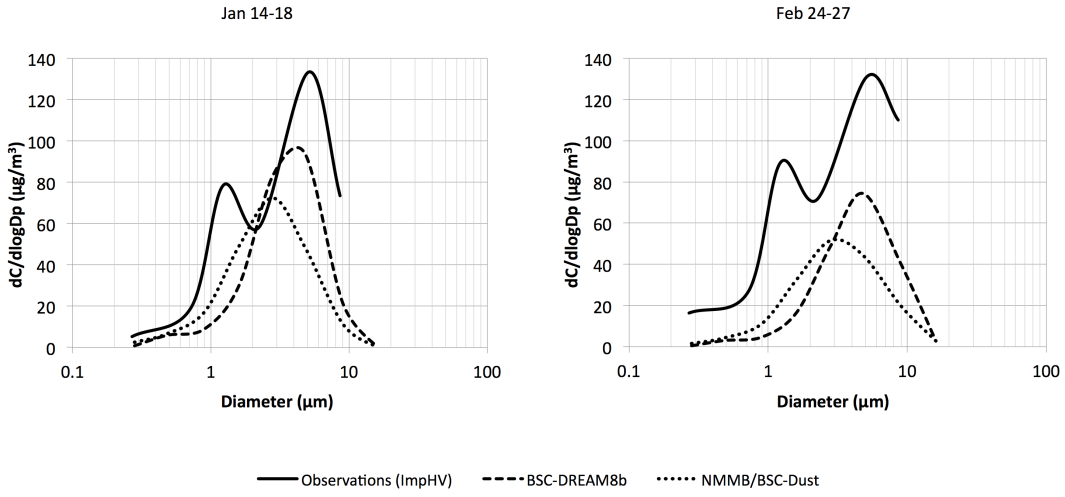

Figure 2.4: PM measured and modelled size distribution for (left) Jan 14-18 and (right) Feb 24-27.

2.3.2 Aerosol Optical Depth (Espargos, Sal Island)

The data from the AERONET site in Cape Verde (located on Espargos, Sal Island) is shown in Figure 2.5. In general, higher AOD values are present during summer months. During winter, AOD values are usually lower, with high values during only specific events. The highest winter peaks occur in the same days as the peaks observed in surface concentration in Santiago Island, highlighting the extent of these episodes of desert dust and long-range transport from the African continent. High extinctions (AOD $>$ 0.15) and low Ångström exponent (AE $<$ 0.75) values point out that the aerosol regime in Cape Verde is dominated by mineral dust due to frequent Saharan dust outbreaks as indicated in the aerosol characterization from Basart et al. (2009). Unlike the surface concentrations, the BSC-DREAM8b model reproduces the magnitude of the column-integrated load during summertime. Considering the 1-year period, a correlation coefficient of 0.58 and a bias of 0.14 were computed from model (which considers only mineral dust transported from the African continent) and observations (which include non-dust aerosols as well). The results from the NMMB/BSC-Dust model are closer to the observations (correlation coefficient $=$ 0.74 and bias $=$ 0.12). AOD estimates are higher during specific dust events such as the ones between January and March. Moreover, the NMMB/BSC-Dust model is also able to describe the observed AOD during springtime (from middle April till the end of May), when the estimates from BSC-DREAM8b are nearly zero.

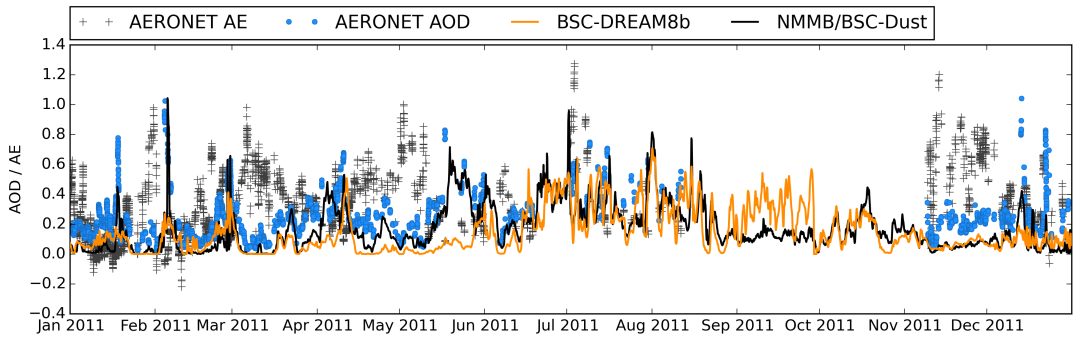

Figure 2.5: Measured and modelled Aerosol Optical Depth (AOD at 550nm) and Ångström Exponent (AE; calculated between 440 and 870nm) in Espargos, Cape Verde.

The fact that on average, the AOD values were higher during the summer period, in opposition to the lower surface concentrations recorded during this period, indicates the existence of aerosol layers at higher altitudes during summer, as indicated previously by Chiapello et al. (1995, 1997), Schepanski et al. (2009) and Tsamalis et al. (2013). Figure 2.6 depicts the averaged vertical

distribution of desert dust concentrations at Cape Verde latitude (15°N), for the winter and summer of 2011, modelled by NMMB/BSC-Dust. Similar distributions were obtained with the BSC-DREAM8b model (not shown here). Indeed, during winter months, transport of Saharan dust occurs at near-surface layers, while in the summer the dust layer is extended to higher levels (up to 5km). These results give additional insights regarding the Praia surface PM size distribution analysis. During the summer period it is probable that the coarser particles, having a higher sedimentation velocity, will fall from higher atmospheric layers to the surface, thus influencing aerosol distribution with peaks at sizes larger than those resulting from direct transport, as seen in the observations depicted in Figure 2.3.

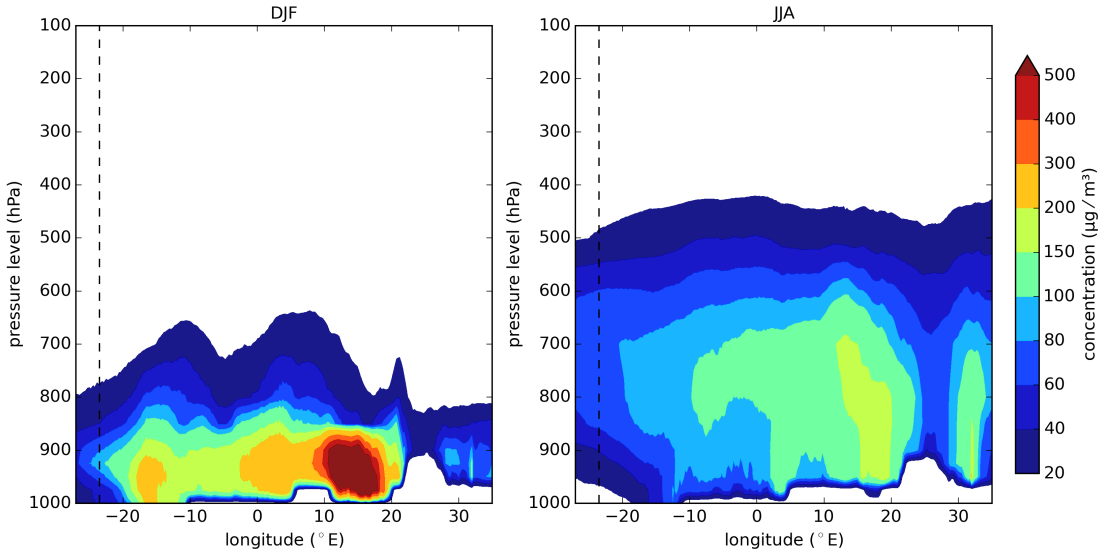

Figure 2.6: Vertical distribution of desert dust concentrations at a fixed latitude of 15°N, for (left) winter (December, January and February) and (right) summer (June, July and August) averages, modelled with NMMB/BSC-Dust. The dashed line represents the longitude of Cape Verde.

2.4 Dust regional variability: from sources and transport patterns to concentrations and AOD

Desert dust seasonal average surface concentrations and AOD, modelled with BSC-DREAM8b and NMMB/BSC-Dust for 2011, are presented in Figures 2.7 and 2.8, respectively. The surface concentrations and seasonal patterns are directly linked to dust emissions, meanwhile the AOD seasonal maps help to identify desert dust long-range transport.

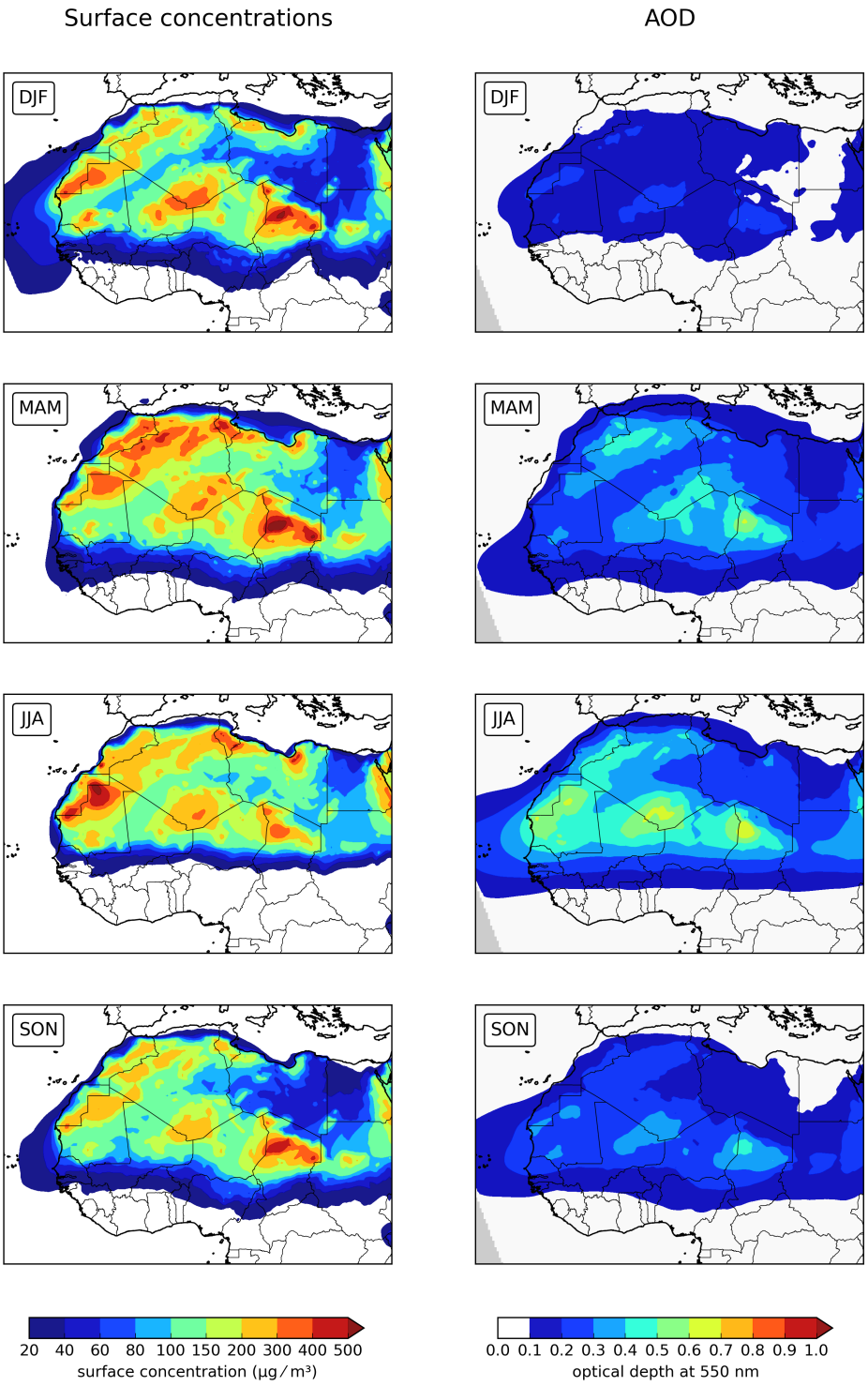

Figure 2.7: Seasonal average of desert dust surface concentrations (left panels) and dust optical depth (right panels), for 2011, modelled with BSC-DREAM8b. DJF corresponds to December, January and February, MAM to March, April and May, JJA to June, July and August and SON to September, October and November.

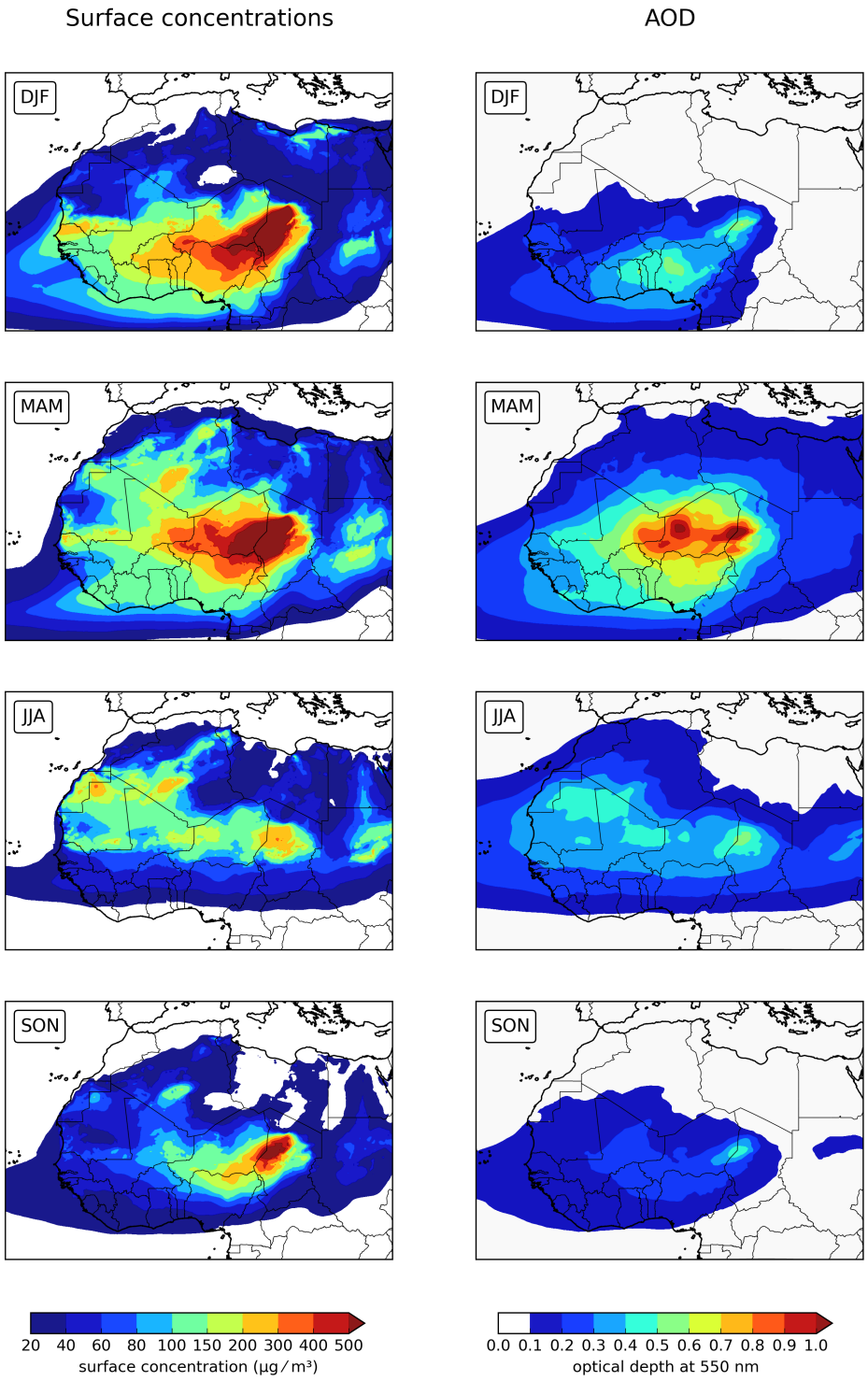

Figure 2.8: Seasonal average of desert dust surface concentrations (left panels) and dust optical depth (right panels), for 2011, modelled with NMMB/BSC-Dust. DJF corresponds to December, January and February, MAM to March, April and May, JJA to June, July and August and SON to September, October and November.

The Bodélé (in Chad) is the area with the highest dust concentrations, achieving maximum values during winter (DJF) and spring (MAM) months. According to Figures 2.7 and 2.8, additional relevant sources include Algeria-Morocco, West Sahara-Mauritania, the Libya desert, Algeria-Tunisia and Algeria-Mali regions. These sources have been, in general, also mentioned in previous studies where satellite-based data were explored for the purpose of identifying dust-source regions (Goudie and Middleton, 2001; Prospero et al., 2002; Engelstaedter et al., 2006; Schepanski et al., 2012; Ginoux et al., 2012). Both models reproduce the typical seasonal cycle of dust emissions in North Africa, which is linked to the latitudinal shift of the intertropical convergence zone (ITCZ). The dust sources located in the Sahel are mostly active during winter and spring, while those located in northern subtropical Saharan latitudes are more active during spring and summer (e.g. Prospero et al., 2002; Ginoux et al., 2004).

As shown by Basart et al. (2012b), the BSC-DREAM8b model tends to overestimate the emissions over Morocco, North Algeria and Tunisia during springtime when dust events are usually driven by low-pressure systems. In contrast, during summer the model tends to reproduce lower surface concentrations than in spring over the main source in the Sahara. Furthermore, the BSC-DREAM8b model underestimates the dust emission from the Southern Saharan sources with a strongly underestimation of the dust transport over the Sahel particularly in wintertime in comparison with NMMB/BSC-Dust. As pointed out in the model evaluation performed by Basart et al. (2012b), this is a problem in the low-level dust transport over the region partly linked to the dry deposition scheme. The updated version of the BSC-DREAM8b model (version 2.0) includes in its emission scheme a topographical approach from Ginoux et al. (2001), which improves the realism of the model dust load in the vicinity of sources, as well as a new dry deposition and sedimentation scheme based on Zhang et al. (2001) (see Basart et al., 2012b).

On the other hand, the NMMB/BSC-Dust model shows lower AOD values in the summer in comparison to spring (Figure 2.8). In the recent work of Ashpole and Washington (2013) based on a classification of satellite-derived maps of daily dust occurrence frequency, it is shown that during summer the high dust occurrences in Central and Western Sahara are found in areas close to the Algeria-Mali-Niger border triple point (TP) or further to the northwest across the west half of the Mali-Algeria border (MAB). TP patterns occur far more frequently in June meanwhile, MAB patterns are more typical of July and August. Differences in surface concentration during summer between BSC-DREAM8b and NMMB/BSC-Dust (Figures 2.7 and 2.8, respectively) highlighted that NMMB/BSC-Dust tends to strongly underestimate the emissions in these particular dust

source regions, as indicated the lower dust surface concentrations modelled in summer. Furthermore, these lower values are associated with a decrease in the AOD at the end of August, as also shown in the AERONET temporal series for Cape Verde (see Figure 2.5). Several causes could induce these summer AOD underestimations over the Sahara. During summer, dust emission is linked mainly to the low-level jets embedded in both the north-easterly Harmattan flow and the south-westerly West African monsoon flow and to cold pool outflows from convective complexes that are sometimes present over the southern Sahara (Ashpole and Washington, 2013; Marsham et al., 2013). These mesoscale convective systems cannot be well captured by global meteorological models or regional dust models (Marsham et al., 2011; Heinold et al., 2013). Additionally, as pointed out by Perez et al. (2011), the topographical approach from Ginoux et al. (2001), included in the emission scheme of the NMMB/BSC-Dust model, tends to omit the Mauritania/Mali border source. Other features of the present model configuration are being investigated as possible factors, such as the NCEP/FNL global meteorological input data used as initial and boundary conditions, possible missing sources in the model and the misrepresentation of small-scale atmospheric convection processes by the model.

In order to obtain the characteristic transport patterns, air masses reaching Cape Verde during 2011 were computed and clustered using the HYSPLIT Trajectory Model (Hybrid Single Particle Lagrangian Integrated Trajectory Model; Draxler and Hess, 1998) forced with NCEP's GDAS meteorological data. Air mass backward trajectories over 96 hours before arrival at Praia, at 250 m, were simulated four times per day, and a "bottom-up" cluster methodology was used to group trajectories into clusters according to their characteristics. Typical meteorological parameters and mineral dust measured and predicted concentrations were then assessed for the several clusters, i.e., for the several transport patterns found. The optimum number of clusters was determined by assessing the total spatial variance as a function of the number of clusters, as proposed by Delcloo and De Backer (2008).

Eight trajectory clusters were found; the mean trajectories of each cluster are depicted in Figure 2.9, as well as their monthly distribution. Figure 2.10 depicts the measured and the BSC-DREAM8b and NMMB/BSC-Dust predicted PM10 concentrations in Praia, for the eight transport patterns found. Both models tend to show lower PM10 values in comparison to the measurements because the measurements include all the aerosols, while the model only considers desert dust.

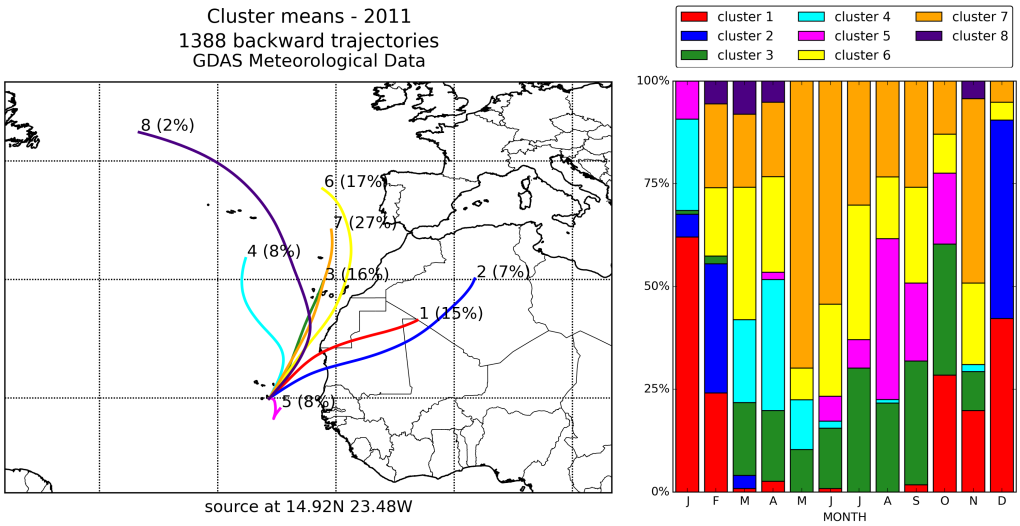

Figure 2.9: (left) 96-hour average back-trajectories for the eight clusters at Praia, Santiago Island (latitude: 14.92 N, longitude: 23.48 W), for 2011, with starting height at 250 m above sea level (percentages in parentheses reflect percentage of total 6-hour periods contributing to the averaged trajectory), and (right) their monthly distribution.

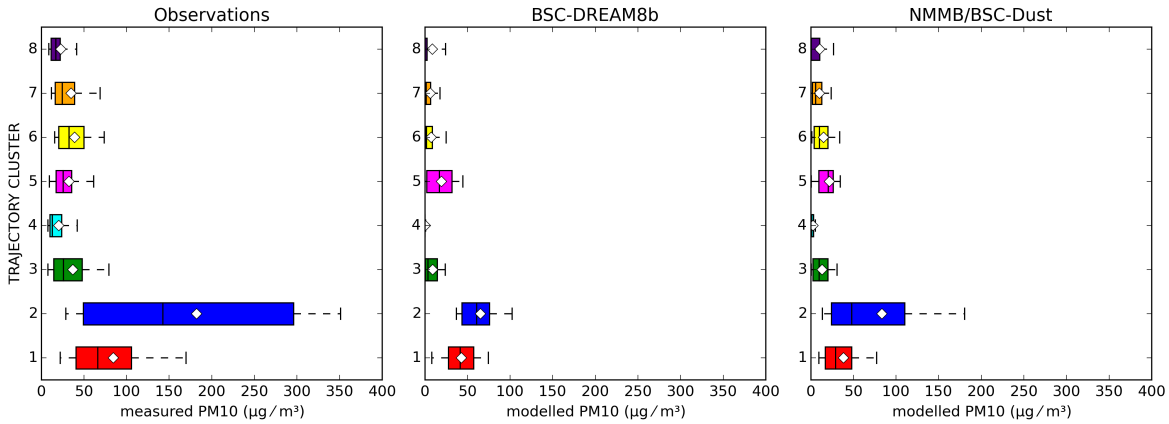

Figure 2.10: PM10 (left) measured and (right) BSC-DREAM8b and NMMB/BSC-Dust modelled PM10 concentrations in Praia, during 2011, according to trajectory clusters. The left and right limits of the box represent the first and third quartiles and the band inside the box represents the median. The ends of the whiskers represent the 10th and the 90th percentiles. White diamonds represent the mean value. Outliers are not shown.

Similar features can be observed in a comparison between the models and measurements, and there are significant differences between the concentrations associated with each cluster. The trajectories grouped in cluster 1 and 2 occur mainly during the winter period (between October and February for cluster 1 and between December and March for cluster 2). Episodes grouped by these clusters are associated with the transport of dust westerly, from the belt extending from Morocco and northern Algeria to the Western Sahara to Cape Verde region. Indeed, the highest desert dust concentrations are found in air masses from cluster 2, followed by air masses from

cluster 1, both for observations and model results. During summer, the air masses that reach Cape Verde at near-surface levels (250 m) describe typical trajectories along the North African coast.

In order to analyse with more detail the winter situation, since this is when the transport of desert dust to Cape Verde at the surface level is stronger, we computed characteristic transport patterns for this period individually, following the same methodology described for the whole year 2011. Seven characteristic transport patterns were found and are presented in Figure 2.11. Figure 2.12 shows the measured and BSC-DREAM8b and NMMB/BSC-Dust predicted PM10 concentrations that are linked to each cluster. The highest measured concentrations occur for cluster 6, followed by cluster 3 and cluster 1. The models exhibit the same behaviour. It is interesting to notice that NMMB/BSC-Dust describes very well the concentrations linked to cluster 6, which occurred on days 5 and 6 of February, 27 and 28 of February, and 30 and 31 of December.

The BSC-DREAM8b and the NMMB/BSC-Dust models estimate, respectively, that the Bodélé region is responsible for 20% and 40% of the emissions from North Africa, and that this source area emits mainly during winter and spring. According to Schepanski et al. (2009), a maximum contribution of dust transported from this source towards the Cape Verde Islands is found during the winter period. Although our results also show that PM surface concentrations are higher during the winter period (see Figure 2.2), the backward trajectories analysis does not indicate Bodélé as one of the main contributors to the PM recorded in Cape Verde. This is supported by Gross et al. (2015), who used the phosphate oxygen isotopes of all the major Saharan dust events of 2011 over the Cape Verde islands to identify the source of phosphorus in dust blown from Africa. Their results indicated that the dust-P sampled in Cape Verde was derived from two major sources: marine sediments and igneous rocks, having no indication of a Bodélé diatomite contribution. Indeed, the air masses responsible for the highest aerosol concentrations in Cape Verde (cluster 2) describe a path over the central Saharan desert area in Algeria, Mali and Mauritania before reaching the Atlantic Ocean. In the scope of SAMUM-2, Weinzierl et al. (2011) computed similar trajectories (relative to the day 19 January 2008, flight L05) associated with particles dominated by mineral dust. Although the computed trajectories did not directly cross the centre of strong dust activation areas, they passed the edges of the dust activation areas in Mali and Algeria, where they were assumed to have obtained their aerosol loading.

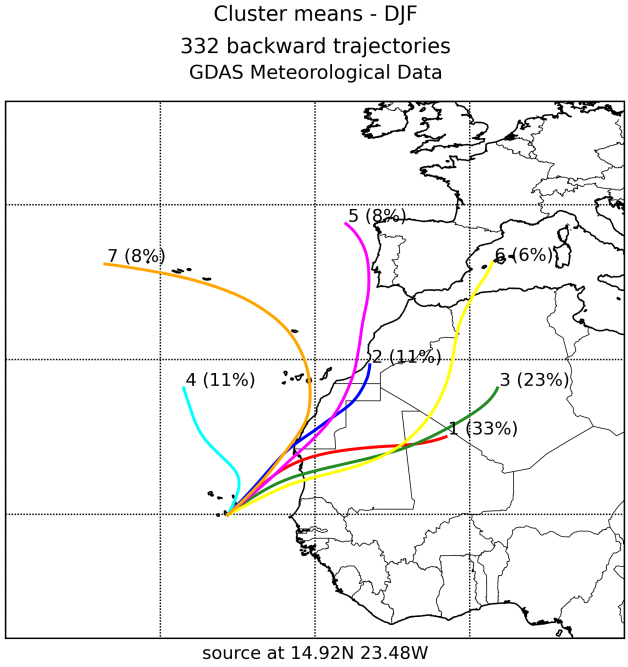

Figure 2.11: 96-hour average back-trajectories for the seven clusters at Praia, Santiago Island (latitude: 14.92 N, longitude: 23.48 W), for December, January and February, with starting height at 250 m above sea level (percentages in parentheses reflect percentage of total 6-hour periods contributing to the averaged trajectory).

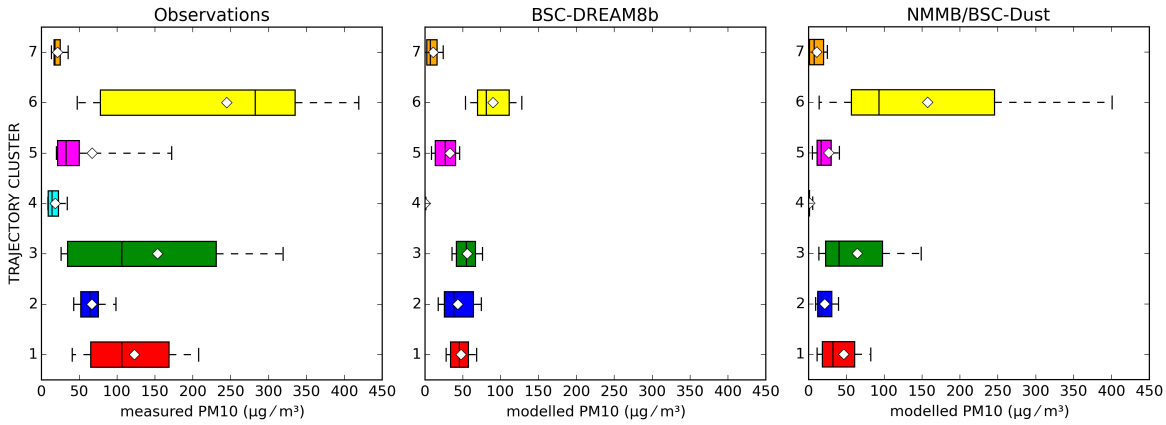

Figure 2.12: PM10 (left) measured and (right) BSC-DREAM8b and NMMB/BSC-Dust modelled PM10 concentrations in Praia, for December, January and February, according to trajectory clusters. The left and right limits of the box represent the first and third quartiles and the band inside the box represents the median. The ends of the whiskers represent the 10th and the 90th percentiles. White diamonds represent the mean value. Outliers are not shown.

2.5 Summary and conclusions

This Chapter provided the characterization of a complete annual cycle of aerosol in Cape Verde. Seasonal patterns were analysed based on a combination of mineral dust modelling with site

aerosol measurements from the CV-Dust Project and optical column data from the AERONET network.

From October till March, significant seasonal intrusions of dust from North West Africa affect Cape Verde at surface levels when atmospheric concentration levels in Praia exhibit very high levels (PM10 observed concentrations reach hourly values up to 710 $\mu g\,m^{-3}$). High aerosol optical depth (AOD) values were observed for Sal Island on the same days as the peaks observed for surface concentration on Santiago Island, highlighting the extent of episodes of long-range transport of desert dust from the African continent. While surface concentrations were higher during winter, AOD were higher during summer, indicating that during this period dust is transported from North Africa at higher altitudes.

The BSC-DREAM8b and the NMMB/BSC-Dust models were applied for a one-year period (2011) over the domain covering Northern Africa, Europe and the Middle East to complement the present analysis. This is the first time that these models have been used to evaluate surface concentration and size distribution in Africa over a complete annual cycle. Both models are able to reproduce the majority of the dust episodes, although the magnitude of the predicted concentrations was lower than those observed. While the dust models take into account only aeolian mineral particles emitted from the deserts, the measurement data set may also reflect non-dust aerosols like sea-salt or biomass burning particles, secondary pollutants and local sources. Results from NMMB/BSC-Dust are in better agreement with observed PM concentrations and AOD through the year. For this model, the comparison between observed and modelled PM10 daily averaged concentrations yields a correlation coefficient of 0.77, denoting the importance of mineral dust contribution for the total aerosol mass, and a 29.0 $\mu g\,m^{-3}$ "bias", of which 12-14 $\mu g\,m^{-3}$ is explained by the observed sea salt contribution to PM10 during 2011. These results allow rough estimation that on a yearly basis, 42% of the PM10 mass observed in Cape Verde is associated with dust transported from North African deserts. PM size distribution modelled with BSC-DREAM8b seems to be in greater agreement with observations than NMMB/BSC-Dust, since the estimated contribution of the larger particles for the total dust mass was higher.

Seasonal differences simulated by the models in terms of dust emissions, air mass circulations and PM concentrations are important for the analyses of observed episodes in Cape Verde. Possible dust-source areas that may affect the Cape Verde region were analysed and found to have distinct seasonal patterns. The most active source in terms of dust emission was the Bodélé region, mainly

between December and May. Other significant sources include the Algeria-Morocco region, West Sahara-Mauritania, the Libya desert, Algeria-Tunisia and Algeria-Mali. According to the backward trajectories analysis, the air masses responsible for the highest aerosol concentrations in Cape Verde describe a path over the central Saharan desert area in Algeria, Mali and Mauritania before reaching the Atlantic Ocean. The NMMB/BSC-Dust model has very good performance in describing these highest concentrations that occur during the winter. On the other hand, this model strongly underestimates the emissions in the Central and Western Sahara during summer.

This Chapter contributes to the characterisation of the processes and sources responsible for aerosol loading in the Cape Verde region. This was one of the goals of the CV-DUST Project, a joint initiative of Aveiro University (UA) and the Technological and Nuclear Institute (ITN), together with Cape Verde University (Uni-CV) and with support from the CVAO and the BSC-CNS. Moreover, this Chapter includes an evaluation exercise of two dust models widely used for operational forecasts that are used on the Sand and Dust Storms Warning Advisory and Assessment System (SDS-WAS) and for research, in a strategic site to study Saharan Atlantic transport. This work is thus useful to all the end users of these models, allowing a comparison between the models and identification of areas where further improvements are needed, such as in terms of model size distribution.

Chapter 3

Influence of the dust size distribution on concentrations and optical depths

3.1 Introduction

In Chapter 2, a comparison between two dust models is presented. Although the NMMB/BSC-Dust model results are in better agreement with observations (PM concentrations and AOD), further improvements are needed in terms of modelling the dust size distribution. Since the size distribution of mineral dust aerosols partially determines their deposition and interactions with clouds, radiation, ecosystems, and other components of the Earth system (Kok, 2011b), it is one of the key modelling factors in order to correctly incorporate dust-radiation and dust-cloud interactions into regional dust models (Perez et al., 2006b).

In this Chapter, we focus on the dust emissions' size distribution considered by the NMMB/BSC-Dust model. The dust size distribution prescribed at source level is particularly important for downwind concentrations and optical parameters, since most of the dust is emitted in sizes that, effectively, do not grow by condensation or coagulation. Once in the atmosphere, dust size distribution evolves, primarily, due to deposition processes (Mahowald et al., 2014). Smaller particles are allowed to be transported for longer distances, while larger particles are deposited closer to the sources.

In atmospheric models, the aerosol size distribution is usually described with bin or modal approaches. In bin, or sectional methods, separate bins for aerosol size ranges are simulated separately, allowing interaction with each other and the gas phase, as well as deposition and transport. For each bin, however, the size distribution within the bin stays constant, which means there is a constant relationship between mass in the bin and the number of particles (Mahowald et al., 2014). The atmospheric models that are applied in this Thesis use the bin method to incorporate the aerosol size distribution.

A number of studies (e.g. Alfaro and Gomes, 2001; Shao, 2001, 2004; Kok, 2011a) proposed distinct parametrizations to predict the dust aerosol size distribution at emission. In this Chapter, we aim to implement one of these parametrizations, derived from Kok's brittle fragmentation theory (Kok, 2011a), and to test the impact of this parametrization in model results.

This Chapter is organized as follows: Section 3.2 describes the NMMB/BSC-Dust model, the dust size distribution currently implemented in the model and the new developments. In Section 3.3, the results are presented and discussed, in terms of surface concentrations size distribution and aerosol column load, comparing model results with available observations. Finally, in Section 3.4 the main conclusions are summarized.

3.2 Methodology

3.2.1 The NMMB/BSC-Dust model

The NMMB/BSC-Dust model, already introduced in Section 2.2.2, is the dust module of the NMMB/BSC Chemical Transport Model (NMMB/BSC-CTM), which, in collaboration with NOAA, the National Centers for Environmental Prediction (NCEP) and the NASA Goddard Institute for Space Studies, is under development at the Barcelona Supercomputing Center (BSC). The main system is built on the meteorological driver NMMB (Nonhydrostatic Multiscale Meteorological Model on the B grid), which is an evolution of the WRF-NMM model and a unified model for a broad range of spatial and temporal scales. The developments made in the BSC include the implementation of the gas-phase chemistry (Jorba et al., 2012), and of the mineral dust (Perez et al., 2011) and sea salt (Spada et al., 2013) modules. The model is fully online coupled, meaning that feedback mechanisms between meteorology and atmospheric pollution processes are considered.

To estimate dust emissions from arid regions, the model calculates the vertical dust flux according to the empirical relationship of Marticorena and Bergametti (1995) and Marticorena et al. (1997). The emissions are then distributed over 8 dust size transport bins (diameters between 0.2 and 20 μm) with intervals taken from Tegen and Lacis (1996).

In this work, we did not change the computation of the dust mass emissions nor the number and range of the size transport bins considered. We focus on the distribution of the total emission flux per the model size bins. Originally, the vertical dust flux was size distributed according to the tri-modal size distribution in source regions of Zender et al. (2003), which is further described hereafter. The numerical code of the model has been adapted to include a new size distribution scheme, following Kok's brittle fragmentation theory (Kok, 2011a).

Two high resolution simulations were performed with the NMMB/BSC-Dust for North Africa, Middle East and Europe (at 0.25º x 0.25º) for the year 2011. The simulation domain is presented in Figure 3.1. Simulation "Z" considers the originally implemented size distribution at emission, while simulation "K" considers the new size distribution at emission, derived from Kok's brittle fragmentation theory. Table 3.1 presents some additional details of the simulations.

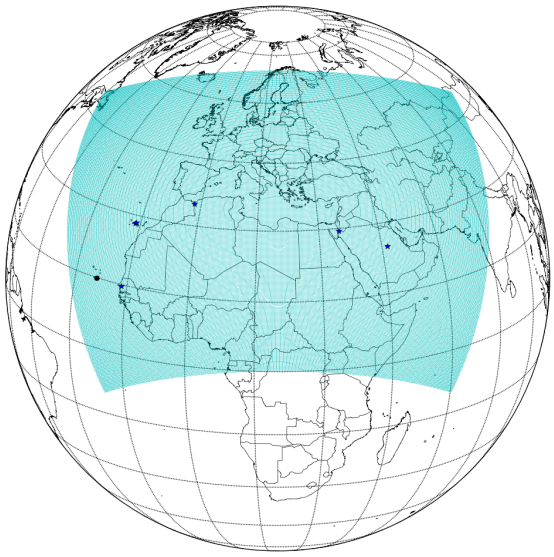

Figure 3.1: Model simulations domain (cyan) and identification of the observation sites: Praia, Cape Verde (14.92°N, 23.48°W; black dot) and the AERONET stations (blue stars) (from left to right) of Bambey-ISRA (14.71°N, 16.48°W), Izaña (28.31°N, 16.50°W), Santa Cruz de Tenerife (28.47°N, 16.25°W), Oujda (34.65°N, 1.90°W), Eilat (29.50°N, 34.92°E) and Solar Village (24.91°N, 46.40°E).

Table 3.1: Mass fraction of the dust emissions per model bin in simulations Z and K. Simulation Z considers the size distribution by Zender et al. (2003), while simulation K considers the size distribution derived from Kok's brittle fragmentation theory (Kok, 2011a).

bin	Size range (μm)	Simulation Z Mass fraction flux per bin Zender et al. (2003)	Simulation K Mass fraction flux per bin Kok (2011)
bin 1	0.2-0.36	0.4%	0.0%
bin 2	0.36-0.6	0.8%	0.1%
bin 3	0.6-1.2	2.7%	1.0%
bin 4	1.2-2.0	7.4%	2.9%
bin 5	2.0-3.6	23.3%	10.7%
bin 6	3.6-6.0	29.6%	22.0%
bin 7	6.0-12.0	27.8%	48.7%
bin 8	12.0-20.0	6.4%	14.5%

Tri-modal size distribution in source regions

Currently, in the original NMMB/BSC-Dust model, total vertical dust mass flux is distributed into the model transport bins by assuming a typical background source size distribution with three log-normal modes as proposed by Zender et al. (2003) following D'Almeida (1987) background dust mode (see Figure 3.2).

In the figure, the parameters of dust in the source regions are shown (mass median diameter D, geometric standard deviation sigma, and mass fraction M), for each dust mode.

The mass fraction of each source mode i that is carried in each transport bin j is the mass overlap $M_{i,j}$. Since the mass in the source modes is assumed to be lognormally distributed, the $M_{i,j}$ is given by

$$M_{i,j} = \frac{1}{2}\left[erf\left(\frac{ln(D_{max,j}/\tilde{D}_{v,j})}{\sqrt{2}\ \ ln\sigma_{g,i}}\right) - erf\left(\frac{ln(D_{min,j}/\tilde{D}_{v,j})}{\sqrt{2}\ \ ln\sigma_{g,i}}\right)\right] \tag{3.1}$$

where erf is the standard error function, $D_{min,j}$ and $D_{max,j}$ are the minimum and maximum diameters of bin j, and v, i and g, i are the mass median diameter and geometric standard deviation of the source modes. The total transported mass of the source modes is the sum of all $M_{i,j}$.

Although this methodology is known as the three background dust modes of D'Almeida (1987), the middle mode dominates dust emissions, accounting for 95.7% of the total flux. The total emission flux is represented in black in Figure 3.2.

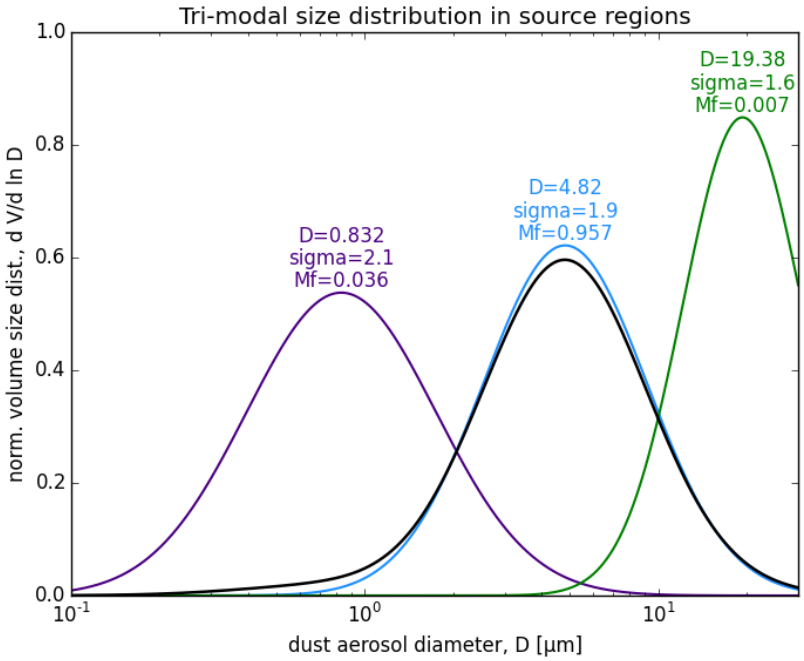

Figure 3.2: The dust aerosol tri-modal size distribution in source regions. Coloured lines indicate each of the three modes (defined by the mass median diameter "D" and the geometric standard deviation "sigma"). The black line represents the sum of the three modes, in the respective weight (given by the mass fraction "Mf").

The mass fraction flux per bin, calculated according to this methodology, is presented in Table 3.1. Most of the dust emission (80.7%) is allocated to the bins 5, 6 and 7, which correspond to particles with diameter from 2 to 12 µm. Particles up to 2 µm carry 11.3% of the total dust emission, while larger particles, with diameter larger than 12 µm, carry 6.4% of the emission. By using this methodology only 98.4% of the calculated mass dust flux is entrained into the atmosphere. The residual, non-transported mass is almost all in the coarse mode centred at 19 µm (see Figure 3.2) which, according to Schulz et al. (1998) may be considered not important for long-range transport.

Kok's size distribution of emitted dust aerosols according to brittle fragmentation theory

Kok (2011a) derived a new size distribution of emitted dust aerosols according to the brittle fragmentation theory, which is applicable when dust emission is predominantly due to the fragmentation of soil dust aggregates by impacting saltators. Major implications of this theory are: (a) emitted dust size distribution is independent from wind friction velocity; (b) the dependence of dust size distribution on soil properties is of secondary importance (Albani et al., 2014). According to Mahowald et al. (2014), the equation derived by Kok (equation 3.2) is in good agreement with

measurements. Moreover, its implementation into atmospheric models has improved agreement with measurements in several regional and global models (Albani et al., 2014; Johnson et al., 2012; Nabat et al., 2012; Zhang et al., 2013).

The dust aerosol size distribution in source regions, according to Kok (2011a), is expressed by

$$\frac{dV_d}{dlnD_d} = \frac{D_d}{c_V}\left[1 + erf\left(\frac{ln(D_d/Ds)}{\sqrt{2}ln\sigma_s}\right)\right] exp\left[-\left(\frac{D_d}{\lambda}\right)^3\right] \tag{3.2}$$

where V_d is the normalized volume of dust aerosols with size D_d, $c_V = 12.62\,\mu m$ is a normalization constant, and $\sigma_s \approx 3.0$ and $Ds \approx 3.4\,\mu m$ are the geometric standard deviation and median diameter by volume of the log-normal distribution of a typical arid soil size distribution in the $\leq$ 20 µm size range. The parameter λ denotes the propagation distance of side branches of cracks created in the dust aggregate by a fragmenting impact; Kok (2011a) obtained $\lambda = 12 \pm 1\mu m$ using least-square fitting to dust PSD measurements.

The dust aerosol size distribution in source regions, after Kok (2011a), is depicted graphically in Figure 3.3, together with the originally implemented distribution in the NMMB/BSC-Dust, using both linear (left subplot) and logarithmic (right subplot) scales in the y-axis.

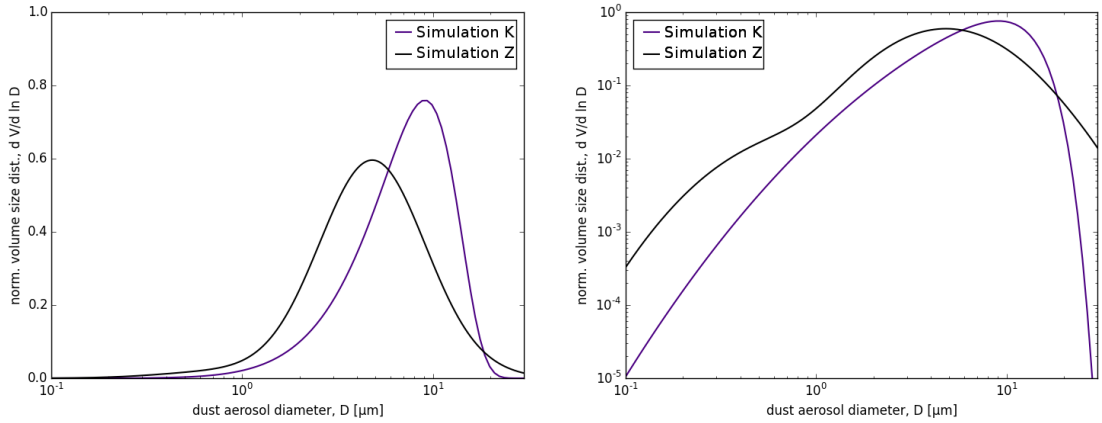

Figure 3.3: Dust size distribution schemes considered in simulations Z and K. In the left panel the schemes are plotted in a linear y-axis scale while in the right panel a y-axis logarithmic scale is used.

Equation 3.2 has been solved using the Riemann summation method, yielding to dust aerosol volume per bin. Then, volume was converted to mass by assuming a density of 2.5 g cm^{-3}, value which was already used in the previous Chapter (see the reasoning presented in Section 2.2.1). The mass fraction flux per bin calculated according to this methodology is presented in Table 3.1.

This methodology leads to lower emissions in the finer bins of the model (up to bin 6) and higher emissions in the coarser ones (bins 7 and 8), when compared to the results obtained with the tri-modal size distribution originally implemented into the model. The total calculated mass dust flux (100%) is now entrained into the atmosphere and further transported away. Particles up to 2 µm carry only 4.0% of the total dust emission. Bins 5, 6 and 7 carry together 81.4% (similar to the 80.7% previously found for the same three bins), however, 48.7% of the total dust emissions are now allocated to bin 7 only, which correspond to particles with diameter from 6 to 12 µm. Larger particles, with diameter above 12 µm, carry 14.5% of the emission.

To include this size distribution scheme in the numerical code of the model, a fortran routine in the preprocessing code of the model has been modified.

Surface concentration and size distribution measurements

Modelled values have been compared against the measurements obtained in Praia, Cape Verde in the framework of CV-DUST Project (Pio et al., 2014), already presented in Section 2.2.1 and widely used through Chapter 2, which include size distribution and concentration measurements at surface level, for 2011. Measurements were based on the optical particle counter method and were carried out using a GRIMM EDM164 Environmental Dust Monitor. The equipment allowed the continuous counting of particles in real time (5 minutes averages) with sizing from 0.25 up to 32 µm, using 31 size channels.

To complement the analysis, column-integrated aerosol optical properties, routinely observed within the AErosol RObotic NETwork (AERONET; http://aeronet.gsfc.nasa.gov Holben et al., 1998; Smirnov et al., 2000), were used. While in Chapter 2 we employed total AOD (direct Sun measurements) to compare with model results, in this Chapter we will use a different data product, called the aerosol spectral de-convolution algorithm (SDA), that utilizes spectral total AOD data to infer the component fine- and coarse-mode optical depths at 500 nm. This algorithm, described in O'Neill et al. (2003), yields fine (sub-micron) and coarse (super-micron) aerosol optical depths at a standard wavelength of 500 nm.

The SDA algorithm fundamentally depends on the assumption that the coarse mode Angstrom exponent and its derivative are close to zero. Its advantage lies in the fact that it produces useful indicators of aerosol size discrimination at the frequency of extinction measurements.

The theoretical underpinning of the SDA technique is that the aerosol population is assumed to be bimodal. This is not always true (Eck et al., 2010), but it is a hypothesis of surprisingly universal applicability (when its not true it clearly produces an optically equivalent bimodal representation of the real aerosol world).

For this study, we used level 2.0 SDA retrievals, namely the fine mode and coarse mode aerosol optical depths at 500 nm. We focus on AERONET sites located in North Africa, with a contiguous dataset record throughout the 1-year study period. Five sites, identified in Table 3.2, were selected.

Table 3.2: The selected AERONET sites.

Name	Country	LON	LAT	height (m)
Bambey-ISRA	Senegal	16.48°W	14.71°N	30
Izaña	Spain	16.50°W	28.31°N	2391
Santa Cruz de Tenerife	Spain	16.25°W	28.47°N	52
Oujda	Morocco	1.90°W	34.65°N	620
Eilat	Israel	34.92°E	29.50°N	15
Solar Village	Saudia Arabia	46.40°E	24.91°N	764

3.3 Results and discussion

The results of the model simulations and comparison with available observations are presented hereafter. It must be highlighted that the NMMB/BSC-Dust model takes into account only aeolian mineral particles emitted from the deserts, whereas measurement data sets may reflect also non-dust aerosols like sea-salt or biomass burning particles, secondary pollutants and local sources, as well as long-range transport of anthropogenic pollution.

3.3.1 PM surface concentrations at Praia (Cape Verde)

As we've seen in Chapter 2, winter months are associated with the highest observed surface concentrations of particulate matter in Cape Verde. Moreover, these maxima are associated with desert dust westerly transport at near-surface levels.

Figure 3.4 shows the monthly mean size distribution of aerosol concentrations, based on observations. The figure reveals the existence of a sub micro mode and multiple aerosol modes in coarse particles. The main mode with maximum at 3-4 μm is more evident during months with strong dust events (January, February and December). At lower intermediate aerosol loadings, a mode

at 5-6 µm becomes predominant. These multiple aerosol modes in coarse particles may reflect the multiple sources and formation/transport processes contributing to the coarse aerosol loading in Praia atmosphere, at ground level (Pio et al., 2014).

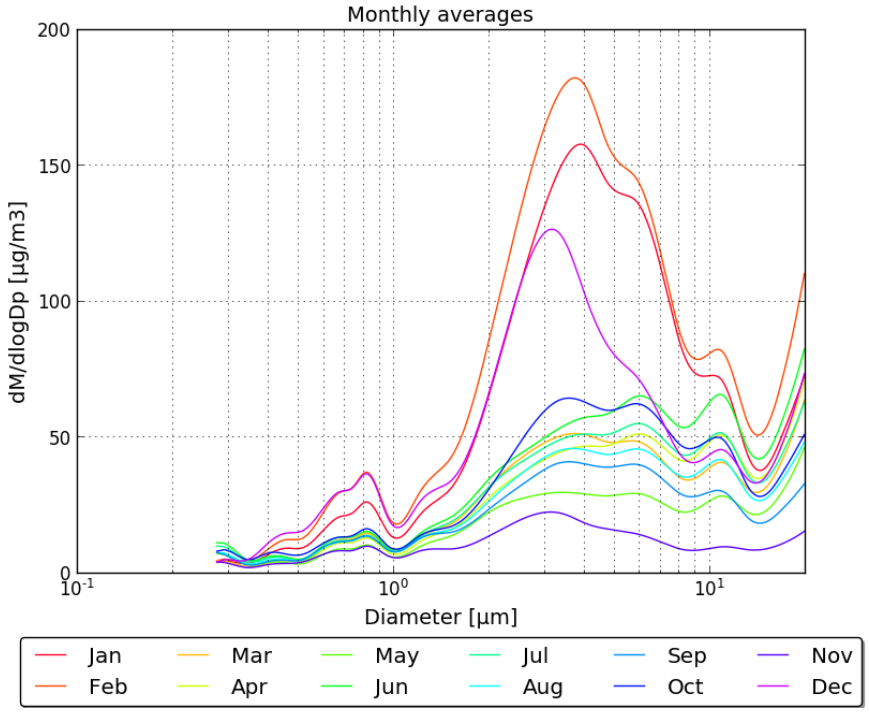

Figure 3.4: Monthly averages of aerosol size distributions observed at Praia, Santiago Island (latitude: 14.92 N, longitude: 23.48 W).

We selected the three months which are highlighted in the analysis of Figure 3.4 (December, January and February), plotting in Figure 3.5 the observed aerosol size distribution according to transport path during these three months (the computation of the characteristic transport patterns for this period was described and presented in the previous Chapter, in Section 2.4). Figure 3.6 shows the modelled size distribution for each characteristic transport pattern, during December, January and February, according to the results of simulations Z (left) and K (right).

Long-range transport patterns influence the observed particle size distribution. Clusters 6, 3, 1 and 5 (presented by order of magnitude) exhibit mass dominance of particles with equivalent aerodynamic diameter between 2.9 and 4.4 µm. A second mode, between 5.2 and 6.9 µm is visible. In measurements grouped in cluster 2, these two modes have the same importance. In other words, cluster 2 presents higher contribution of larger particles for the total mass. This can be related with the fact that dust sources are closer from the receptor / less deposition during transport.

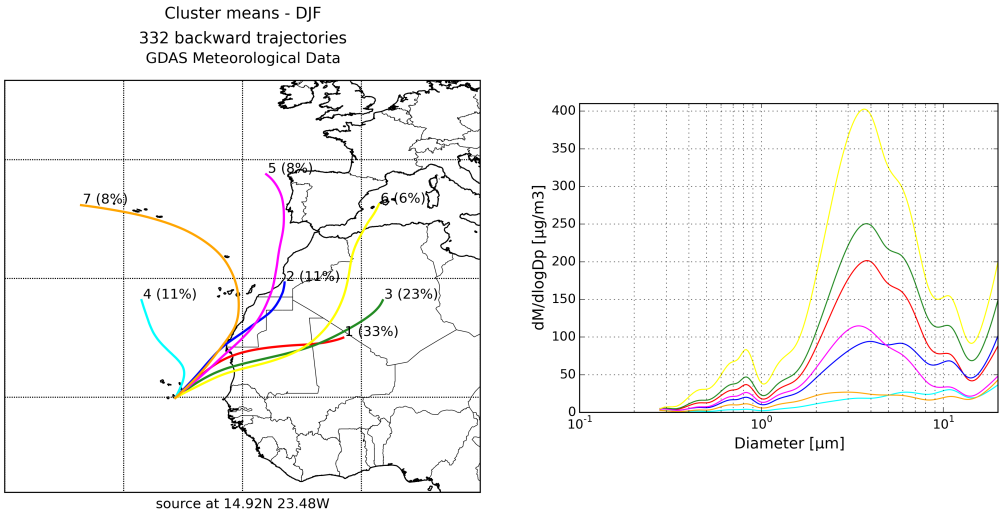

Figure 3.5: Characteristic transport patterns (left) and associated aerosol size distributions (right) observed at Praia, Santiago Island (latitude: 14.92 N, longitude: 23.48 W), during January, February and December 2011.

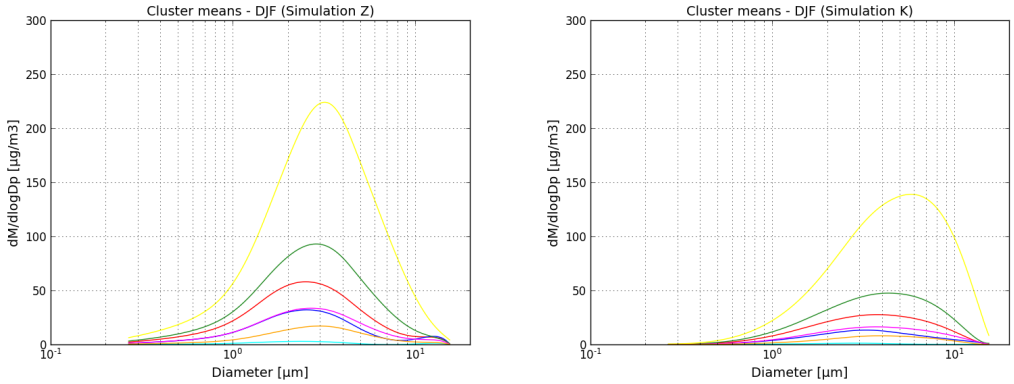

Figure 3.6: PM modelled size distribution during January, February and December 2011 in Praia, Cape Verde, according to the characteristic transport paths. Left plot shows the results of Simulation Z and right plot the results from Simulation K.

Clusters 4 and 7 are distinct from all the others. These clusters groups pure marine air masses, and observations within this group exhibit mass dominance of particles with equivalent aerodynamic diameter higher than 10 µm. Very coarse particles are probably of local origin in the island.

Model results exhibit mass dominance of particles with equivalent aerodynamic diameter between 2.0 and 3.6 µm in the simulation with the originally implemented size distribution at emission (simulation Z), and between 3.6 and 6.0 µm in the simulation K (see Figure 3.6). However, it must be highlighted that the mass concentrations are in general lower with the Kok's scheme. This is probably related with the increase in the deposition phenomena along transport, which remove the coarser fractions of the dust from the load-column, since with the new size distribution scheme the mass fraction flux of the coarser bins is higher.

Results with the new size distribution scheme are also analysed for the complete annual cycle. Figure 3.7 presents the time series of PM10 and PM2.5 concentrations with the two model setups. Table 3.3 shows a summary of the mean and standard deviation of observations and simulations.

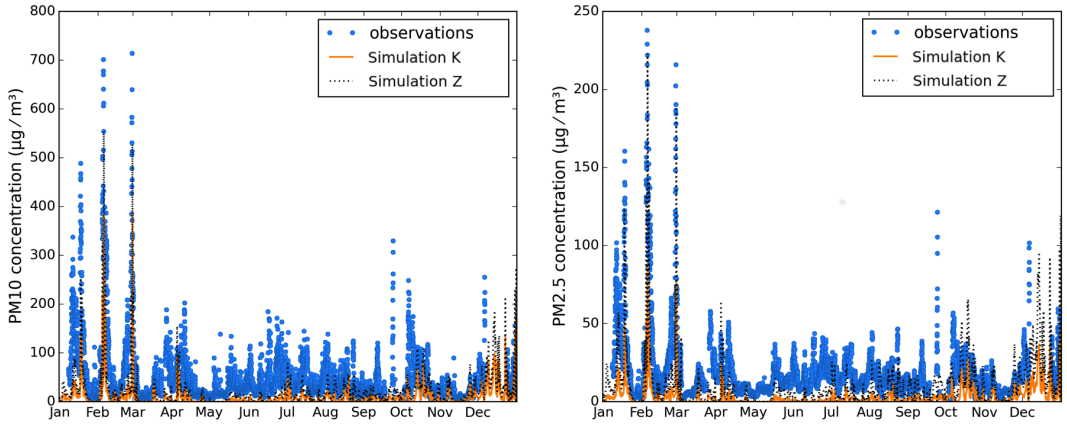

Figure 3.7: Measured and modelled PM10 (left) and PM2.5 (right) concentrations in Praia, Cape Verde.

Table 3.3: PM10 and PM2.5 mean concentration and standard deviation of observations and simulations Z and K.

	PM10 ($\mu g\, m^{-3}$)	PM2.5 ($\mu g\, m^{-3}$)
observations	49.7 ± 62.3	19.5 ± 21.0
simulation Z	20.7 ± 36.5	10.0 ± 16.3
simulation K	10.2 ± 23.1	3.2 ± 6.3

In agreement with what was presented in Chapter 2, Figure 3.8 shows the seasonal analysis of observed and modelled surface PM size distributions for Praia, Cape Verde.

PM concentrations simulated with simulation K (modified size distribution scheme according to Kok (2011)), are much lower than the observations. Praia's PM10 mean concentrations with simulation K are nearly half of the concentrations simulated by simulation Z. When we look to PM2.5 results, the drop in mean concentrations from simulations Z to K is even stronger (mean values drop from 10.0 to 3.2 $\mu g\, m^{-3}$).

In the discussion of these results, it is important to notice that the model was not tuned from simulation Z to simulation K. The goal of tuning is to minimise some difference between the model output and selected observations and theories. In this case, since we want to evaluate the effect in the outputs of changing the size distribution scheme, we decided to keep all the other inputs and parameters, and the tuning as well. We understand the surface concentrations obtained with simulation K are unrealistic when compared to the observations.

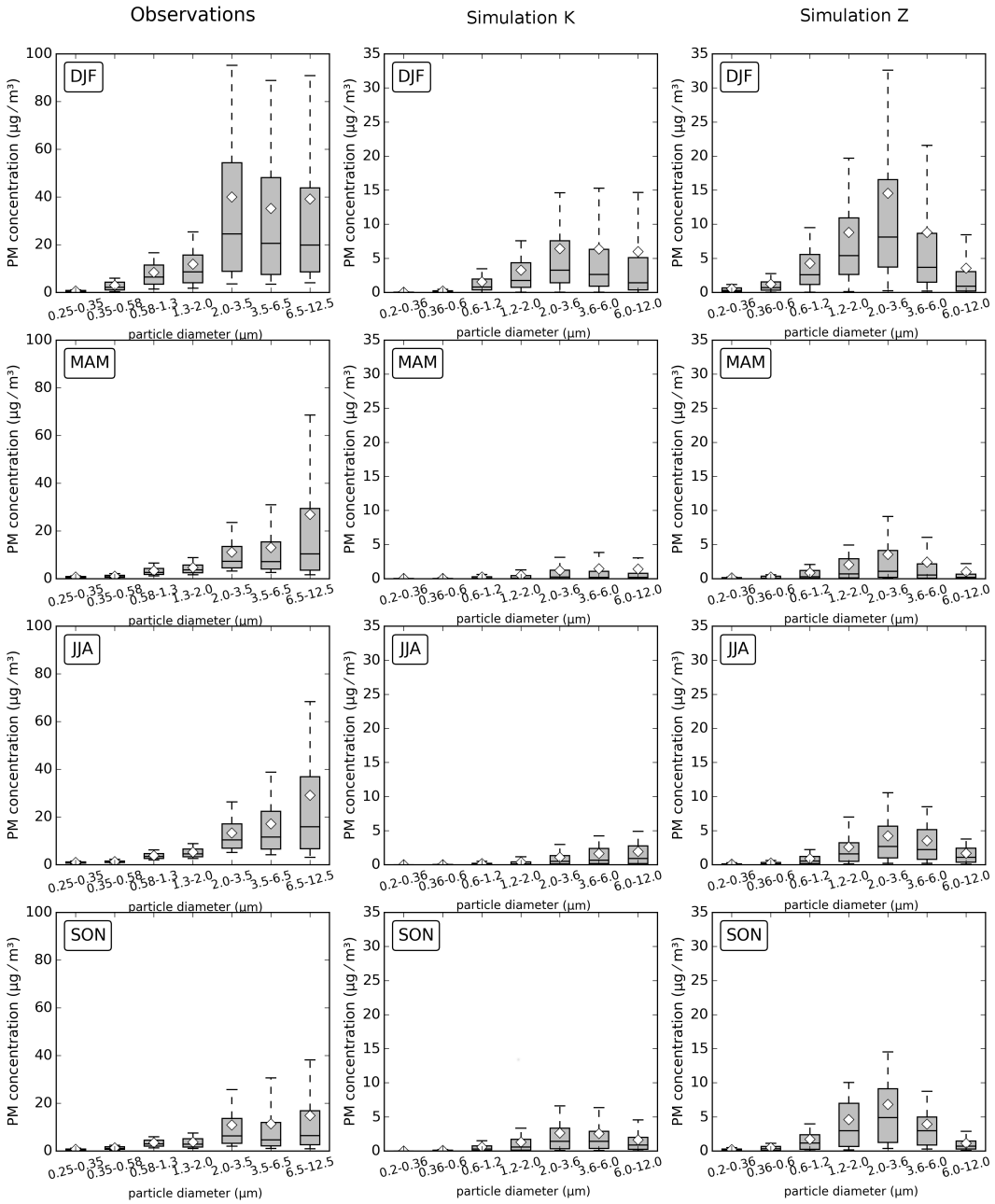

Figure 3.8: Seasonal analysis of the observed (lef panels) and modelled (centre and right panels) size distribution surface PM concentrations, for Praia, Cape Verde, 2011. DJF corresponds to December, January and February, MAM to March, April and May, JJA to June, July and August and SON to September, October and November. The bottom and top of the box represent the first and third quartiles and the band inside the box represents the median. The ends of the whiskers represent the 10th and the 90th percentiles. White diamonds represent the mean value. Outliers are not shown.

In the model, the concentrations in the atmosphere are constrained by emissions and deposition. To obtain better results with simulation K in future studies, we recommend to address deposition phenomena together with the size distribution scheme. In numerical models, such phenomena are numerically represented by size-dependent parametrizations of dry and wet deposition. Albani

et al. (2014), for example, tested changes in dust emission size distributions, together with changes in the wet deposition scheme. The use of deposition observations to validate model outputs is crucial. Moreover, model tuning could be performed after the choice of the best setups / parametrizations, in order to achieve the best result possible.

3.3.2 Aerosol optical depths

In addition to surface concentrations, model results were compared with AOD observations from the AERONET sites distributed over North and West Africa and Middle East. Results are shown for Bambey-ISRA (Figure 3.9), Izaña (Figure 3.10), Santa Cruz de Tenerife (Figure 3.11), Oujda (Figure 3.12), Eilat (Figure 3.13) and Solar Village (Figure 3.14). Comparison between simulations and AERONET observations over North and West Africa points out that, with the original scheme (Simulation Z), model seems to be not well balanced between fine and coarse modes. In stations like Izaña (Figure 3.10) and Santa Cruz de Tenerife, the fine mode aerosol optical depth is overestimated by the model. AOD fine fraction is in better agreement with observations using Kok's size distribution scheme. Nevertheless, with Kok's scheme, total AOD is generally underestimated.

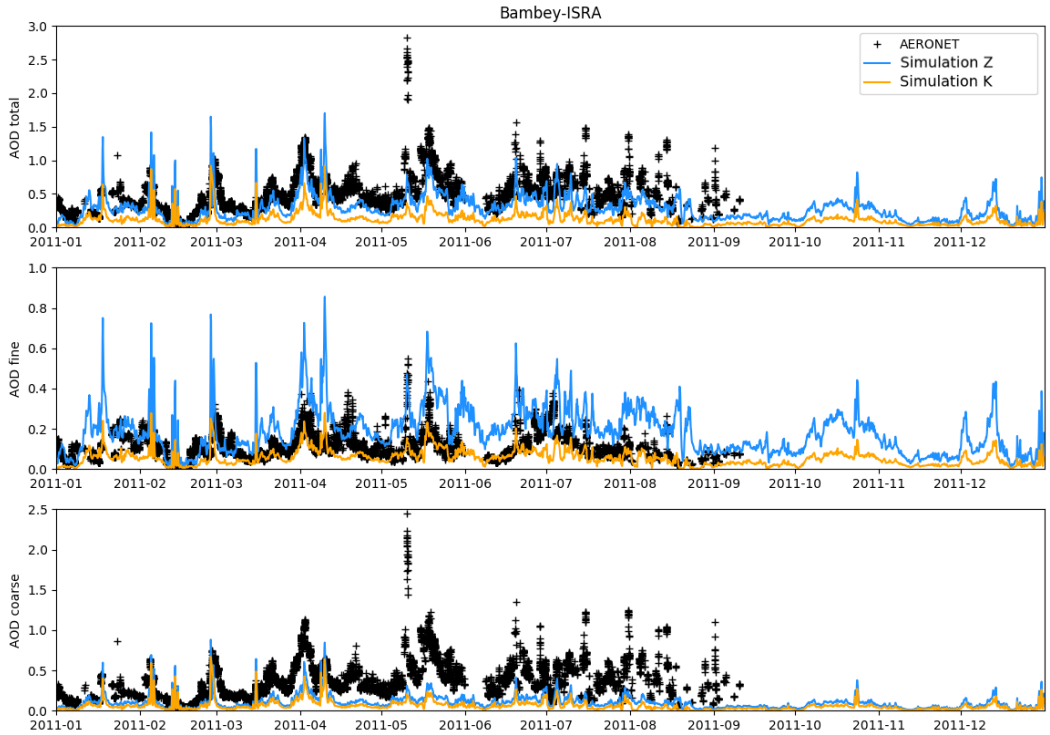

Figure 3.9: Measured and modelled Aerosol Optical Depth (AOD at 550 nm) in Bambey-ISRA, Senegal. The top panel shows total AOD, centre and bottom panels show fine and coarse AOD fractions, respectively.

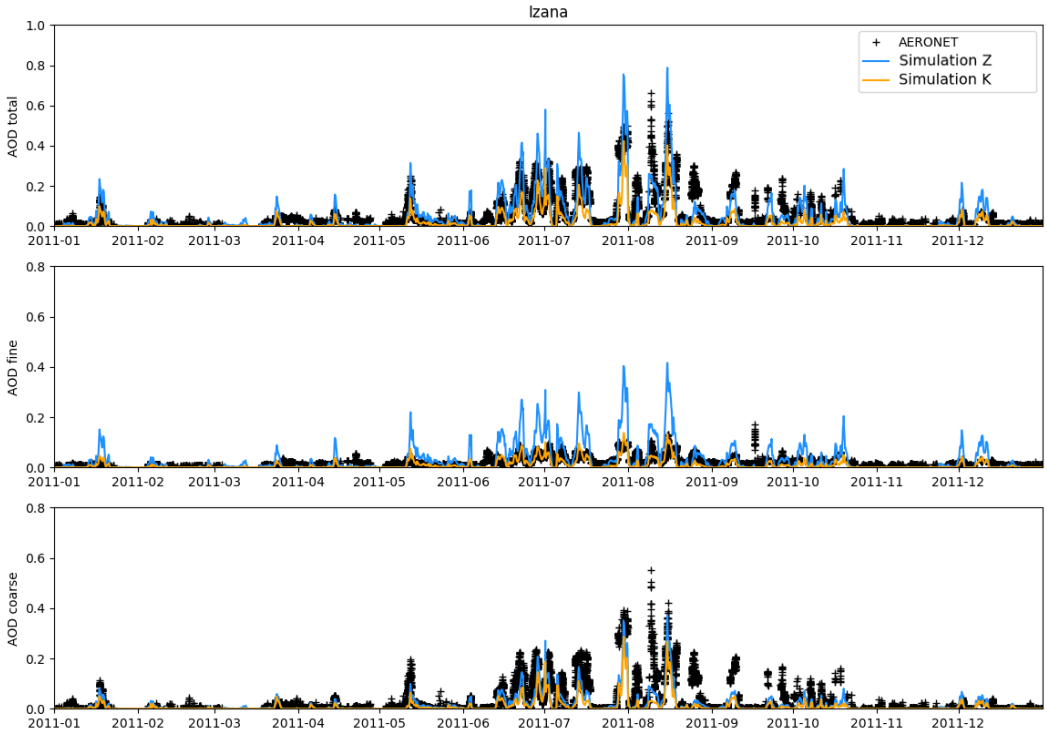

Figure 3.10: Measured and modelled Aerosol Optical Depth (AOD at 550 nm) in Izaña, Spain. The top panel shows total AOD, centre and bottom panels show fine and coarse AOD fractions, respectively.

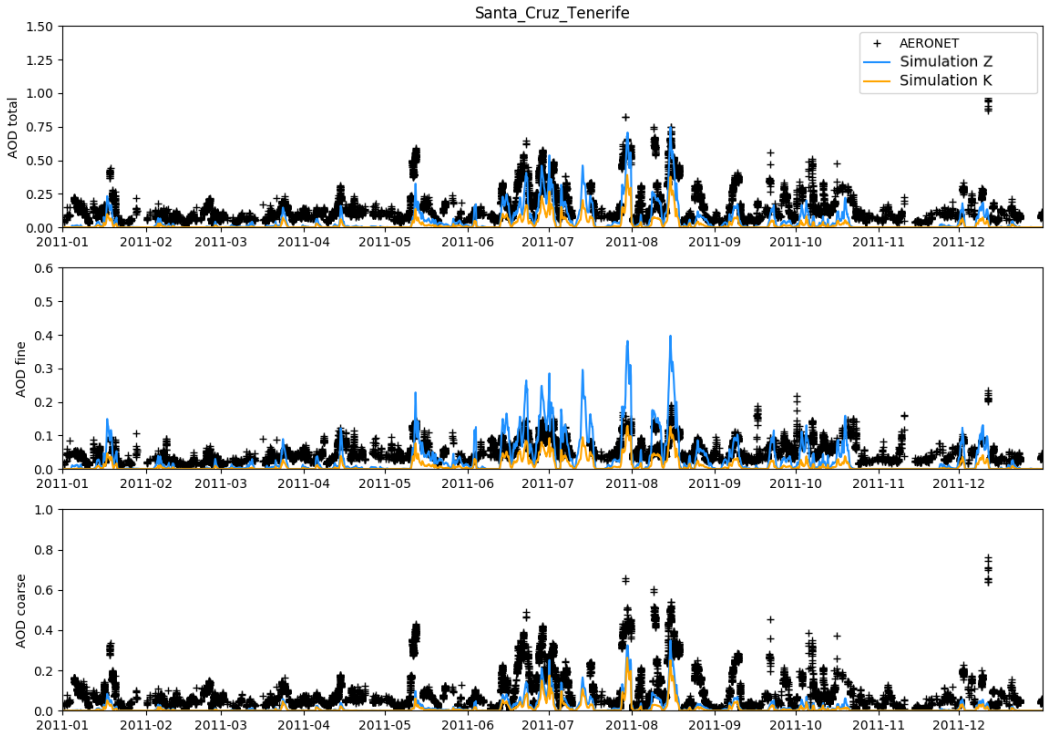

Figure 3.11: Measured and modelled Aerosol Optical Depth (AOD at 550 nm) in Santa Cruz de Tenerife, Spain. The top panel shows total AOD, centre and bottom panels show fine and coarse AOD fractions, respectively.

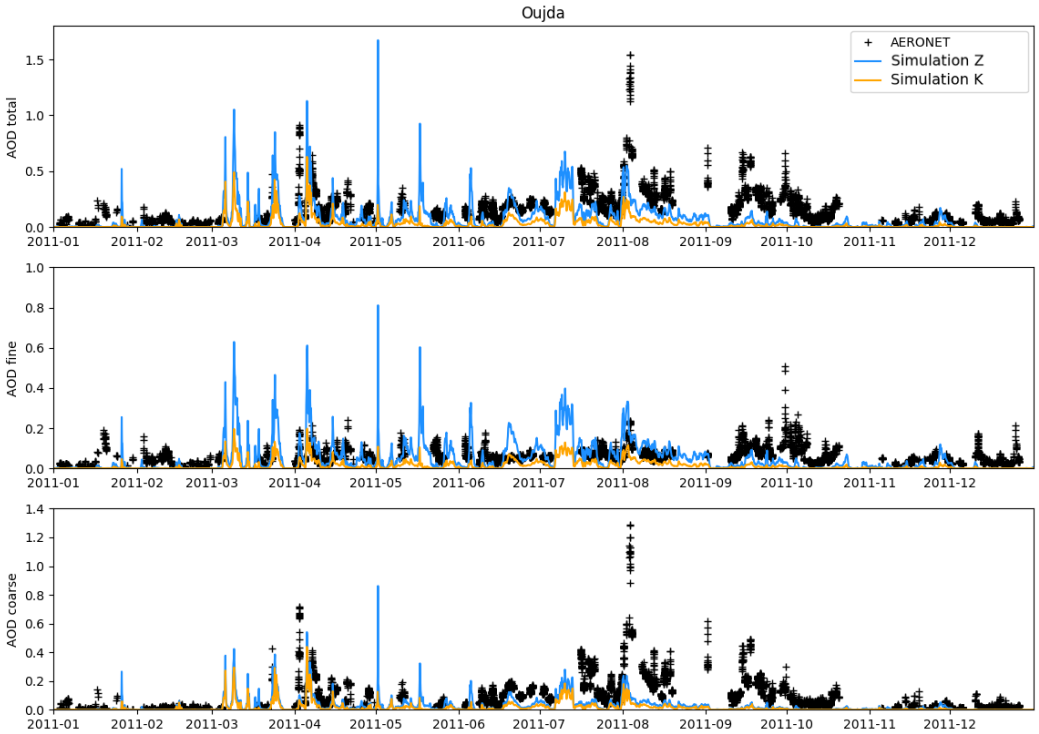

Figure 3.12: Measured and modelled Aerosol Optical Depth (AOD at 550 nm) in Oujda, Morocco. The top panel shows total AOD, centre and bottom panels show fine and coarse AOD fractions, respectively.

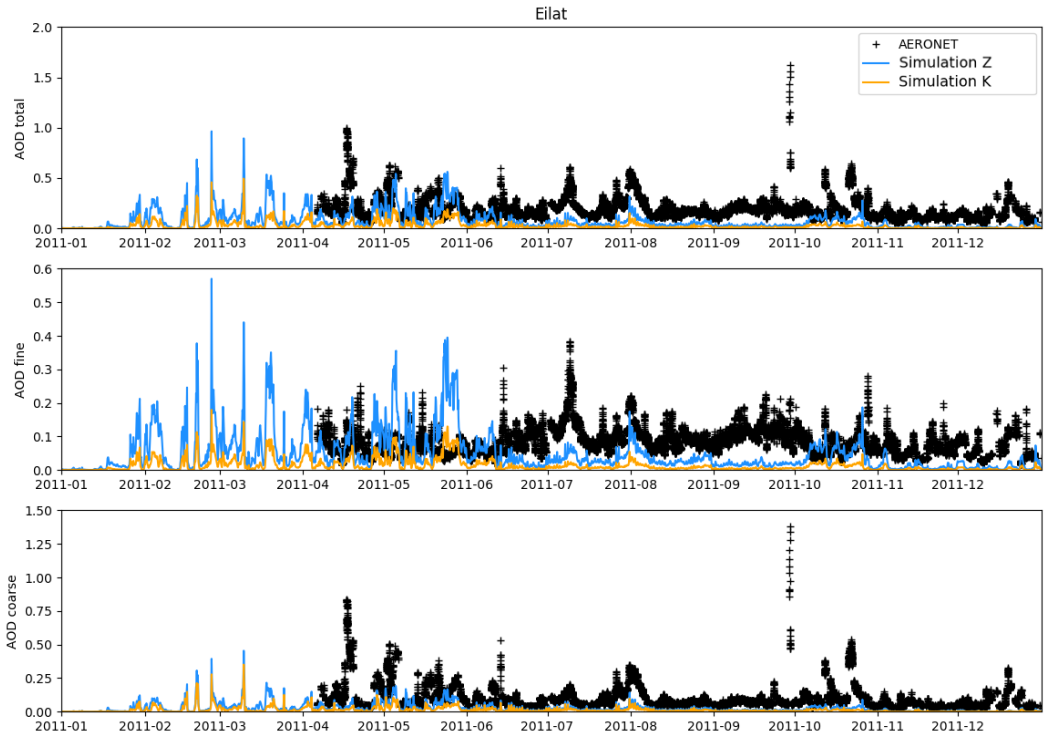

Figure 3.13: Measured and modelled Aerosol Optical Depth (AOD at 550 nm) in Eilat, Israel. The top panel shows total AOD, centre and bottom panels show fine and coarse AOD fractions, respectively.

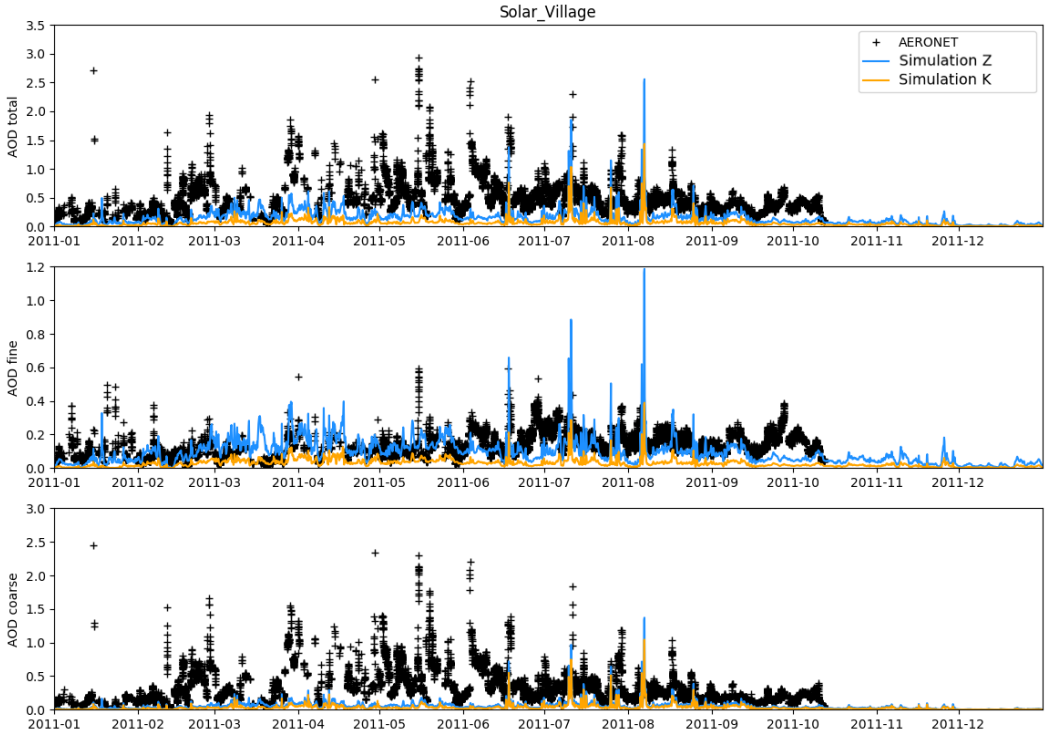

Figure 3.14: Measured and modelled Aerosol Optical Depth (AOD at 550 nm) in Solar Village, Saudi Arabia. The top panel shows total AOD, centre and bottom panels show fine and coarse AOD fractions, respectively.

Izaña is the site where the improvements are more notorious. In this site, the originally implemented scheme tends to overestimate the fine fraction, particularly between May and August. Results obtained with the new scheme seem to be in better agreement with observations. The Willmott's index of agreement refined version (dr) was computed (Willmott et al., 2012) and confirms the improvement for the fine fraction of the aerosol optical depth – dr increases from 0.53 to 0.81 (see Table 3.4). However, when the total AOD is considered (see Table 3.5), dr decreases from 0.88 to 0.78 and bias from 0.00 to 0.05. A similar behavior is found in Santa Cruz de Tenerife. In fact, these two sites are located very close to each other, in the Canary Islands (Spain) but Izaña is located at 2391 m, while Santa Cruz de Tenerife at 52 m.

In Bambey-ISRA, in Senegal, the modelled AOD fine fraction is also in better agreement with observations when the new size emission scheme is considered – dr increases from 0.49 to 0.60. However, total AOD is underestimated with this scheme, since the overestimation of the fine fraction registered with the originally implemented scheme was somehow balancing the underestimation of the coarser fraction. A similar behaviour is found in Eilat, Israel, mainly between April and middle June.

Table 3.4: Statistical parameters computed for AOD fine fraction, for simulations Z and K. "dr" stands for the Willmott's index of agreement refined version, "r" is the correlation coefficient, "RMS" the root mean square error, and "bias" the mean difference between measured and modelled values.

	dr		r		RMS		bias	
AERONET site	Z	K	Z	K	Z	K	Z	K
Bambey-ISRA	0.49	0.60	0.47	0.48	0.14	0.07	−0.10	0.05
Izaña	0.53	0.81	0.75	0.75	0.07	0.02	−0.03	0.01
Santa Cruz de Tenerife	0.71	0.57	0.70	0.70	0.05	0.05	0.01	0.04
Oujda	0.51	0.44	0.23	0.23	0.06	0.07	0.03	0.05
Eilat	0.33	0.37	−0.06	−0.06	0.08	0.08	0.04	0.07
Solar Village	0.48	0.42	0.15	0.18	0.09	0.13	0.04	0.11

Table 3.5: Statistical parameters computed for total AOD, for simulations Z and K. "dr" stands for the Willmott's index of agreement refined version, "r" is the correlation coefficient, "RMS" the root mean square error, and "bias" the mean difference between measured and modelled values.

	dr		r		RMS		bias	
AERONET site	Z	K	Z	K	Z	K	Z	K
Bambey-ISRA	0.72	0.49	0.67	0.62	0.27	0.43	0.00	0.05
Izaña	0.88	0.78	0.82	0.79	0.07	0.08	0.17	0.36
Santa Cruz de Tenerife	0.77	0.56	0.80	0.78	0.12	0.17	0.13	0.17
Oujda	0.61	0.47	0.66	0.70	0.17	0.20	0.11	0.15
Eilat	0.46	0.40	0.32	0.39	0.18	0.21	0.10	0.13
Solar Village	0.47	0.43	0.37	0.35	0.42	0.50	0.32	0.41

In Oujda, located in North-East Morocco, the implementation of the new size distribution scheme seems to lead to an improvement of model results, as huge peaks of AOD tend to disappear. However, the measurement dataset has large missing data periods, which make it difficult to conclude about model agreement with observations.

In Solar Village, model results from simulation Z are in better agreement with observations. Regarding this site, located in the middle of the Arabian Peninsula and far from the Persian Gulf or other industrialized areas, previous studies have reported that the model underestimates some important dust storms in spring while it overestimates some episodes in summer leading to a weak overall correlation (Perez et al., 2011). By using the new size distribution scheme, model underestimation during spring events is even more evident.

3.4 Summary and conclusions

A new methodology to distribute the total vertical dust flux by each model size bin was derived from Kok's brittle fragmentation theory (Kok, 2011a) and implemented in the NMMB/BSC-Dust

model, without changing the computation of the total dust emission flux nor the number and range of the size transport bins considered. Two high resolution simulations were performed for the year 2011, the first with the originally implemented size distribution scheme and the second with the newly implemented one. Kok's size distribution function leads to a decrease in the fine model bins emissions and an increase in the coarser ones, which has impact in the modelled downwind concentrations and optical parameters.

Model results were compared with surface observations in Praia, Cape Verde. Model outputs obtained with the new emission scheme (simulation K) exhibit mass dominance of particles with equivalent aerodynamic diameter between 3.6 and 6.0 µm, which is agreement with observations. However, PM10 and PM2.5 concentrations are strongly underestimated in simulation K. The fact that mass concentrations are in general lower with the new scheme is probably related with the increase in the deposition phenomena along transport, which remove the coarser fractions of the dust from the load-column, since with the new size distribution scheme the mass fraction flux of the coarser bins is higher.

It is important to note the model was not tuned from simulation Z to simulation K. The goal of tuning is to minimise some difference between the model output and selected observations and theories. In this case, since we want to evaluate the effect in the outputs of changing the size distribution scheme, we decided to keep all the other inputs and parameters, and the tuning as well. By changing the size distribution scheme, modelling results, in particular surface concentrations, do not improve in comparison with the original size distribution currently implemented in the model.

To complement surface observations, model results were compared with AOD observations from AERONET sites distributed over the domain. In some sites, like Izaña or Santa Cruz de Tenerife, an improvement in the simulation with the new size distribution scheme is registered. In other sites, like Bambey-ISRA and Eilat, modelled AOD fine fraction is also in better agreement with observations when the new size emission scheme is considered, however total AOD is now underestimated, since the overestimation of the fine fraction registered with the originally implemented scheme was balancing the underestimation of the coarser fraction. In general, model performance over Arabian Peninsula is worst than over North and West Africa.

The results presented in this Chapter should be complemented with a more exhaustive evaluation of the impact of Kok's size distribution on the dust deposition rates over the domain.

After these simulations were done, Kok et al. (2014) proposed a new parametrization for mineral dust emissions (total vertical dust flux). This parametrization will be assessed in Chapter 5 using, however, a different atmospheric model.

Part Three. Mineral dust over Portugal

Chapter 4

Characterization of the particulate matter levels in Portugal

This chapter is based on: Gama, C., Monteiro, A., Pio, C., Miranda, A.I., Baldasano, J.M., Tchepel, O. (2018) Temporal patterns and trends of particulate matter over Portugal: a long-term analysis of background concentrations. Air Quality, Atmosphere and Health. doi:10.1007/s11869-018-0546-8

4.1 Introduction

Atmospheric aerosols affect air quality and climate; their impacts have been evidenced in various research works across urban, regional, and global scales (Calvo et al., 2013; Fuzzi et al., 2015). Furthermore, exposure to atmospheric aerosols may affect human health (WHO-OCDE, 2015). In the past decades, many studies highlighted the role of ambient airborne particulate matter (PM) as an important environmental pollutant for cardiopulmonary diseases and lung cancer (e.g. Valavanidis et al., 2008; López-Villarrubia et al., 2016).

In addition to primary emission sources, PM concentrations can be significantly influenced by secondary aerosol formation in the atmosphere, which is not only dependent on the precursor's emissions but also on meteorological conditions and geographical location. Furthermore, additionally to local pollution sources, air quality is affected by the long-range transport of air masses that contribute to regional background pollution levels and to air pollution episodes. In this context,

North African dust outbreaks may influence air quality in Europe, especially on the Mediterranean Basin (Pey et al., 2013).

Due to the geographic location of Portugal and the dominant wind regime (Valverde et al., 2015), influenced by the presence of the semi-permanent Azores high-pressure and the Icelandic low-pressure systems over the North Atlantic Ocean, it is expected that, in most of the year, transport of maritime air promotes the decrease of anthropogenic and mineral PM concentrations (Almeida et al., 2013b). Nevertheless, Portugal has been facing air quality problems, being PM10, together with O_3, the main critical pollutants. Furthermore, results from Monteiro et al. (2017b) evidence that human health protection will be even more critical in the future, particularly for PM; in 2050, due to the warmer and dryer conditions and the expected increase of background concentrations, degradation of air quality is expected to occur.

In the last years, several studies focused on the characterization of PM levels and composition over specific cities or regions in Portugal, based on intensive experimental campaigns. PM composition and sources have been documented for Lisbon (Almeida et al., 2006, 2009) and Porto (Custódio et al., 2016; Diapouli et al., 2017). Another study worth mention within the scope of this work is the paper by Cruz et al. (2016), in which PM levels in Portugal (mainland and islands) were analysed throughout a 3-year period.

The aim of this Chapter is to provide a characterization of the aerosol background levels in Portugal, based on the long-term observations of PM10 and PM2.5 concentrations. This is the first attempt to characterize the aerosol over Portugal with such a long record (10 years) of observations and a large number of monitoring stations. The results of this study bring new insights on the temporal patterns and trends of PM levels over Portugal and, also, on the distribution between fine and coarse particulate matter.

4.2 Methodology

Surface data from the Portuguese air quality monitoring network (see http://qualar.apambiente.pt/) is used in this section to characterize PM levels in Portugal. We focus on PM10 and PM2.5 concentrations collected over the last 10 years, more precisely, observations recorded from January 2007 to December 2016. The aerosol coarse fraction, PMc (the size fraction between 2.5 and 10 µm), was estimated through the subtraction of PM2.5 from collocated PM10.

Air quality data is analysed in terms of temporal patterns, long-term trends and legal limits compliance. Temporal patterns (which include daily, weekly and monthly cycles) and long-term trends of concentrations were performed using the OpenAir package for R (Carslaw and Ropkins, 2012; Ropkins and Carslaw, 2012).

4.2.1 Data

In Portugal, the air quality stations from the national air quality monitoring network are classified by the type of influence (traffic, industrial or background) and the area characteristics (urban, suburban or rural). Within the scope and aim of the present study, we consider the background influenced sites, only. Sites from Azores and Madeira islands are not included in this characterization.

Data quality objectives for air quality assessment are defined in the EU Directive 2008/50/EC (EU, 2008) as a percentage of hourly data availability along the year. The minimum percentage of data capture for PM10 and PM2.5 is 90%. Despite the minimum 90% of data quality objectives, in some cases, measurements from stations with a minimum annual data capture of 75% are used to achieve data continuation over time. Between 2007 and 2016, we could gather data for 8 rural, 4 suburban and 8 urban sites, distributed along mainland Portugal. Details on the location and classification of the stations used can be found in Table 4.1, together with the information on data completeness relative to the period 2007-2016. Figure 4.1 depicts the 10-year mean concentrations observed in each of the monitoring stations.

Among the selected stations, 13 measure PM10 only and 7 (4 rural and 3 urban) measure both PM10 and PM2.5 concentrations. For the study period, FUN is the station with higher percentage of data, both for PM10 (97.2%) and PM2.5 (94.0%). However, it must be noted that the percentages presented in Table 4.1 were computed considering as general temporal coverage the 10-year period, without taking into account the stations operational starting dates. As an example, the ALV station, which measures PM10 concentrations since 01/01/2009, has in fact a much higher data collection efficiency (97.4%) when its 8-year period of operation its considered.

All the selected monitoring stations are automatic and use the beta attenuation method to measure PM10 and PM2.5 concentrations.

Table 4.1: List of QUALAR background stations with data completeness > = 75% during the period 2007-2016. Coordinates and surrounding environment type classification (urb: urban; sub: suburban; rur: rural) are included.

Code	Name	LON	LAT	height (m)	type	PM10	PM2.5
ALV	Alverca	-9.040	38.896	22	urb	78.0%	-
ARC	Arcos	-8.894	38.529	2	urb	79.1%	-
CHA	Chamusca	-8.468	39.353	143	rur	95.9%	92.2%
CUS	Custóias Matosinhos	-8.645	41.201	100	sub	82.6%	-
ERM	Ermesinde Valongo	-8.551	41.217	140	urb	83.6%	-
ERV	Ervedeira	-8.893	39.922	60	rur	93.4%	92.9%
FPO	Fernando Pó	-8.691	38.636	57	rur	87.3%	84.3%
FRN	Fornelo do Monte	-8.100	40.640	741	rur	95.9%	-
FRO	Frossos - Braga	-8.454	41.566	51	sub	87.7%	-
FUN	Fundão	-7.300	40.232	473	rur	97.2%	94.0%
IGE	Inst. Geof. Coimbra	-8.412	40.206	145	urb	93.8%	-
ILH	Ílhavo	-8.672	40.588	32	sub	92.7%	-
LAR	Laranjeiro	-9.159	38.663	63	urb	94.2%	78.1%
LOU	Loures-Centro	-9.166	38.828	10	urb	86.1%	-
MEM	Mem Martins	-9.348	38.784	173	urb	87.3%	84.5%
MOV	Montemor-o-Velho	-8.677	40.183	96	rur	87.9%	-
MVE	Monte Velho	-8.799	38.076	53	rur	94.4%	-
OLI	Olivais	-9.109	38.768	32	urb	90.6%	87.7%
TER	Terena	-7.398	38.616	187	rur	82.8%	-
VCO	Mindelo V. Conde	-8.736	41.345	25	sub	82.9%	-

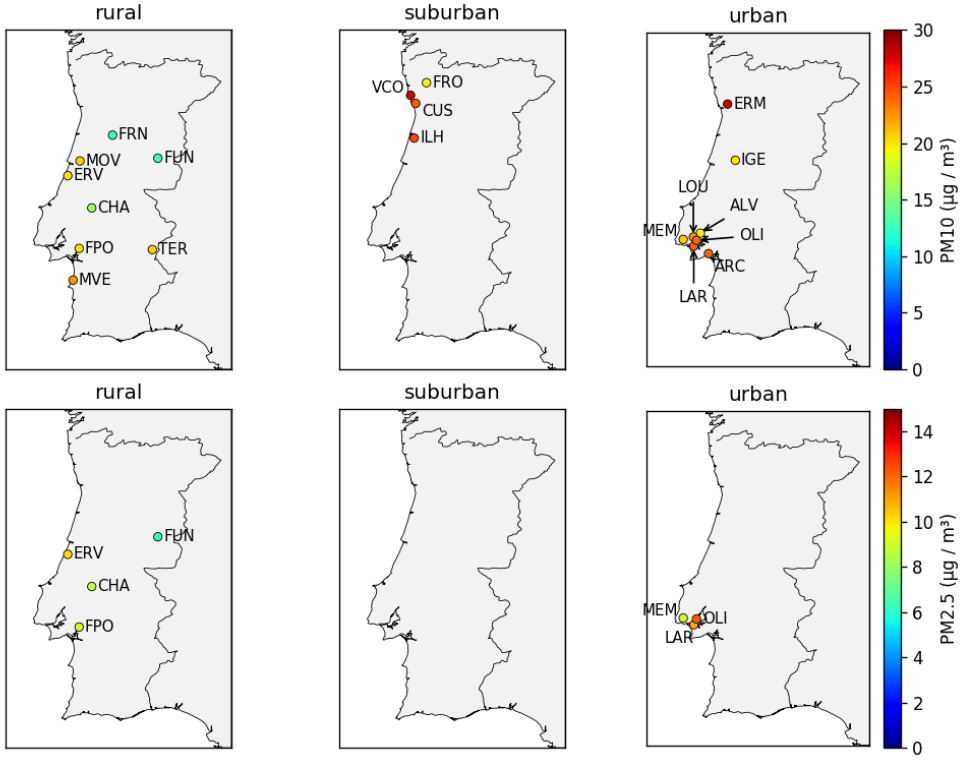

Figure 4.1: Spatial variation of the PM10 and PM2.5 mean concentrations observed at background stations between 2007 and 2016, according to the monitoring station environmental classification.

4.2.2 Methods

By simply plotting data in different ways, a visual analysis can often give valuable insights. As such, a comparison of PM concentrations between different locations or monitoring station types can reveal for example, information concerning the likely sources.

Hourly measurements from the selected monitoring stations were processed to prepare datasets with different time scales. Moreover, in this analysis, data were grouped according to station type. In the study of PM temporal cycles or patterns, four different plots are produced: (i) day of the week variation, (ii) mean hour of day variation, (iii) a combined hour of day – day of the week plot and (iv) a monthly plot. In these plots, relative to PM10, PM2.5 and PMc concentrations, the mean and the 95% confidence interval in the mean are depicted, relative to the 10 years data, aggregated by the time scale and the stations classification. The daily cycle of PM concentrations (mean hour of the day variation) is also plotted, split by season.

PM10, PM2.5 and PMc long-term temporal trends have been calculated with the Openair's smoothTrend function, a non-parametric method to calculate time series trends. This function generates a plot of monthly averaged concentrations, fits a smooth line to the data and shows the 95% confidence interval of the fit. The smooth line is determined using the generalized additive modelling approach (see Carslaw et al. (2007) for background information on the use of this approach in the air quality field). The amount of smoothness in the trend is optimised automatically. In this analysis, data has been deseasonalized using the seasonal-trend decomposition procedure based on locally weighted scatterplot smoothing, LOESS (Cleveland et al., 1990).

4.3 Results and Discussion

4.3.1 Temporal patterns in PM concentrations

Urban and suburban sites are characterized by higher PM levels, in comparison with rural ones (see Figure 4.1), and exhibit common typical temporal cycles. Figures 4.2, 4.3 and 4.4 show the monthly variability through an average year, the daily variability through an average week and the diurnal variability per average week and per average day, of the PM10, PM2.5 and PMc concentrations, respectively, observed between 2007 and 2016 and grouped by station type.

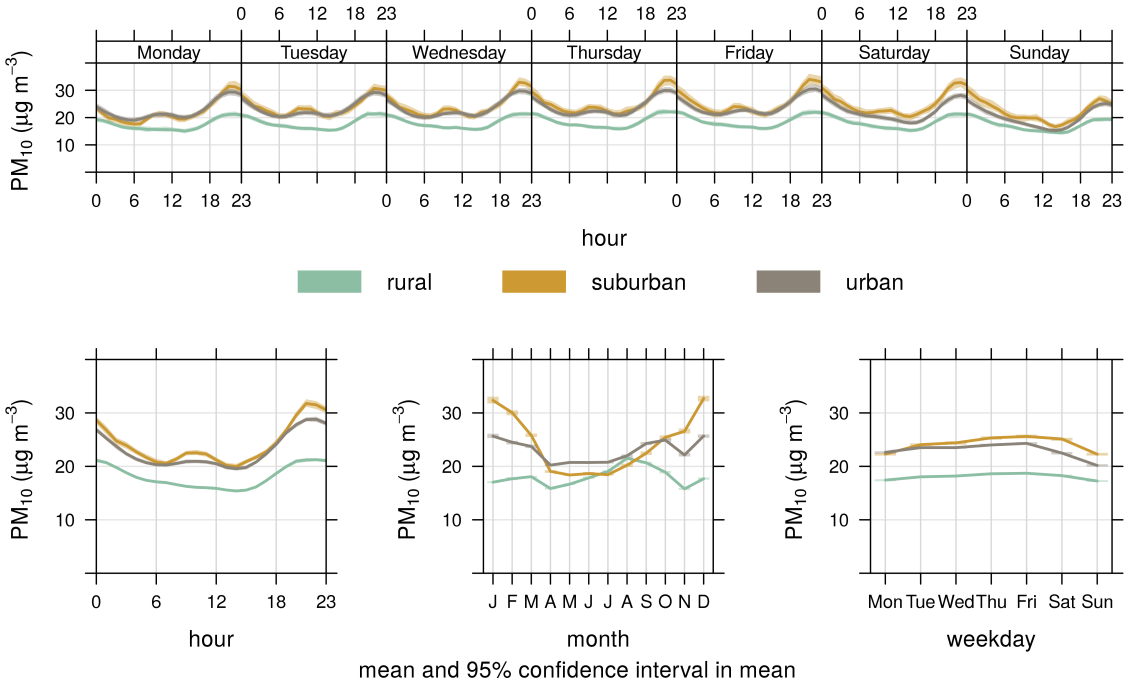

Figure 4.2: Hourly, daily and monthly variability of the PM10 concentrations observed at background stations between 2007 and 2016.

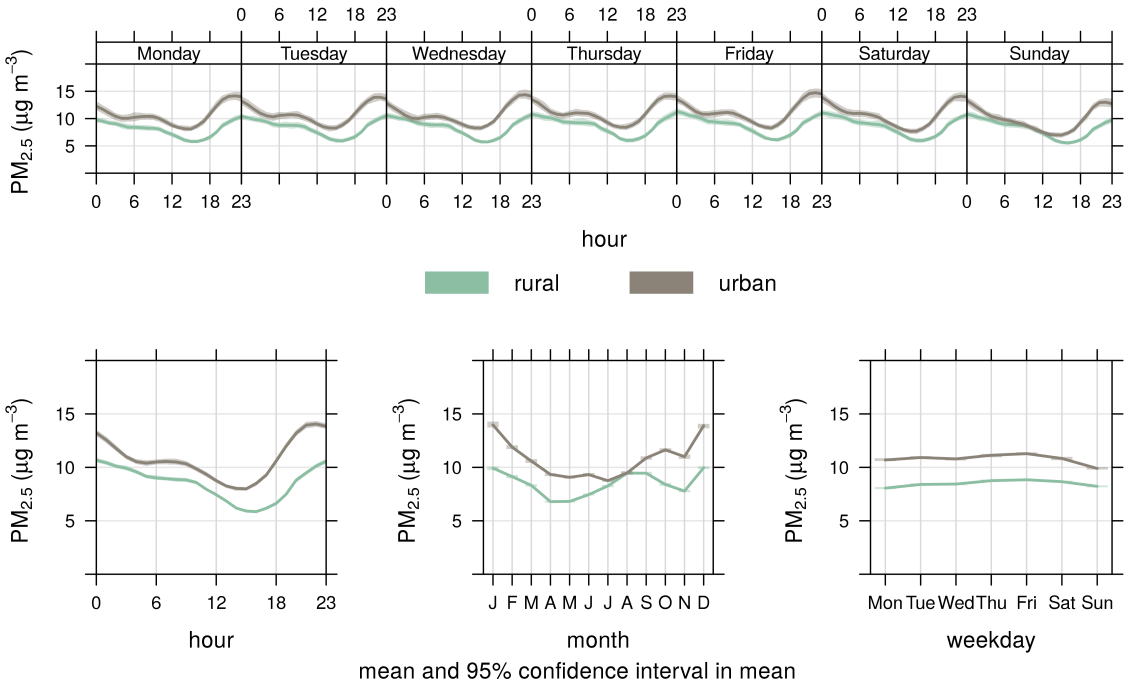

Figure 4.3: Hourly, daily and monthly variability of the PM2.5 concentrations observed at background stations between 2007 and 2016.

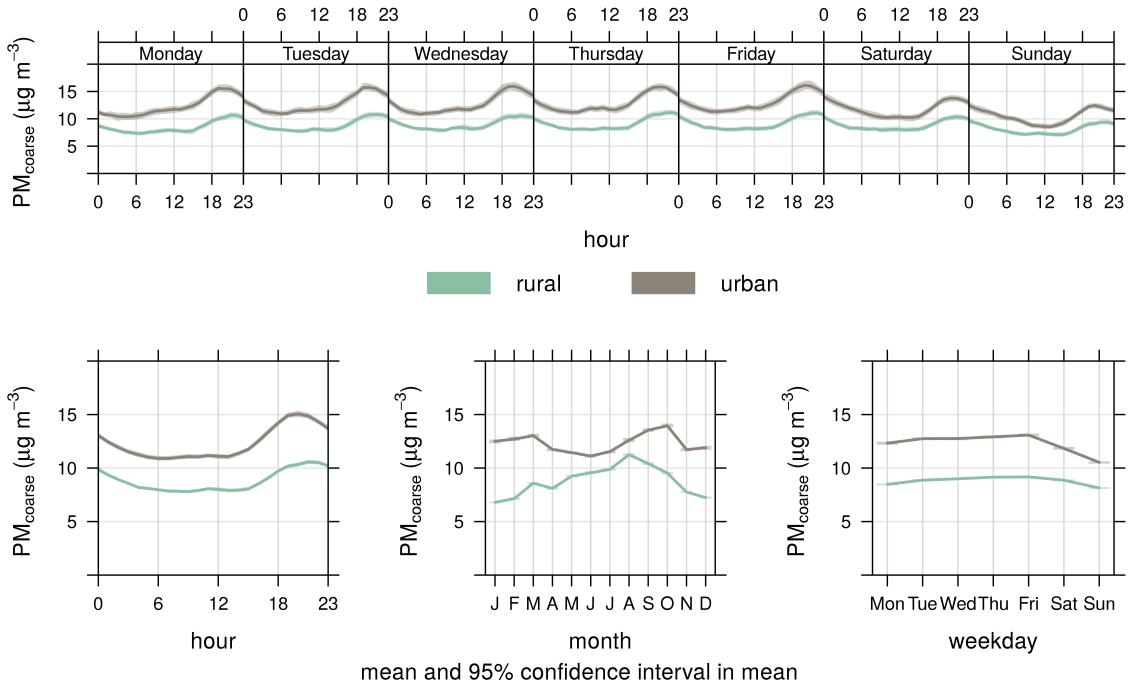

Figure 4.4: Hourly, daily and monthly variability of the PMc concentrations estimated at background stations between 2007 and 2016.

In general, during weekdays, urban and suburban sites show a dip in PM10 concentrations during the night (between 00h and 07h) which then rise between 07h and 10h, dropping again between 10h and 14h. During the afternoon, concentrations increase, being the highest peak of the day usually achieved between 20h and 23h. This profile is similar to those found by Harrison et al. (2012) relative to specific UK urban background stations. On Sundays, for the same group of stations, the peak in the early morning is not significant (probably due to the absence of the morning rush-hour traffic) and concentrations reach their minimum values in the beginning of the afternoon (around 14h). They then rise until around 21h, achieving then the highest peak of the day, which is, as expected, lower than during the week-days.

The combined hour of day – day of the week plot for PM2.5 shows a cycle similar to the PM10 one. Apart from the magnitude of concentrations, the main differences rely on the morning rise of concentrations, which is weaker for PM2.5, and on the differences between week-days and Sundays. The larger difference, between week-days and Sundays, in the magnitude of PM10 concentrations during late evening peaks at urban sites, reflects the importance of coarse particles of anthropogenic origin in Portuguese urban areas. Indeed, Figure 4.4 shows that the PM coarse fraction is about 3 $\mu g\,m^{-3}$ higher during week-days than during Sundays, at urban sites.

The late evening peak shown in the mean hour of day plots is related with, both, the daily evolution of the atmospheric boundary layer, which gets thinner during the night, and the evening contribution of domestic sources such as heating (Borrego et al., 2010; Gonçalves et al., 2012; Vicente et al., 2015) and cooking (Ots et al., 2016). In addition, according to Harrison et al. (2012), there may exist a contribution of semivolatile material condensing on ambient particles with the lower night-time temperatures. All these causes are more important during winter (due to thinner and more stable boundary layers, more emissions from heating, colder night-time temperatures), which may explain why the intensity of this late evening peak is much stronger during winter (see in Figure 4.5 the PM10 concentrations daily variability split by season).

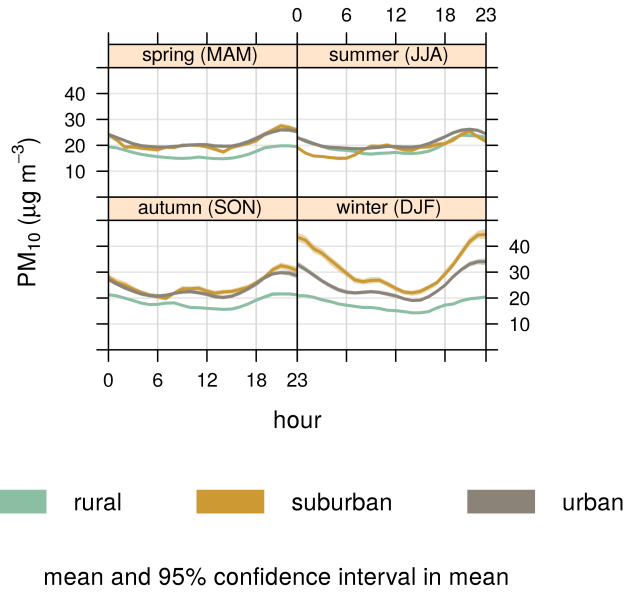

Figure 4.5: Daily variability split by season of the PM10 concentrations observed at background stations between 2007 and 2016.

It is at suburban sites that we find the larger differences between seasonally averaged daily cycles. On those stations, during winter, the PM10 late evening peak concentration is 20 $\mu g\, m^{-3}$ higher than during summer. This fact suggests a greater use of residential wood combustion in the urban suburbs than in the city centres, as it happens in other European cities such as London (Fuller et al., 2014) and Berlin (Wagener et al., 2012). It is important to notice that in this analysis we are including monitoring stations with different geographical locations (see Figure 4.1): the 4 suburban monitoring stations are located in the North of Portugal (in Aveiro, Porto and Braga districts), while from the 8 urban monitoring stations, 6 are located in Great Lisbon region (Lisbon and Setúbal districts), one in Coimbra and another one in Porto district. The

different geographical locations might as well contribute to the differences found between the two groups of stations.

As shown in Figures 4.2 and 4.5, rural sites present PM10 higher levels during summer. Indeed, most of the rural sites (FPO, FRN, FUN and TER) exhibit pronounced seasonal patterns, with the highest PM10 concentrations observed during August or August/September, when the monthly mean PM10 concentrations are about to 6 to 8 $\mu g\,m^{-3}$ higher than in the rest of the year. Cruz et al. (2016), who analysed PM levels in Portugal throughout a 3-year period, attributed this behaviour to the influence of high-altitude mountain stations. In that study, only two monitoring sites (FUN and Douro Norte, a station, which is not considered in our characterization due to non-compliance with the data coverage threshold) present the highest PM10 concentrations during summer. The authors relate this with enhancement of secondary particulate formation, arising from photochemical reactions between biogenic VOC compounds and anthropogenic precursors transported from populated coastal areas in the north and the centre of the country.

In our results, we also observe this seasonal trend in low altitude stations (FPO and TER). We agree that the summer maximum might partially result from photochemically driven secondary formation of aerosols (Alves et al., 2001), which is not exclusive of high-altitude stations as our results show. Indeed, Figure 4.3 also shows an increment in rural PM2.5 concentrations during summer. However, our data analysis suggests, with PMc higher summer levels at rural sites (see Figure 4.4), that other factors are influencing particulate mass increase in the rural summer atmosphere. Possible reasons which may also contribute for the PM10 summer maximum are local dust emissions from dry soils, the impact of forest fires and long-range transport of African desert dust. In addition, differences in the precipitation patterns between winter and summer may play a huge role in PM concentrations, due to the effect of precipitation scavenging on PM removal from the atmosphere.

Other sites, such as ERM, ERV, FRO, ILH and VCO are characterized by higher average PM10 concentrations during winter. In this group of stations all types of areas are included: urban (ERM), suburban (FRO, ILH and VCO) and rural (ERV).

4.3.2 Relationship between PM2.5 and PM10 and between PM2.5 and PMc

Figure 4.6 shows the simultaneously measured PM2.5 vs. PM10 daily mass concentrations for the 7 sites that measured both pollutants between 2007 and 2016. PM2.5 and PM10 mass concentrations are correlated and slope values for individual sites range from 0.44 to 0.54. These values are lower than the ones calculated by Dingenen et al. (2004) for 11 European sites, using "binned" PM2.5 and PM10 24-h values, which range from 0.57 to 0.89. Putaud et al. (2010) observed "binned" PM2.5/PM10 ratios between 0.44 and 0.90, in 34 European sites, having not found any clear relationship between PM2.5/PM10 ratio and the type of site or its location in Europe. In our study, we found as well no clear relationship between the value of the PM2.5/PM10 ratio and the type of monitoring station. Ratios computed for individual stations range from 0.44 to 0.52 for urban and from 0.44 to 0.54 for rural stations. The mean PM2.5 vs. PM10 ratios for urban and rural monitoring stations are very similar (0.48 and 0.49, respectively).

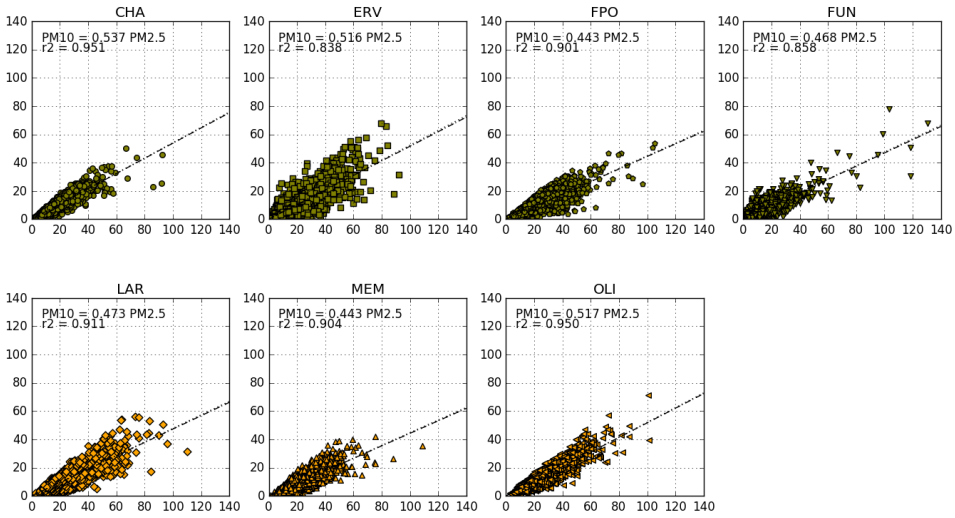

Figure 4.6: Ratio between PM2.5 and PM10 concentrations observed at individual background monitoring stations between 2007 and 2016. Rural stations data is represented with green dots in the top panel while data from urban stations is represented by yellow dots in the bottom panel.

Lower PM2.5/PM10 ratios are associated with spatial and temporal conditions where the observed PM levels are dominated by coarse particles. Higher ratios are observed at sites where secondary aerosol sources, which produce fine particles, are predominant (Dingenen et al., 2004), or where fuel combustion is amongst the main sources of particulate matter emissions. The values we calculated for the Portuguese background monitoring stations indicate that we have a significant contribution of the coarser fraction to the total PM10.

In order to analyse with more detail the fine and coarse contribution to the total aerosol mass, Figure 4.7 shows the daily variability split by season of the PM2.5 and PMc concentrations, at rural and urban background stations. In general, background stations exhibit similar magnitude of PM2.5 and PMc concentrations.

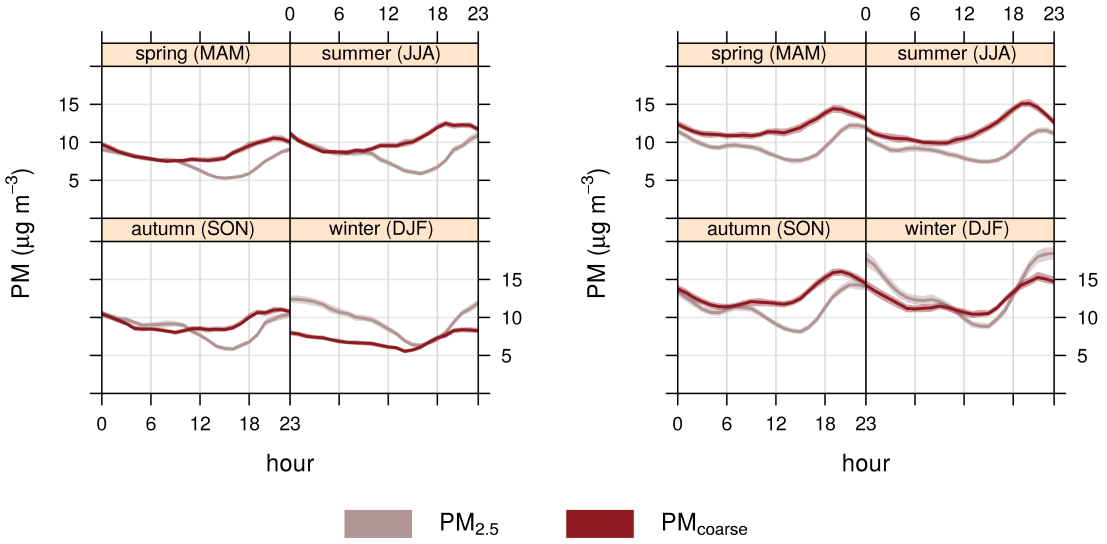

Figure 4.7: Daily variability split by season of the PM2.5 and PMc concentrations observed at rural (left plot) and urban (right plot) background stations between 2007 and 2016.

PM2.5 concentrations are higher during winter. The relative contribution of the PM2.5 fraction to the total aerosol mass is in average higher in rural than in urban background stations (mainly during winter). In other words, Portuguese urban background stations show a contribution of anthropogenic emissions to the PMc concentrations. These findings are in accordance with Almeida et al. (2006), which found that during autumn/winter, a predominant fraction of coarse soil dust observed in an urban area (in the outskirts of Lisbon) originates from anthropogenic activities. Indeed, most cities with pollution from transport and other combustion sources show a non-combustion source which is mainly attributed to dust re-suspension (from vehicle non-exhaust sources, construction activities, soil dust, etc.), which forms part of the coarser fraction PMc.

Figure 4.8 shows PM2.5 vs. PMc daily mass concentrations for the 7 sites with data between 2007 and 2016. There is no clear relationship between the value of the PM2.5/PMc ratio and the type of monitoring station. At urban sites, the correlation coefficient between fine and coarse particulate matter concentrations indicates a robust relationship between the two variables. This relationship may denote similar PM sources in the atmosphere.

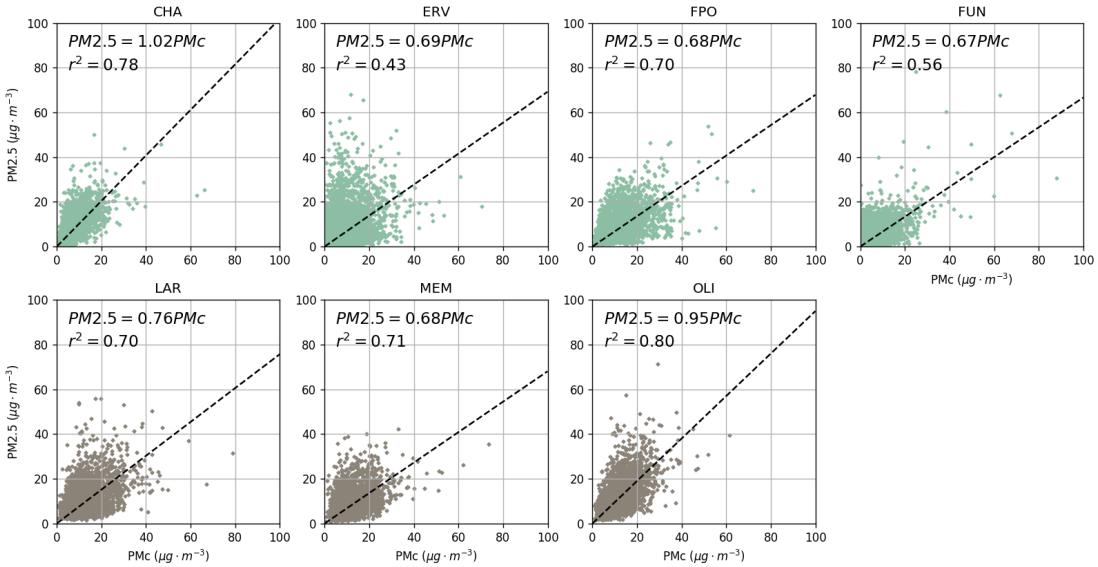

Figure 4.8: Ratio between PM2.5 and PMc concentrations observed at individual background monitoring stations between 2007 and 2016. Rural stations data is represented with green dots in the top panel while data from urban stations is represented by grey dots in the bottom panel.

The rural sites ERV and FUN show lower values of correlation between PM2.5 and PMc. ERV monitoring station is located at about 5 km from the seashore, which means that it might be influenced by sea-spray. However, sea-spray influences mainly large particles (Cesari et al., 2018; Slezakova et al., 2007). The scatter plot of PM2.5 and PMc concentrations shows a large number of points with larger PM2.5 than PMc concentrations, which indicates that sea-spray is not the main contributor in these cases.

4.3.3 Long term temporal trends

In previous sections PM temporal patterns were presented. In this section, the trend in PM concentrations through the last decade is discussed. Figures 4.9, 4.10 and 4.11 show the smooth trend for PM2.5, PM10 and PMc concentrations observed at background stations between 2007 and 2016, according to type of station.

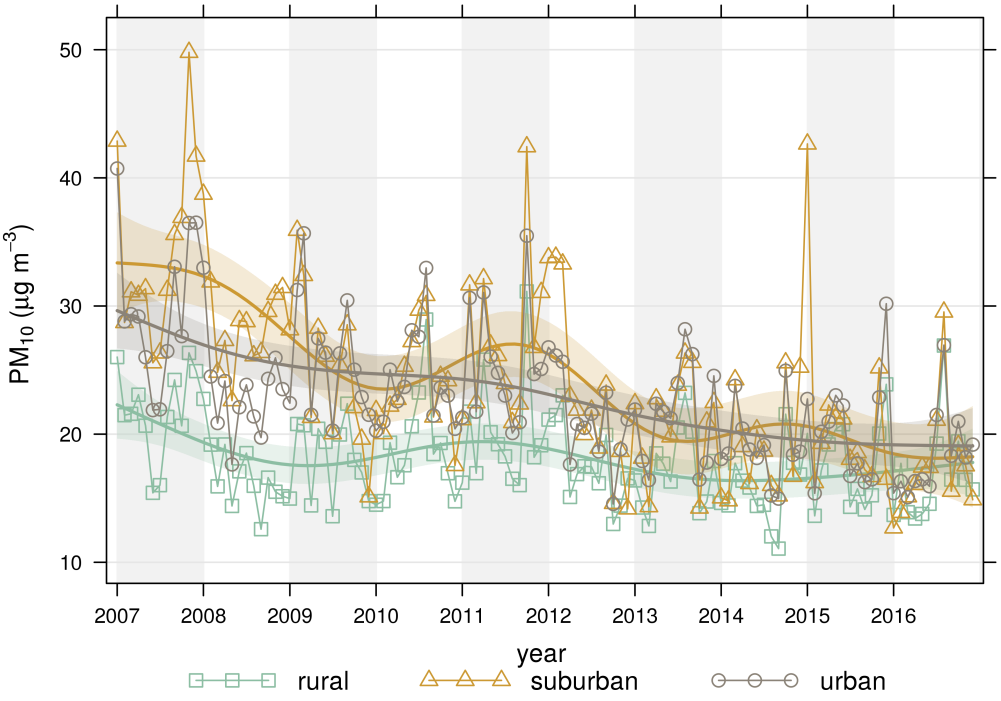

Figure 4.9: Trends in the monthly mean PM10 concentrations observed at background stations between 2007 and 2016.

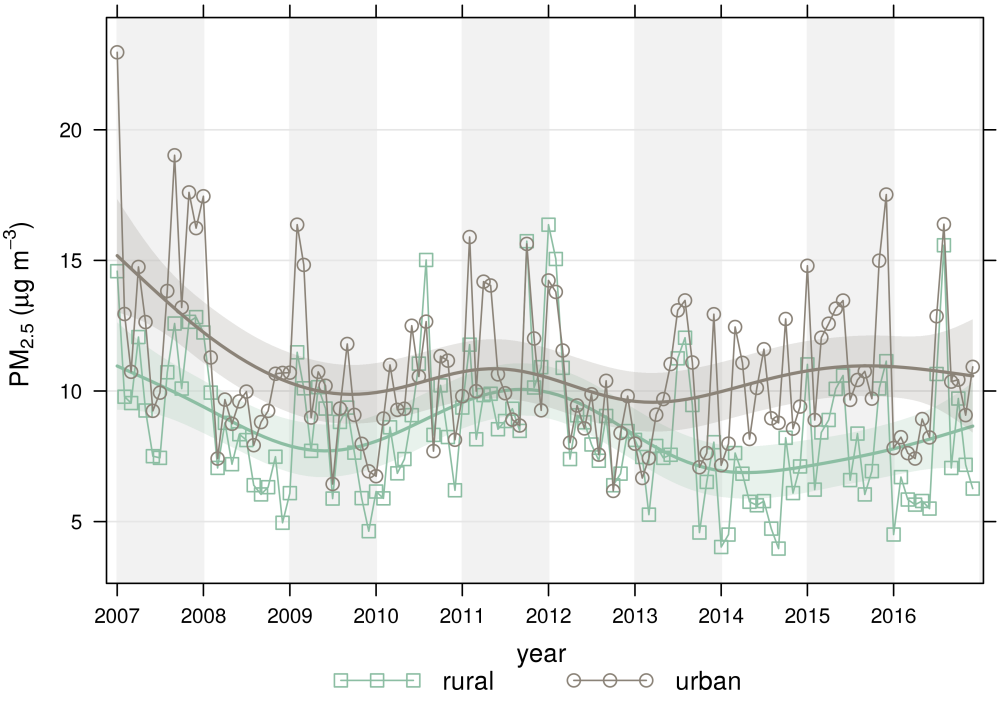

Figure 4.10: Trends in the monthly mean PM2.5 concentrations observed at background stations between 2007 and 2016.

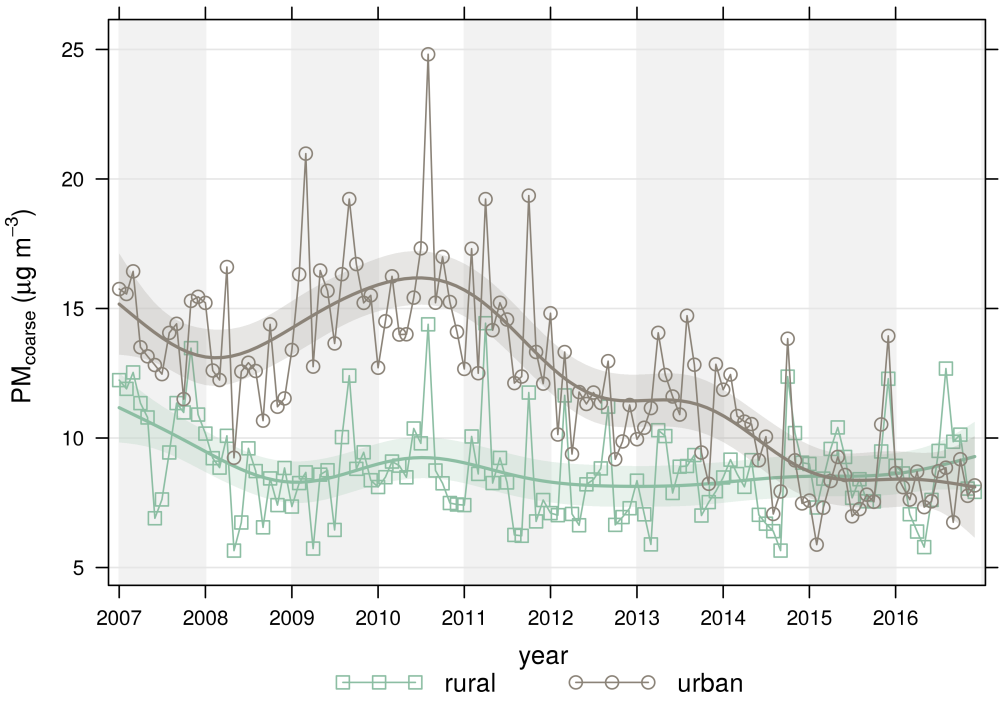

Figure 4.11: Trends in the monthly mean PMc concentrations estimated at background stations between 2007 and 2016.

A decreasing trend is observed in PM10 concentrations, mainly for the urban and suburban stations. For rural stations, the observed trend is less evident, and concentrations are more stable through the 10-year period in analysis. While, back in 2007 there was a large difference between PM10 levels observed at suburban, urban and rural stations, ten years later, in 2016, the three types of stations measure a similar range of mean concentration values. The monthly mean concentrations fit has, in January 2007, values of 22.3, 29.6 and 33.4 $\mu g\,m^{-3}$ for rural, urban and suburban stations, respectively. Ten years later, values are 17.8, 19.1 and 18.2 $\mu g\,m^{-3}$, respectively. PM10 concentrations decreased by 20%, 35% and 45% at Portuguese rural, urban and suburban areas, respectively, between 2007 and 2016.

The trend in PM2.5 concentrations (see Figure 4.10) is not as evident for PM10. The fit to the monthly mean concentrations has, in January 2007, concentration values of 10.1 and 15.2 $\mu g\,m^{-3}$ for rural and urban stations, respectively, while ten years later, these values are 8.7 and 10.6 $\mu g\,m^{-3}$, respectively.

It is interesting to notice that at urban stations, PM10 concentrations decrease more than PM2.5. Over the last decade and according to our results, PM10 and PM2.5 concentrations registered

a reduction of approximately 10 and 5 $\mu g\,m^{-3}$, respectively. Urban stations registered a huge decrease in the aerosol coarse concentrations, PMc (see Figure 4.11).

The improvement in the air quality might be partly related to the Portuguese economic crisis. Indeed, Monteiro et al. (2017a) found a relationship between the reductions in energy consumption (registered at transports, industry and residential sectors) and PM10 concentrations in Lisbon and Porto municipalities. Moreover, the economic crises severely affected construction activity within cities, which may affect positively PM10 concentrations due to a reduction in dust production and re-suspension.

4.3.4 Air Quality Objectives

In this section we aim to assess the compliance of the ambient air quality legislation throughout the last decade. However, in line with the scope of this work, this assessment uses background monitoring stations data. It is expected that an assessment considering also traffic and industrial monitoring stations would have different (worst) results.

The Air Quality Directive (Directive 2008/50/EC) establishes objectives for ambient air quality designed to avoid, prevent, or reduce, harmful effects on human health and on the environment as a whole. For PM10, daily (50 $\mu g\,m^{-3}$) and yearly (40 $\mu g\,m^{-3}$) limit values are defined for the protection of the human health. According to the Directive, the daily limit value for the protection of human health cannot be exceeded more than 35 times a calendar year. For PM2.5, the Air Quality Directive defines an annual value of 25 $\mu g\,m^{-3}$ which entered into force in 2010 as a target value and as a limit value after 2015.

Table 4.2 summarizes the exceedances to the PM10 daily limit value for the protection of human health. During the study period, from the 20 background air quality stations analysed, 5 urban or suburban background stations have surpassed the maximum number of exceedances allowed to the daily limit value in one or more years. In general, although rural background stations show exceedances, they accomplish the legislation regarding the protection of human health. While between 2007 and 2012 we had at least one background station each year with more than 35 exceedances, between 2013 and 2016 all the background stations analysed, despite their surrounding environment classification, have accomplished the values established in the Directive 2008/50/EC for the protection of the human health.

Table 4.2: Number of exceedances to the PM10 daily limit value for the protection of human health during the period 2007-2016, per station and per calendar year. Bold values highlight the stations where the limit value was exceeded more than 35 times a calendar year.

Code	2007	2008	2009	2010	2011	2012	2013	2014	2015	2016
ALV	-	-	6	8	6	0	2	3	5	8
ARC	0	4	34	9	20	5	5	4	14	7
CHA	2	1	0	3	3	1	2	3	2	7
CUS	**73**	13	32	33	**45**	16	17	1	2	0
ERM	**86**	33	**39**	34	**59**	22	19	8	2	8
ERV	18	4	1	6	19	15	2	3	16	2
FPO	13	7	8	6	6	10	0	0	5	13
FRN	1	3	1	6	4	3	6	2	2	7
FRO	**49**	23	18	10	14	14	3	1	2	0
FUN	1	1	0	7	0	6	1	2	2	5
IGE	29	4	2	2	12	8	2	6	5	4
ILH	**37**	19	1	7	**39**	**51**	17	18	34	6
LAR	27	10	34	18	29	6	5	6	12	8
LOU	25	9	13	5	9	1	0	2	5	6
MEM	15	5	9	2	6	0	1	3	6	4
MOV	13	9	4	3	24	9	4	2	10	5
MVE	22	2	1	4	3	2	0	2	3	5
OLI	23	13	15	11	29	7	4	2	7	8
TER	4	5	5	7	24	10	1	2	5	11
VCO	**115**	**83**	**59**	2	**39**	33	20	10	5	5

The exceedances presented in Table 4.2 are calculated using daily PM10 concentrations and are a result of the maximum daily concentration values through the year. Although trends computed in section 4.3.3 are based in monthly mean concentrations, the results of both analysis are in agreement. The situations of non-compliance with legislation also follow a decreasing tendency.

PM10 and PM2.5 mean concentrations per calendar year are presented in Figure 4.12. Among the 20 air quality monitoring stations, only one station (VCO, a suburban station located in the Porto Litoral zone) surpassed the annual limit for PM10 concentrations, in 2007. Regarding PM2.5 concentrations, all the 7 monitoring stations are compliant with the legislation. Nevertheless, it is important to remember that we are considering background monitoring stations only. The conclusions of this analysis could be different when considering traffic and industrial monitoring stations as well.

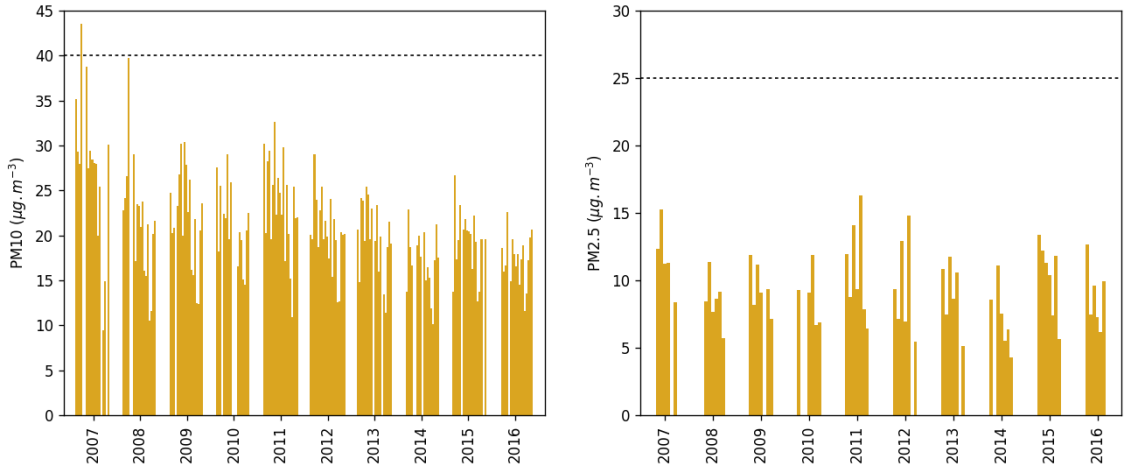

Figure 4.12: Mean PM10 and PM2.5 concentrations observed at background stations per calendar year, from 2007 till 2016. The dashed line represents the PM10 yearly limit value for the protection of the human health and the PM2.5 target/limit value, as defined by the Directive 2008/50/EC.

Contributions from natural sources can be assessed but cannot be controlled. Therefore, according to the Directive 2008/50/EC, where natural contributions to pollutants in ambient air can be determined with sufficient certainty, and where exceedances are due in whole or in part to these natural contributions, these may be subtracted when assessing compliance with air quality limit values. In the next Chapter, a modelling approach will be presented and then, in Chapter 6, it will be used to assess the impact of the aeolian dust, transported from North African deserts, in the particulate matter levels in Portugal.

4.4 Conclusions

The aerosol background levels in Portugal are analysed based on data gathered from 2007 to 2016. Compliance with the Directive 2008/50/EC has been assessed and a decreasing tendency was found within the number of non-compliance situations. While, between 2007 and 2012 we had at least one background station each year with more than 35 exceedances, between 2013 and 2016 all the background stations analysed, despite their type, have accomplished the values established for the protection of human health.

A decreasing trend is observed in PM10 concentrations, mainly for the urban and suburban stations. Our analysis shows that the main factor contributing to the PM10 decrease in urban areas is the decrease in the PMc concentrations. While in January 2007 there was a large difference

between PM10 levels observed at suburban, urban and rural stations (33.4, 29.6 and 22.3 $\mu g\,m^{-3}$), ten years later, values are 17.8, 19.1 and 18.2 $\mu g\,m^{-3}$, respectively.

PM10 and PM2.5 concentrations are characterized by typical temporal patterns. Along the day, concentrations follow the expected patterns with rural sites exhibiting less variability through the day and urban and suburban sites characterized by two main peaks during the day: one during the morning, and the largest one at late evening.

The results of this study point out the importance of coarse particles of anthropogenic origin in Portugal. This conclusion is supported by the larger differences between weekdays and Sundays in PM10 than PM2.5. PMc is about to 3 $\mu g\,m^{-3}$ higher during week-days than during Sundays, at urban sites.

It is on suburban sites that the larger differences between the PM10 characteristic daily cycle of each season are found. In this group of stations, the highest daily concentrations (observed at late evening / during the night) during winter are in average 20 $\mu g\,m^{-3}$ higher than during summer. PM2.5 concentrations could not be assessed at suburban stations.

This work provides an import insight on temporal variations of PM10, PM2.5 and PMc concentrations over Portugal and summarizes trends through the last decade. Our study contributes to the characterization of background levels of particulate matter and to the ongoing discussion on sources and processes influencing those concentrations.

Chapter 5

Aerosol forecast over Portugal

5.1 Introduction

Air quality models (AQMs) are numerical representations of the atmospheric processes. AQMs are important tools to understand the behaviour of pollutants in the atmosphere, especially the relationship between emissions, atmospheric transport, chemistry and deposition. Moreover, AQMs permit prediction of pollution levels in areas of significant public exposure. This information, when delivered timely to the population, allows the adoption of preventive measures aimed at individuals that are particularly sensitive to air pollution.

Since 2007, an air quality forecast system based on numerical simulations of atmospheric physical and chemical properties, is running operationally at the University of Aveiro. The genesis of this system (Monteiro et al., 2005) was based on the MM5-CHIMERE models system. Nowadays, the operational air quality forecast system includes WRF meteorological simulations (Skamarock et al., 2008), which drive the CHIMERE air quality model (Menut et al., 2013). Recently, a non-climatic representation of African dust transport was included in the operational forecast system, firstly using the BSC-DREAM8b dust model (Basart et al., 2012b) and later applying CHIMERE's own module for the dust emissions and transport. The main features of this set-up are described in Section 5.2.

The Portuguese air quality forecast system has been extensively tested and validated; those exercises outlined the reasonably good skills of the CHIMERE model for ozone and other gaseous pollutants concentrations. Particulate matter presents a higher complexity than ozone. Many

studies have recognized the difficulty of models to simulate the mass of PM over Europe (e.g. Matthias, 2008; Pay et al., 2010). As summarized by Basart et al. (2012a), the underestimation of PM10 may be related with the lack of fugitive dust emissions and resuspended matter, a possible underestimation of primary carbonaceous particles, the inaccuracy of secondary organic aerosol formation, the difficulty in representing primary PM emission from wood burning and other sources not considered in the emission inventory such as pollutant sources over North Africa and a more general lack of process knowledge on aerosol removal, dispersion and transport processes.

In this Chapter, we aim to evaluate a complete annual cycle of aerosol forecasts over Portugal, using ground-level PM10 and PM2.5 concentrations from the air quality monitoring network and AERONET, and also LIDAR observations obtained during specific Saharan dust events. Focusing on the modelling of dust emissions and transport from North Africa, experimental air quality forecasts, which are described in Section 5.3, are implemented for the same year in analysis, in order to test improvements in the system. The results of those tests are assessed and their limitations are discussed in Section 5.4.

5.2 Description of the operational air quality forecast system

The Portuguese operational air quality forecast system is based on daily simulations of the WRF and CHIMERE numerical models, which are further described below. The system can be accessed by the general public in http://previsao-qar.web.ua.pt/. The results are shown in the Internet for the actual day and the following one, and include both the air quality index and the main pollutants (PM10, PM2.5, O_3 and NO_2) concentrations (Figure 5.1). The spatial distribution of the air quality index / pollutant concentration is presented on top of a basemap with a zoom-in capability, which helps the user to identify the location where he/she is interested in. The system also provides detailed pollutant time series for the spatial location selected by the user.

5.2.1 The WRF meteorological model

The Weather Research and Forecasting (WRF) Model is a state-of-the-art mesoscale numerical weather prediction system designed for both atmospheric research and operational forecasting needs. The effort to develop WRF began in the latter 1990's, in the United States of America, being a collaborative partnership principally among the National Center for Atmospheric Research

(NCAR), the National Oceanic and Atmospheric Administration (represented by the National Centers for Environmental Prediction (NCEP) and the (then) Forecast Systems Laboratory (FSL)), the Air Force Weather Agency (AFWA), the Naval Research Laboratory, the University of Oklahoma, and the Federal Aviation Administration (FAA).

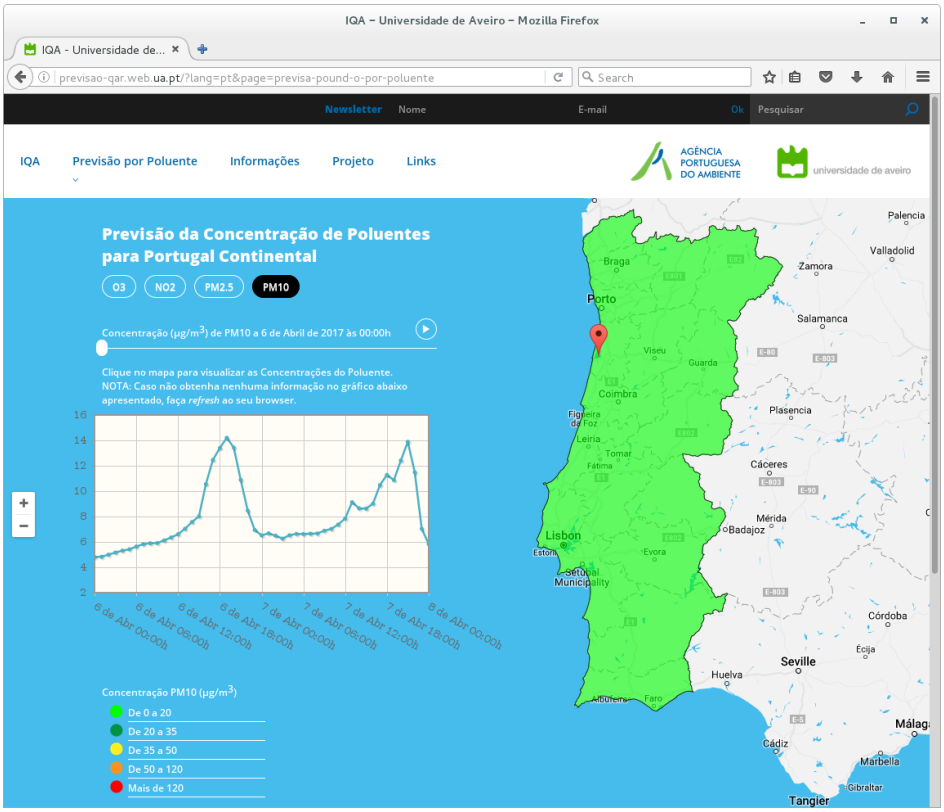

Figure 5.1: Aspect and capabilities of the Portuguese operational air quality forecast system website.

The WRF system contains two dynamical solvers, referred to as the ARW (Advanced Research WRF) core and the NMM (Nonhydrostatic Mesoscale Model) core. In the Portuguese operational air quality forecast system, the ARW version 3 (Skamarock et al., 2008) is used. The ARW dynamics solver integrates the compressible, nonhydrostatic Euler equations. The equations are cast in flux form using variables that have conservation properties, and are formulated using a terrain-following mass vertical coordinate. WRF offers a host of options for atmospheric processes. The set of options chosen for the Portuguese operational air quality forecast are shown in Table 5.1. The meteorological outputs from the WRF are used as inputs for the chemistry transport model CHIMERE, which is described in the next Section.

Table 5.1: WRF options selected for the Portuguese operational air quality forecast

solver	ARW
physics schemes	
microphysics	WSM6 scheme (Hong and Lim, 2006)
cumulus parametrizations	Kain-Fritsch scheme (Kain, 2004)
planetary boundary layer	ACM2 scheme (Pleim, 2007)
atmospheric radiation	RRTMG scheme (Iacono et al., 2008)
grid-nesting techniques	one-way interactive

5.2.2 The CHIMERE chemical transport model

CHIMERE is a state-of-the-art Eulerian off-line chemistry transport model (CTM). It computes the atmospheric concentrations of tens of gas-phase and aerosol species over local to continental domains (from 1 km to few degrees resolution), given meteorological fields, primary pollutant emissions and chemical boundary conditions. The general principle of a CTM like CHIMERE is depicted in Figure 5.2. The key processes affecting the chemical concentrations are: emissions, transport (advection and mixing), chemistry and deposition.

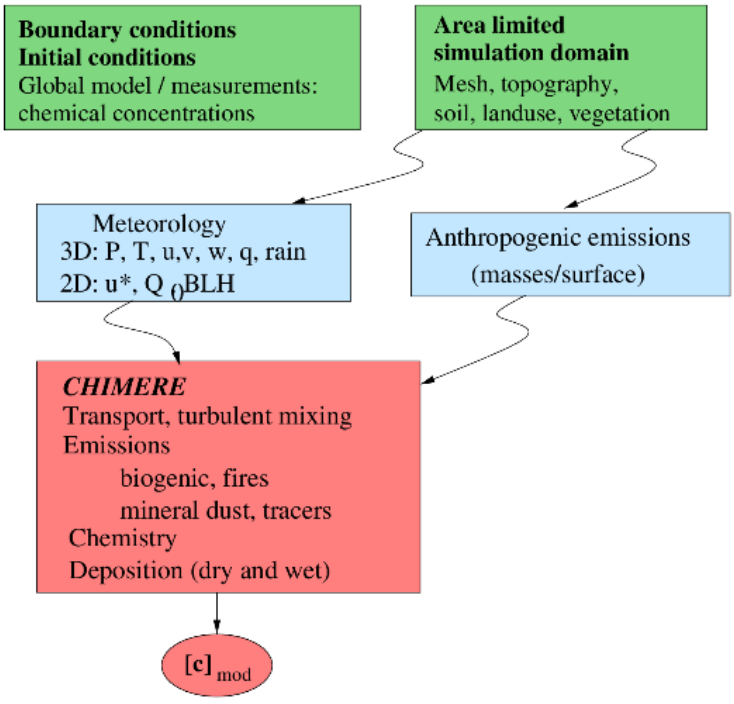

Figure 5.2: General principle of a chemistry-transport model such as CHIMERE. In the box Meteorology, $u*$ stands for the friction velocity, Q_0 the surface sensible heat flux, L the Monin-Obukhov length and BLH the boundary layer height. $[c]_{mod}$ are the chemical concentrations fields simulated by the model. adapted from http://www.lmd.polytechnique.fr/chimere/docs/CHIMEREdoc2016a.pdf

The model is mainly used for pollution event analysis, scenario studies and operational forecast. CHIMERE is part of the operational air quality of regional air quality networks in France, Italy, Spain, Portugal and Netherlands, and is included in the PREV'AIR system, MACC (Monitoring atmospheric composition and climate) and CAMS (Copernicus Atmosphere Monitoring Service) regional forecasting services, etc. It has been involved in numerous intercomparison studies mainly focusing on ozone and PM10 (Vautard et al., 2007; van Loon et al., 2007; Solazzo et al., 2012; Zyryanov et al., 2012). It is currently involved in the EURODELTA-Trends multi-model chemistry-transport experiment, which has as main objective to assess the efficiency of air pollutant emissions mitigation measures in improving regional-scale air quality (Colette et al., 2017). The model has been mainly applied over Europe, but also over Africa and Asia for dust simulations (Schmechtig et al., 2011; Cuesta et al., 2015) and over Central America during the MILAGRO project to study organic aerosols (Hodzic et al., 2009).

CHIMERE proposes many different options for simulations, which make it also a powerful research tool for testing parametrizations' hypotheses. It can run with several vertical resolutions and chemical mechanisms, and with a wide range of complexity. The set of options in use within the Portuguese operational air quality forecast are summarized in Table 5.2.

Table 5.2: CHIMERE version and options selected for the Portuguese operational air quality forecast

model version	2016a1
chemistry mechanism	Melchior reduced
chemically-active aerosols	yes
number of aerosol size sections	10
horizontal and vertical advection schemes	Van Leer I
radiative processes	Fast-JX model
boundary conditions	LMDz-INCA (gaseous and particular species), GOCART (mineral dust)

In the Portuguese operational air quality forecast system, three nested domains covering part of the North Africa and Europe are used (Figure 5.3), with horizontal resolutions of 125x125 km^2, 25x25 km^2 and 5x5 km^2 for the innermost domain covering Portugal. The vertical resolution in CHIMERE varies upward in a geometric progression. This means the lowest atmospheric layers are more refined, since these layers are critical for the modelling of boundary layer contamination, particularly in urban areas, but also in marine areas in order to model correctly the sea-salt emissions, and in arid areas, for mineral dust emissions (Mailler et al., 2017). Although the most frequently used vertical discretization consists of 8 vertical levels (Menut et al., 2013), in the Portuguese operational air quality forecast a better representation of the free troposphere is

employed, using 24 levels up to the 200hPa pressure level. The first model layer, which is closer to the surface, has a thickness of 3hPa, about 30m. With this vertical discretization we aim to better reproduce the long-range transport of dust from North Africa, as suggested by Menut et al. (2013).

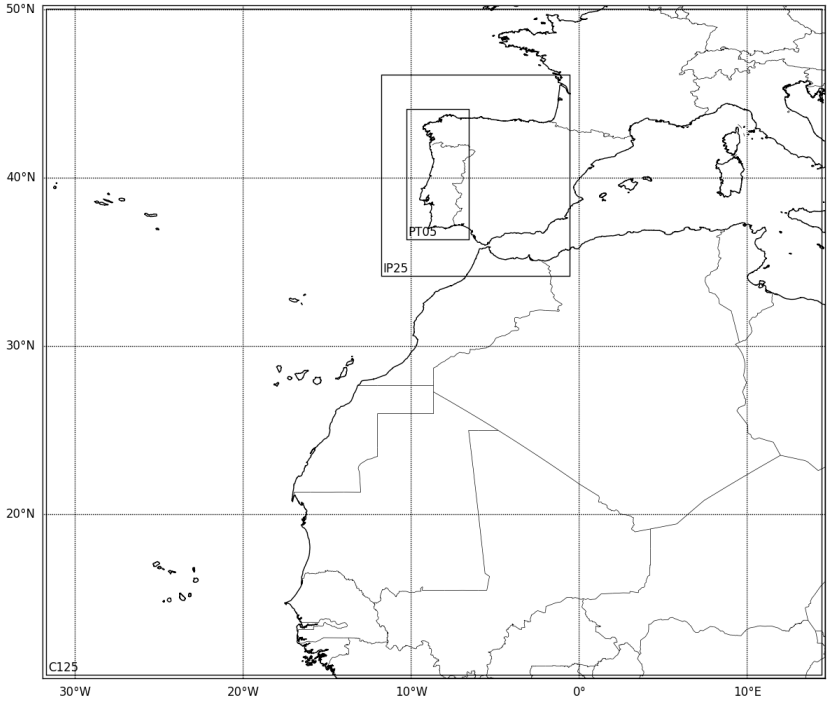

Figure 5.3: CHIMERE domais in the operational air quality forecast system.

At the boundaries of the outermost domain, climatologies from global model simulations are used. The outputs from LMDz-INCA (Szopa et al., 2009) are used for all gaseous and aerosol species, except for mineral dust. For this species, simulations from the GOCART model are used (Ginoux et al., 2001). For the nested domains, the boundary conditions are updated every hour using the previously done coarse CHIMERE simulation. The initial conditions are defined by the 24-h forecast from the previous-day model run.

In addition to the meteorological fields (from WRF) and to the chemical boundary conditions, the air quality modelling system must be fed with primary pollutant emissions. The main human activities emissions (traffic, industries and agriculture, among others) are derived based on data from the annual UNECE/EMEP emission database (available at http://www.ceip.at), following a procedure of spatial and temporal downscaling. The spatial allocation of surface emissions on

the CHIMERE grid is based on a classification among four landuse types: urban, crop, water or forest. Then, for each grid cell, hourly estimates are derived, assuming:

- seasonal factors provided by the Institute of Energy Research for each country and SNAP sector. The application of these factors redistributes the yearly EMEP emissions towards monthly emissions.
- 24-hour profiles for each day of week and for each SNAP sector, which follow the guidelines provided by the Institute for Energy Economics and Rational Use of Energy, University of Stuttgart (Ebel et al., 1994). The application of these factors redistributes the monthly emissions towards hourly emissions.
- hourly emissions from all SNAP sectors, gridded over the CHIMERE simulation domain, are aggregated to a single flux per emitted pollutant.

In addition, EMEP pollutants are split into model species, depending on the chemical mechanism selected in the simulation. In the Portuguese operational air quality forecast system, the 7 inventory pollutants (CO, NOx, SOx, NMVOC, NH_3, PM10 and PM2.5) are split into the 42 reduced Melchior species and 8 chemical operators.

Natural emissions estimates are also taken into account by the model, namely biogenic emissions, sea salt and dust. Forest fire emissions are not included in the simulations. The emissions related to the vegetation are computed online using the MEGAN model (Guenther et al., 2006). Sea salt fluxes are calculated according to Monahan (1986).

Dust emission fluxes are calculated anywhere over the globe, using the parametrization of Marticorena and Bergametti (1995) for saltation and the dust production model proposed by Alfaro and Gomes (2001) for sandblasting. This calculation requires land-use data, which is used to provide a desert mask specifying what surface is potentially erodible. In these simulations, the USGS database, STATSGO-FAO, is employed, and the erodible land-use type applied as a desert mask for dust fluxes calculation is barren soil (white sand).

5.3 Assessment of different model configurations

In order to test improvements in the performance of the Portuguese air quality forecast system, several hypothesis are launched and implemented, producing "experimental" air quality forecasts for the whole 2016. We want to know if the best available parametrization for dust emissions are used and what is the impact of a better resolved topography in dust emission and transport models. Thus, model resolution and mineral dust production schemes are the focus of the "experimental" forecast systems. For the last topic, we took advantage of the schemes already implemented in the version 2016a1 of the CHIMERE model.

Three different forecasting configurations were designed (see details in the next sections and/or Table 5.3 for a summary of the simulations). In order to evaluate modelling results, the outputs of these "experimental" forecasts, for a whole year (2016), are compared with the operational runs and with observations, such as particulate matter concentrations recorded at background sites from the Portuguese air quality monitoring network. As explained in the previous chapter, measurements from stations with a minimum annual data capture of 75% are considered. Taking into account the defined data quality objectives, for 2016 and for PM10, we could gather data for 10 rural, 4 suburban and 13 urban monitoring stations with a background influence (Table 5.4).

Table 5.3: Summary of the simulations.

simulation	domains	resolution	dust emissions
oper	original	125-25-05	Alfaro and Gomes (2001)
exp01	experimental	27-09-03	Alfaro and Gomes (2001)
exp02	experimental	27-09-03	Marticorena and Bergametti (1995)
exp03	experimental	27-09-03	Kok et al. (2014)

In addition to PM10 and PM2.5 concentrations, satellite data, namely the Dust RGB product, is employed to characterize desert dust outbreaks. This product, which is an RGB composite based upon infrared channel data from the MSG satellite, was designed by EUMETSAT to monitor the evolution of dust storms during both day and night. The Dust RGB makes use of channel differences that are close to IR windows near 8.7 µm and 12.0 µm. The resulting product depicts dust in magenta and purple colours over land, depending on the whether it is day or night, respectively. A dusty atmosphere can also be tracked over water as magenta colouring. Cold, thick, high-level clouds have red-brown tones and thin Cirrus clouds appear very dark, nearly black.

Table 5.4: List of QUALAR background stations with data completeness $> = 75\%$ for the year 2016. Coordinates and surrounding environment type classification (urb: urban; sub: suburban; rur: rural) are included.

Code	Name	LON	LAT	height (m)	type	PM10	PM2.5
ALV	Alverca	-9.040	38.896	22	urb	98.9%	-
ARC	Arcos	-8.894	38.529	2	urb	97.8%	-
CER	Cerro	-7.680	37.312	300	rur	85.5%	88.5%
CHA	Chamusca	-8.468	39.353	143	rur	98.1%	96.7%
ERV	Ervedeira	-8.893	39.922	60	rur	81.1%	81.1%
FID	Fidalguinhos	-9.049	38.650	24	urb	89.3%	-
FPO	Fernando Pó	-8.691	38.636	57	rur	91.0%	90.4%
FRN	Fornelo do Monte	-8.100	40.640	741	rur	87.7%	-
FUN	Fundão	-7.300	40.232	473	rur	92.1%	-
IGE	Inst. Geof. Coimbra	-8.412	40.206	145	urb	91.8%	-
ILH	Ílhavo	-8.672	40.588	32	sub	94.3%	-
JMG	Joaquim Magalhães	-7.928	37.014	4	urb	94.3%	-
LAR	Laranjeiro	-9.159	38.663	63	urb	91.8%	-
LEC	Leça do Balio	-8.630	41.220	40	sub	92.6%	-
LNH	Lourinhã	-9.246	39.278	143	urb	96.7%	94.0%
LOU	Loures-Centro	-9.166	38.828	10	urb	94.8%	-
MAL	Malpique	-8.251	37.091	45	urb	96.2%	-
MEM	Mem Martins	-9.348	38.784	173	urb	98.1%	95.6%
MOV	Montemor-o-Velho	-8.677	40.183	96	rur	79.2%	-
MVE	Monte Velho	-8.799	38.076	53	rur	84.4%	-
OLI	Olivais	-9.109	38.768	32	urb	97.3%	95.9%
PFE	Paços de Ferreira	-8.376	41.274	300	urb	88.3%	-
QMA	Quinta do Marquês	-9.324	38.697	48	urb	96.4%	-
REB	Reboleira	-9.232	38.753	132	urb	91.3%	-
TER	Terena	-7.398	38.616	187	rur	98.4%	87.7%
VCO	Mindelo V. Conde	-8.736	41.345	25	sub	93.7%	-
VNT	V. Nova Telha-Maia	-8.662	41.259	88	sub	86.6%	-

5.3.1 Domains and horizontal resolution

For the experimental forecasts, we increase the resolution of the three nested domains. Furthermore, we extend north and eastwards the outermost domain (see Figure 5.4). With this change we intend to include in the model domain regions where the anthropogenic emissions may be significant for the background European (and Portuguese) levels.

In all the experimental forecasts, the simulations are performed over the same horizontal domains as the ones defined for WRF, with a constant resolution of 27 km by 27 km, 9 km by 9 km, and 3 km by 3 km. The vertical levels of the WRF simulations are projected onto CHIMERE 24 levels, from the surface up to 200 hPa.

Wind and dust simulations are reported to improve over Asia due to a better-resolved topography (Liu and Westphal, 2001). Recently, Basart et al. (2016) demonstrate how the dust prediction in

the vicinity of complex terrains improves using high-horizontal resolution simulations. Topography alters the meteorology of dust emission and transport in many ways. The Atlas Mountains, for example, with a 2500 km extension from western Sahara towards Tunisia and peak altitudes up to more than 4000 m a.s.l., play a dominant role in local and mesoscale atmospheric circulation patterns (Pey et al., 2013). This may affect the height of injection of the dust in the atmosphere, which will have effects on downwind air quality at surface levels.

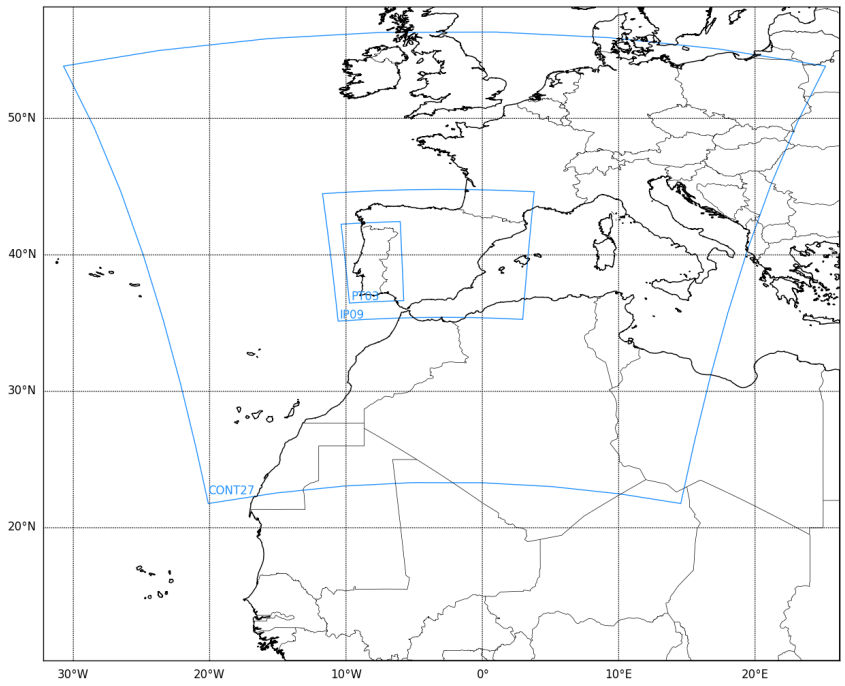

Figure 5.4: CHIMERE domains in the experimental air quality forecast system.

5.3.2 Mineral dust production schemes

Three different Dust Production Models, implemented in the CHIMERE version 2016a1, are tested over our forecast system domains: (i) the Marticorena and Bergametti (1995) scheme, which uses the White (1986) equation and constant distribution of emitted mass fluxes into the three emissions modes; (ii) the Alfaro and Gomes (2001) scheme, which employs the Marticorena and Bergametti (1995) scheme for saltation and estimates the vertical flux using cohesion kinetic energies scheme, in the numerically optimized version presented in Menut et al. (2005); and (iii) the Kok et al. (2014) scheme, in which the vertical dust flux is directly diagnosed for one emissions mode.

The parametrization from Kok et al. (2014) depends only on the wind friction velocity and the soil's threshold friction velocity. Moreover, it accounts for two processes missing from most existing parametrizations: a soil's increased ability to produce dust under saltation bombardment as it becomes more erodible, and the increased scaling of the dust flux with wind speed as a soil becomes less erodible.

5.4 Results and discussion

We have seen in Chapter 4 how the particulate matter background concentrations are distributed along Portugal and how they have varied over the last 10 years. Focusing now on the year 2016, Figures 5.5 and 5.6 present the time-series of PM10 and PM2.5 concentrations recorded that year.

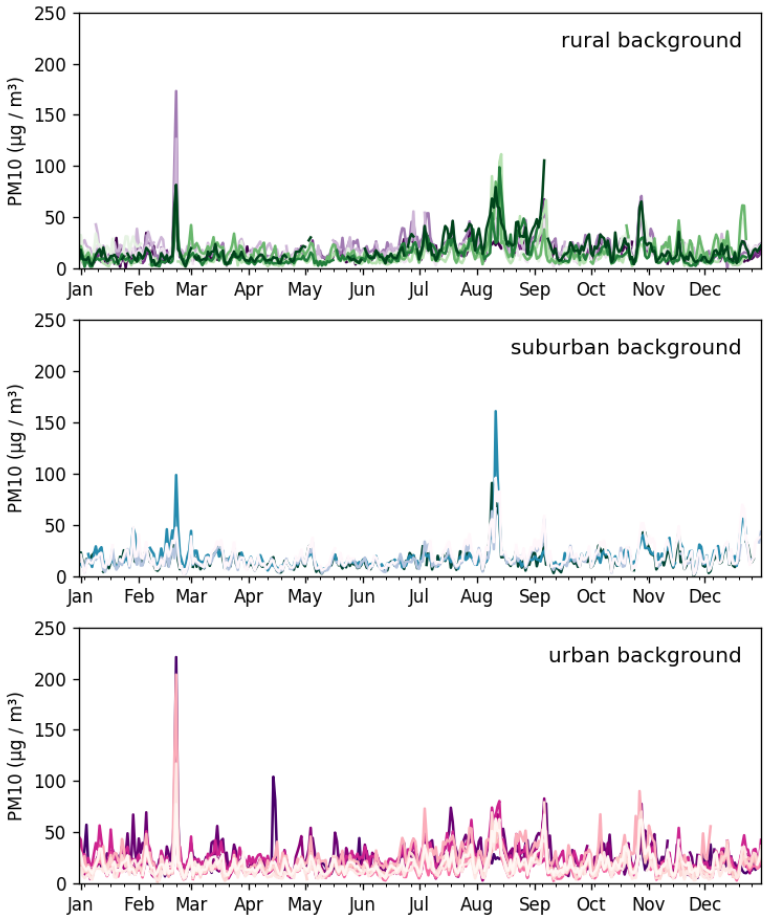

Figure 5.5: PM10 daily concentrations recorded in background stations from the Portuguese monitoring network, during 2016.

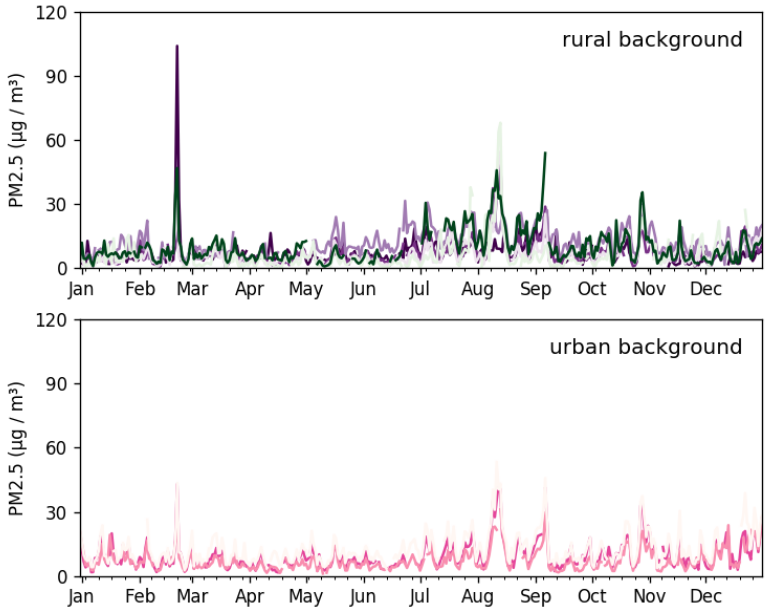

Figure 5.6: PM2.5 daily concentrations recorded in background stations from the Portuguese monitoring network, during 2016.

During 2016, the strongest PM episodes occurred in late February and middle August. These two episodes, which are highlighted in the PM10 and PM2.5 datasets from rural to urban sites (Figures 5.5 and 5.6), affected the whole country, from South to North. As we will see, the episode in February is associated with desert dust advection from North Africa and is investigated in the next section.

5.4.1 Dust outbreak in February 2016

A strong PM episode occurs in late February 2016, affecting roughly all background monitoring stations in Portugal. This episode was due to a vast plume of sand and dust blown northward from the Sahara desert and got "famous" when the European Space Agency astronaut Tim Peake captured an image of Saharan dust plume getting pulled into Europe (Figure 5.7) and posted it to his Twitter account.

Figure 5.7: Dust hovering over Portugal and Spain on Feb 21, 2016, as seen from the International Space Station (Twitter/@astro_timpeake).

Synoptic scenario

The synoptic conditions, which helped to pull the dust northward from its source, are investigated. As we see in Figure 5.8, which shows the 500 hPa geopotential height and winds at 2 km from the WRF simulations, the synoptic situation is characterized by both a cut-off low and the North African high. The presence of these two synoptic systems corresponds to one of the typical synoptic situations leading to dust transport over the Iberian Peninsula (Escudero et al., 2005; Rodríguez et al., 2003).

A cut-off low corresponds to a closed low in the upper troposphere that has become completely detached (cut off) from the basic westerly current usually being advected equatorward of the mid-latitude westerlies (Gimeno et al., 2007). These systems are slow moving and often stay over the same region for several days, therefore capable of considerably affecting the weather conditions at the surface. Moreover, these features play a significant role in the tropospheric ozone balance through dissipation and mixing of stratospheric ozone (Song et al., 2016; Li et al., 2015). As we will see, this system may as well play a significant role in the emission and transport of desert dust from North Africa to the Iberian Peninsula.

The cut-off low formed on February 19 at mid-upper levels over the Atlas Mountains, after the southward displacement and detachment of the bottom of a trough that protruded from the British Isles to the Iberian Peninsula the day before. This structure later drifted toward the Moroccan coast, and then northward to the south of Cape St. Vincent. It was finally dissipated

over the Iberian Peninsula at the end of February 22. This synoptic situation is similar to the one associated to the strong dust episode of October 2008, described by Cabello et al. (2012).

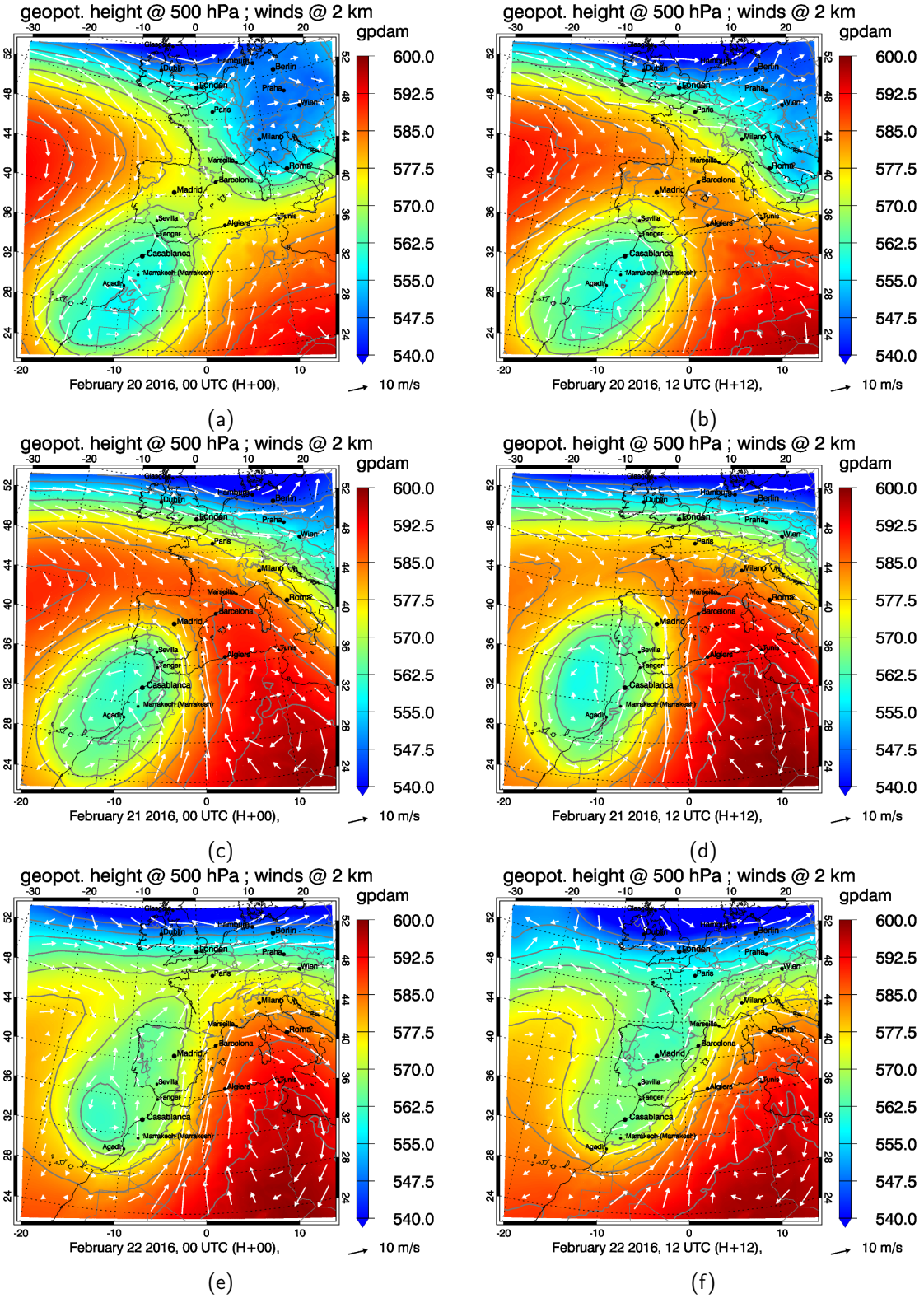

Figure 5.8: Evolution of the synoptic situation at the 500 hPa geopotential height and winds at 2 km, from 20 to 22 February 2016 [courtesy of Annika Vogel].

Dust emission and transport

The evolution of the dust outbreak is illustrated in Figure 5.9, which shows a sequence of the false colour RGB dust images from MSG-SEVIRI, from February 20 00H to February 21 18H. At February 21, 12H, a dust hotspot is identified in the Morocco - Algeria border, along the Atlas Mountains. This dust layer is advected over the Iberian Peninsula and, at 18H, starts to enter Spain passing over Malaga. During the night, the dust layer continues to enter Spain, moving westerly.

On the February 22 at 06H the dust hotspot is visible over Spain and over Central Portugal and the dust injection into the atmosphere in North Africa is not visible anymore. At 12H the dust cloud affects mainly Central Spain and Central Portugal and at 18H it can be seen dissipating north and westwards.

According to Cazorla et al. (2017), no significant visibility reduction was reported in the north-facing downslope areas of the Tell Atlas and in the Rif Mountains, close or at the coast of Algeria and Morocco. This indicates that dust was uplifted before passing over the northern slope of the Atlas Mountains and the North African coast.

Vertical distribution of desert dust

The vertical distribution of aerosol concentrations can be studied using lidar data. Aerosol layers may be identified by the analysis of the range-corrected signal and particle linear depolarization ratios allow the identification of dust. Figure 5.10 shows the evolution of the aerosol layer above Évora (38.6ºN, 7.9ºW), from 20 to 22 February 2016. The Saharan dust layer comprises heights from 2.5 to 3.5 km on February 20 at night. The aerosol layer then descends towards surface levels. Indeed, surface air quality monitoring stations show high PM concentrations after February 21 09H.

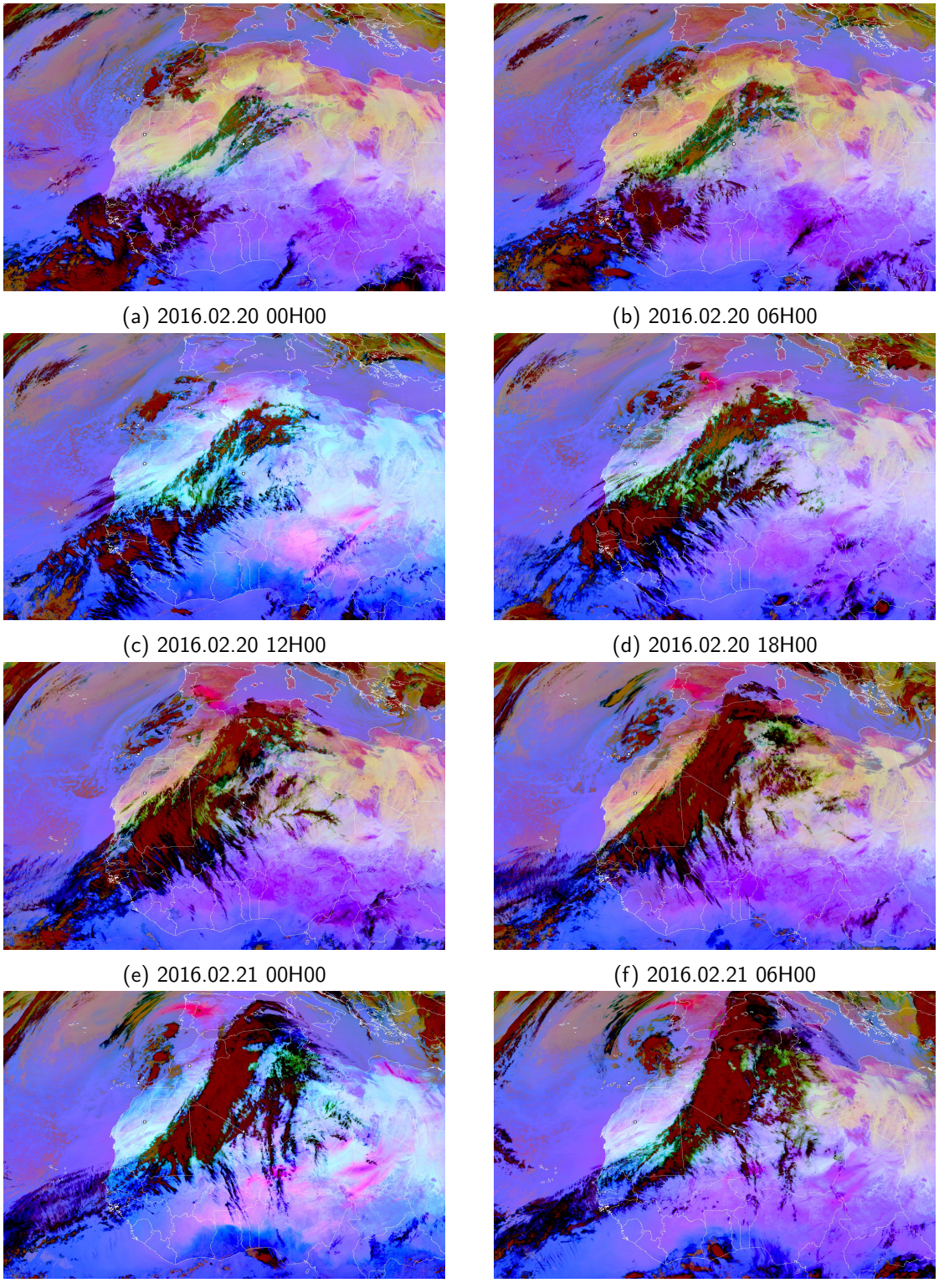

(a) 2016.02.20 00H00 (b) 2016.02.20 06H00

(c) 2016.02.20 12H00 (d) 2016.02.20 18H00

(e) 2016.02.21 00H00 (f) 2016.02.21 06H00

(g) 2016.02.21 12H00 (h) 2016.02.21 18H00

Figure 5.9: Dust RGB Composite from SEVIRI.

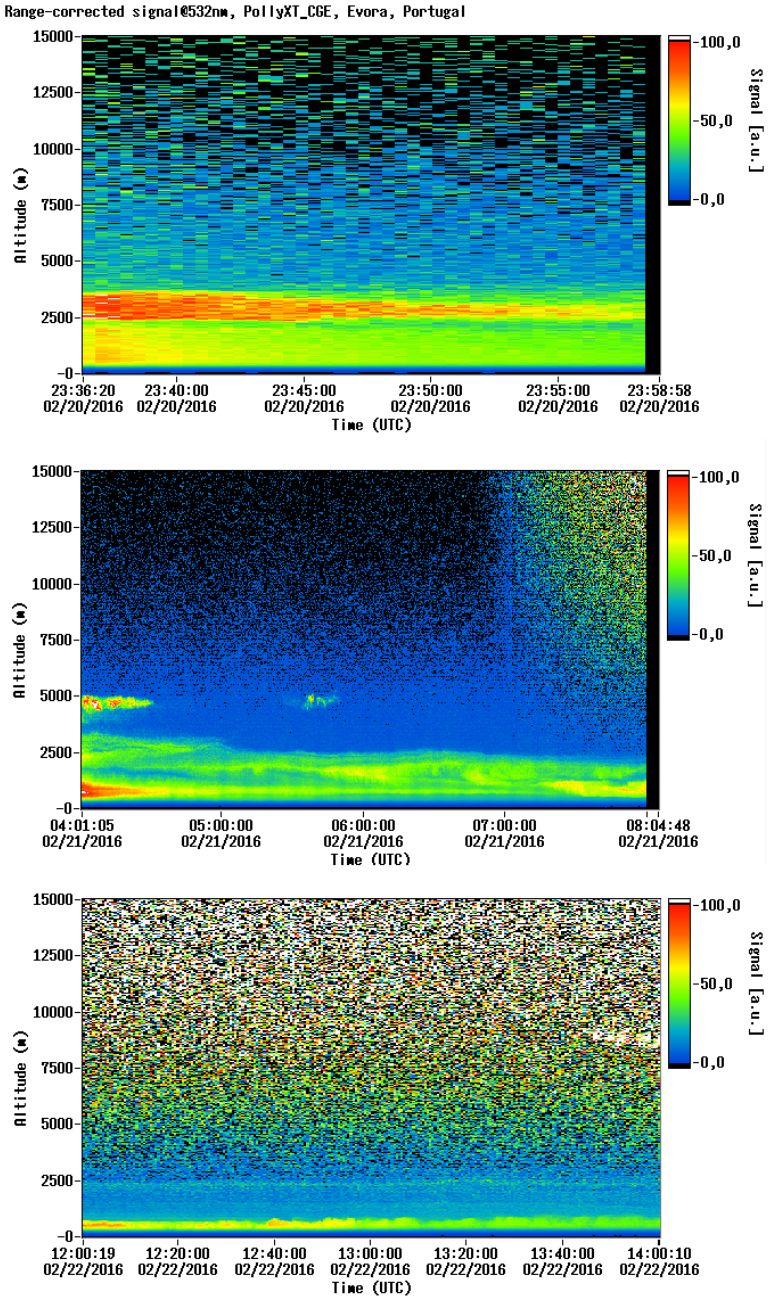

Figure 5.10: Lidar measurements of the range-corrected signal at 532 nm [available at http://polly.rsd.tropos.de].

Model performance

Figure 5.11 shows model simulation results (aerosol optical depth) for the coarser domain, from the operational forecast (125 x 125 km^2 resolution) and from an experimental simulation (27 x 27 km^2), both runs using the dust production model by Alfaro and Gomes (2001).

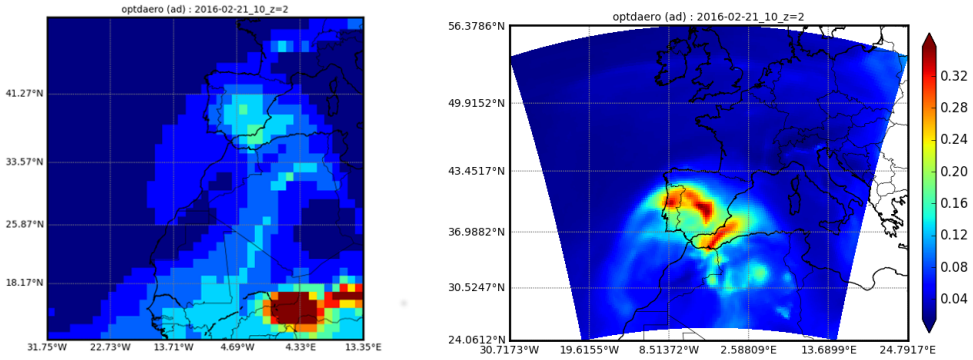

Figure 5.11: Aerosol optical depth simulated by WRF-CHIMERE for Feb 21 10H, with different model domains and resolution. Left map shows results with a 125 x 125 km^2 and right map shows results with a 27 x 27 km^2 horizontal resolution.

Considering the coarser domain, model resolution plays a big role in the model outputs. Both emissions and transport are affected by this increase in model resolution. However, when we look to the inner domain, differences are not so important. Figure 5.12 shows surface concentrations modelled by the four different forecast configurations, and also observations, during this unusually intense dust outbreak.

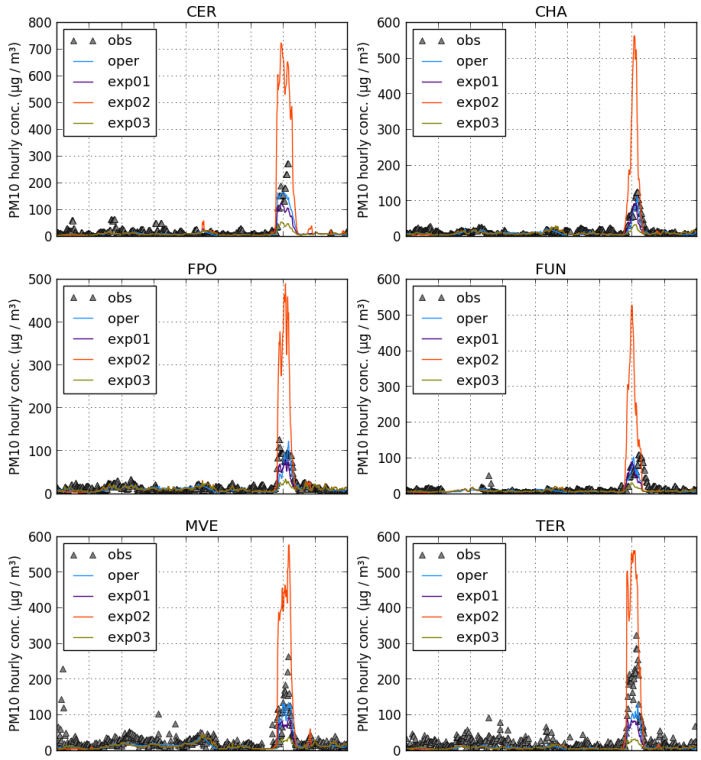

Figure 5.12: PM10 concentrations observed and modelled by the four different forecast configurations, for rural background Portuguese monitoring stations with available data during February 2016 dust outbreak.

From the analysis of Figure 5.12, the simulation exp02, considering Marticorena and Bergametti (1995) dust production model, is highlighted, predicting much higher surface concentrations than the others. Moreover, results obtained with this parametrization are much higher than observations. On the other hand, results from simulation exp03, with Kok et al. (2014) dust production model, appear to be lower than observations. From this very preliminary analysis, the Alfaro and Gomes (2001) parametrization is the one which originates the best agreement between observations and model results, for PM concentrations in Portugal.

The evolution of the aerosol optical depth predicted by the forecasts using Alfaro and Gomes (2001) is shown in Figures 5.13. In addition, Figure 5.14 shows the evolution of aerosol vertical profiles over Évora, modelled by CHIMERE. By comparing, qualitatively, modelled optical depth with dust RGB maps (Figure 5.9) and dust vertical distribution modelled over Évora with vertically resolved lidar particle backscatter coefficients (Figure 5.10), we can say model appears to be in agreement with observations.

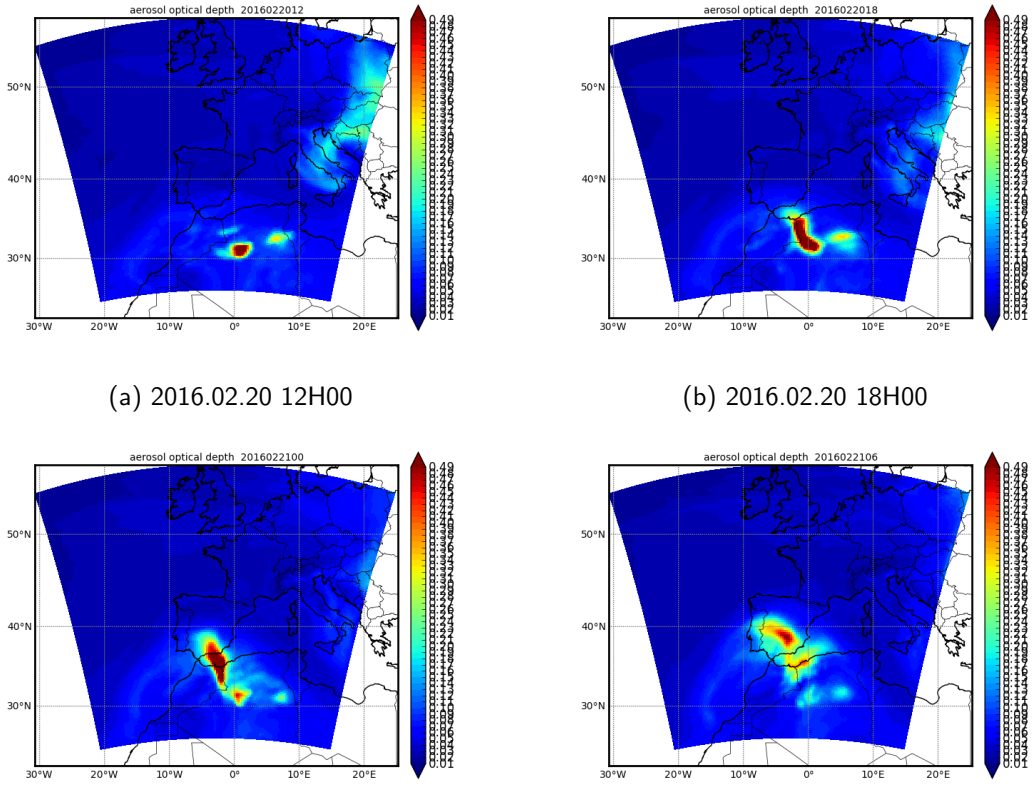

(a) 2016.02.20 12H00

(b) 2016.02.20 18H00

(c) 2016.02.21 00H00

(d) 2016.02.21 06H00

Figure 5.13: Aerosol optical depth over the outermost domain, simulated by WRF-CHIMERE exp01, between Feb 20 and 21, 2016. *(cont.)*

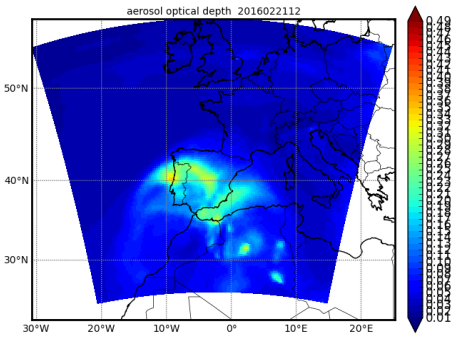

(e) 2016.02.21 12H00

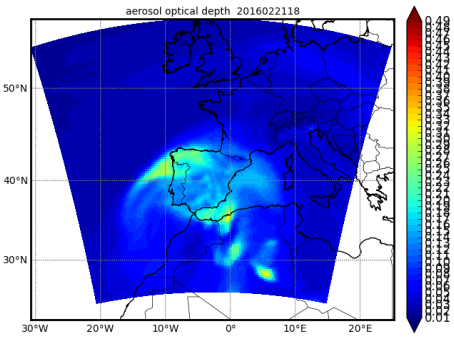

(f) 2016.02.21 18H00

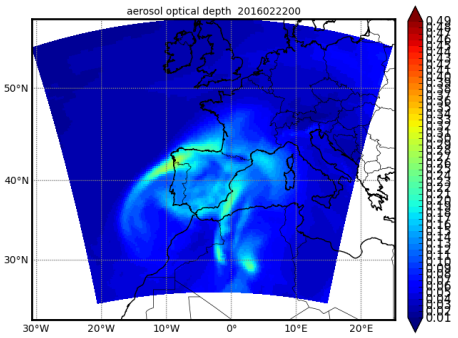

(g) 2016.02.21 00H00

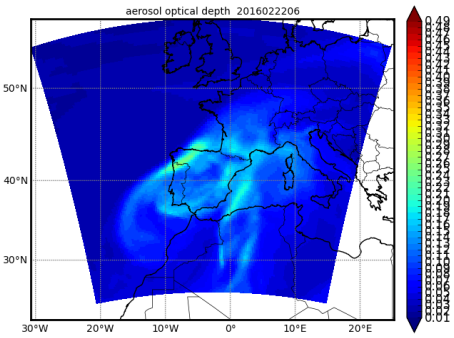

(h) 2016.02.21 06H00

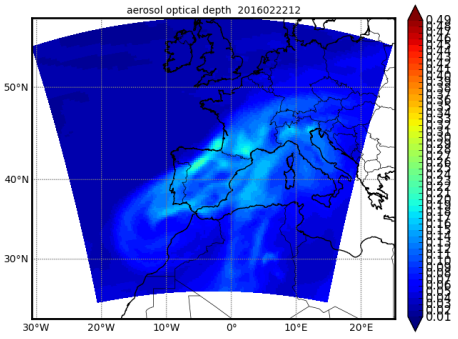

(i) 2016.02.21 12H00

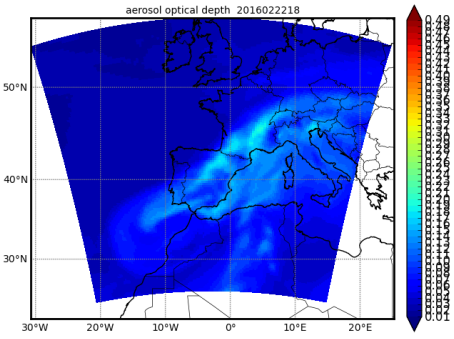

(j) 2016.02.21 18H00

Figure 5.13: Aerosol optical depth over the outermost domain, simulated by WRF-CHIMERE exp01, between Feb 20 and 21, 2016.

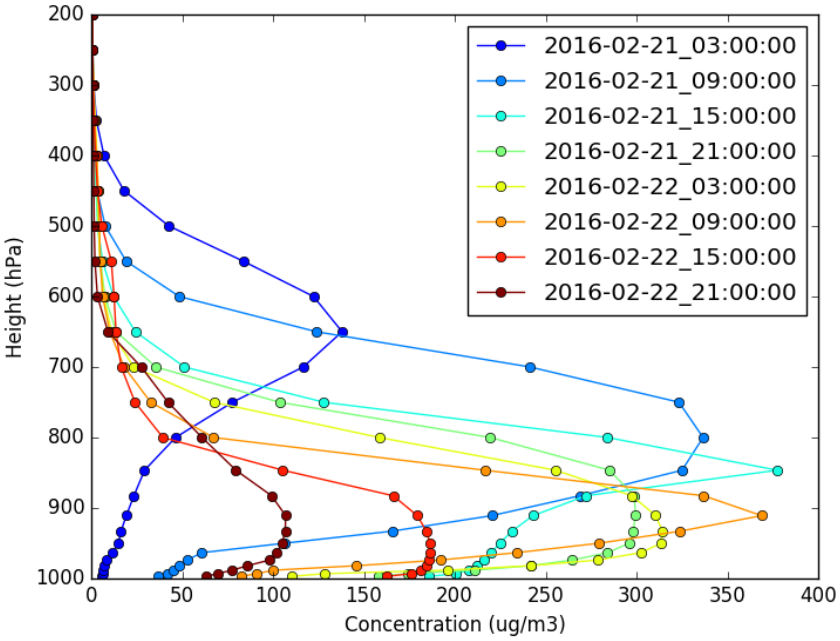

Figure 5.14: Vertical profiles of dust concentrations over Évora, modelled by WRF-CHIMERE.

5.4.2 A one-year period analysis

The modelled concentrations by the operational forecast and "experimental" simulations are compared with the observations from the national air quality monitoring network for a complete year. Figure 5.15 shows the annual mean PM10 concentrations for the four different simulations, as well as the observed mean values.

Simulations exp02, using the dust production model of Marticorena and Bergametti (1995) predict the highest PM concentrations over Portugal. Results with Kok et al. (2014) or with Alfaro and Gomes (2001) yield similar values for annual mean concentrations over Portugal. Differences between oper and exp01 are related to the experimental domains and resolution only, since both simulations run with Alfaro and Gomes (2001) dust production model. Higher resolution allows better details, particularly in Center and North coast, and in Lisbon area. We think this is related to a better resolution of the anthropogenic emissions, which are downscaled for the model grid resolution during CHIMERE pre-processing step.

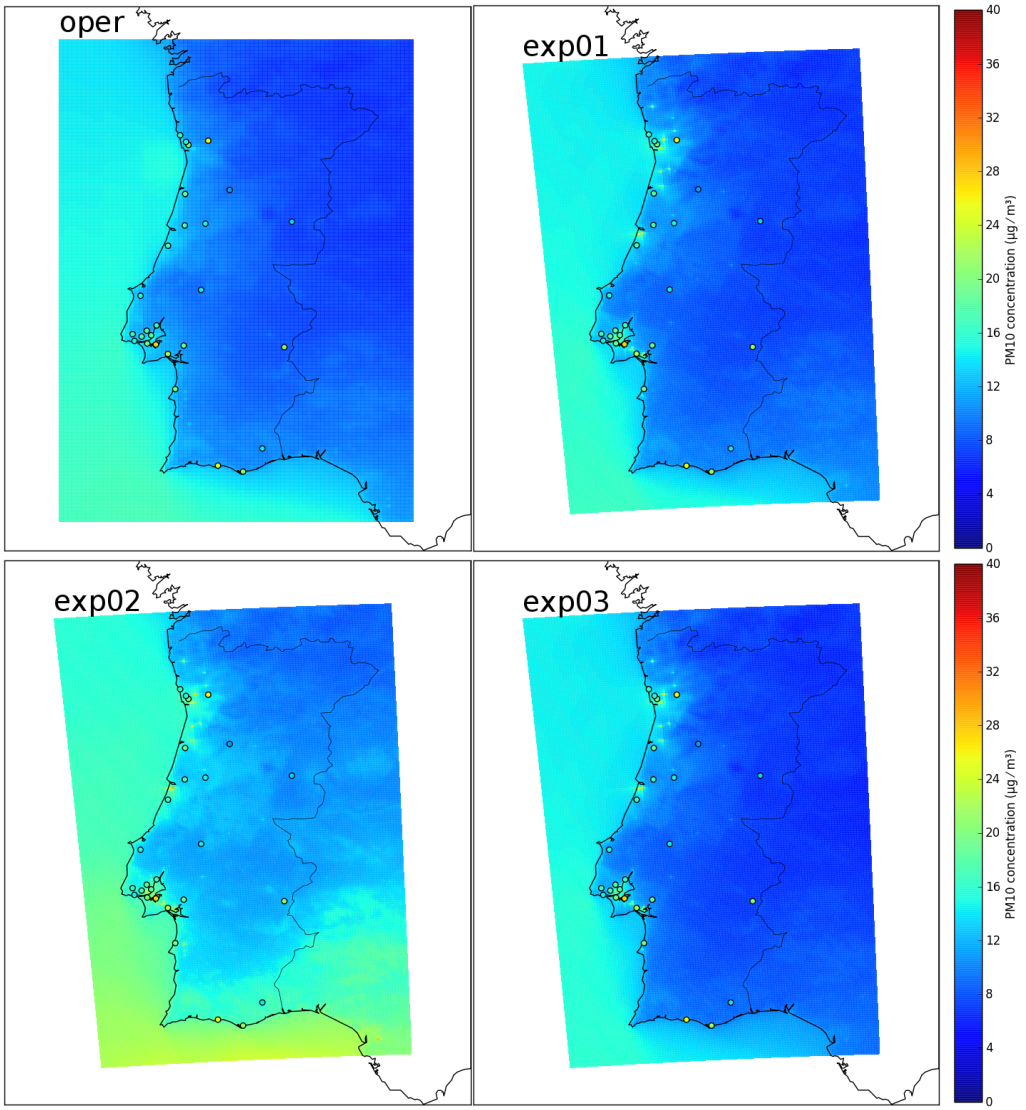

Figure 5.15: Maps of PM10 annual mean concentrations during 2016, as modelled by WRF-CHIMERE assuming, from left to right and top to bottom: (oper) operational forecast, using Alfaro and Gomes (2001) parametrization for dust emission; (exp01) Alfaro and Gomes (2001) parametrization for dust emission and higher resolution domains (exp02) Marticorena and Bergametti (1995) parametrization for dust emission and higher resolution domains; (exp03) Kok et al. (2014) parametrization for dust emission and higher resolution domains. All maps include in circles the mean PM10 concentrations observed during 2016 in background monitoring sites.

To assess model agreement with observations in a daily basis, Taylor diagrams (Taylor, 2001) are presented in Figure 5.16, relative to PM10 in urban, suburban and rural monitoring sites. The Taylor diagram is one of the more useful methods for evaluating model performance, since it provides a way of showing simultaneously how three complementary model performance statistics vary: the correlation coefficient (R), the standard deviation (sigma) and the root-mean-square (RMS) error.

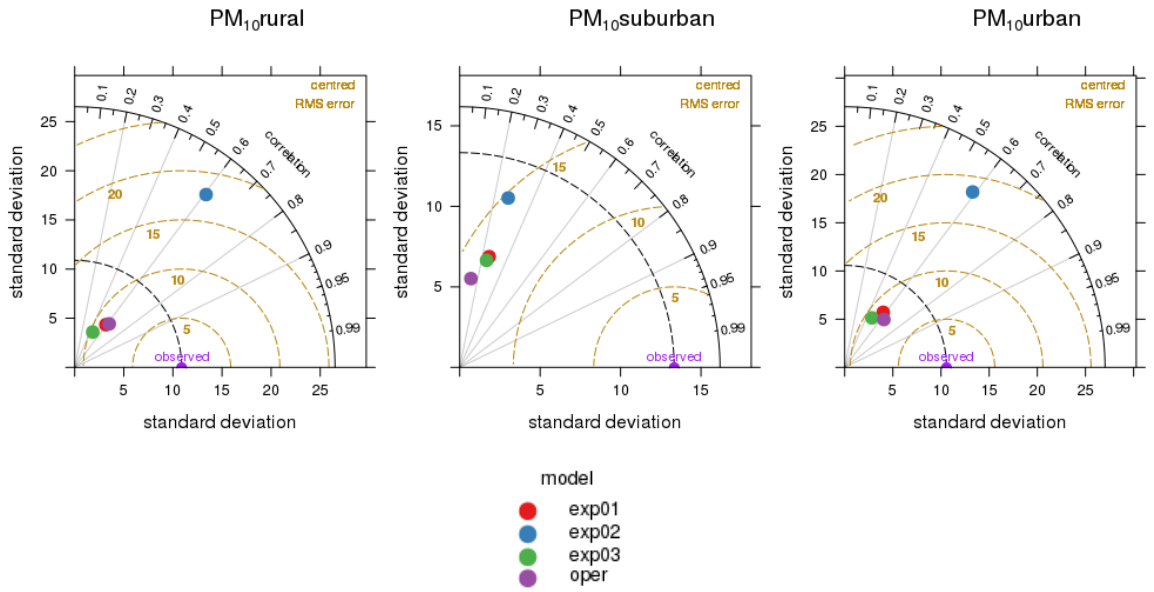

Figure 5.16: Taylor diagrams relative to the WRF-CHIMERE performance for four different configurations (oper, exp01, exp02 and exp03, defined in Table 5.3), used to predict PM10 concentrations at (top left) rural background, (top right) suburban background, and (bottom) urban background monitoring sites.

In Taylor diagrams, concentric dashed lines emanating from the 'observed' point show the value of the RMS error. Variability in the observations and model results is represented by the standard deviation, which is measured as the radial distance from the origin of the plot. The correlation coefficient is shown on the arc and points that lie closest to the x-axis have the highest correlation.

The analysis of the Taylor diagrams highlights exp02 simulations, which results show higher variability than with other model set-ups. For rural and urban sites, forecasts produced with this set-up, using Marticorena and Bergametti (1995) parametrization have more variability than observations (they extend beyond Taylor diagrams' dashed line). This behaviour is not seen in the suburban sites, probably because suburban sites have the highest PM10 observed concentrations, with a huge variability (see Chapter 4).

The statistical indicators obtained with oper, exp01 and exp03 simulations are similar: correlation coefficients between 0.4 and 0.6 and RMS errors between 8 and 10 $\mu g\,m^{-3}$, in rural and urban sites. The four WRF-CHIMERE simulations show a lower performance at suburban sites, with higher RMS errors and lower correlation coefficients (R values below 0.3). This indicates the difficulty of models to simulate PM10 concentrations in suburban areas. It is in this group of stations that the highest improvement due to increase in model resolution, from oper to exp01, occurs.

From the results already presented, the simulations using Alfaro and Gomes (2001) dust production model and the new domains with higher spatial resolution are the ones that better describe reality. Figure 5.17 shows the monthly mean PM10 concentrations, modelled with the selected setup, as well as the observed mean values. Moreover, Figure 5.18 shows scatter plots of observed and modelled PM10 concentrations with this configuration, for all background sites with valid data for 2016.

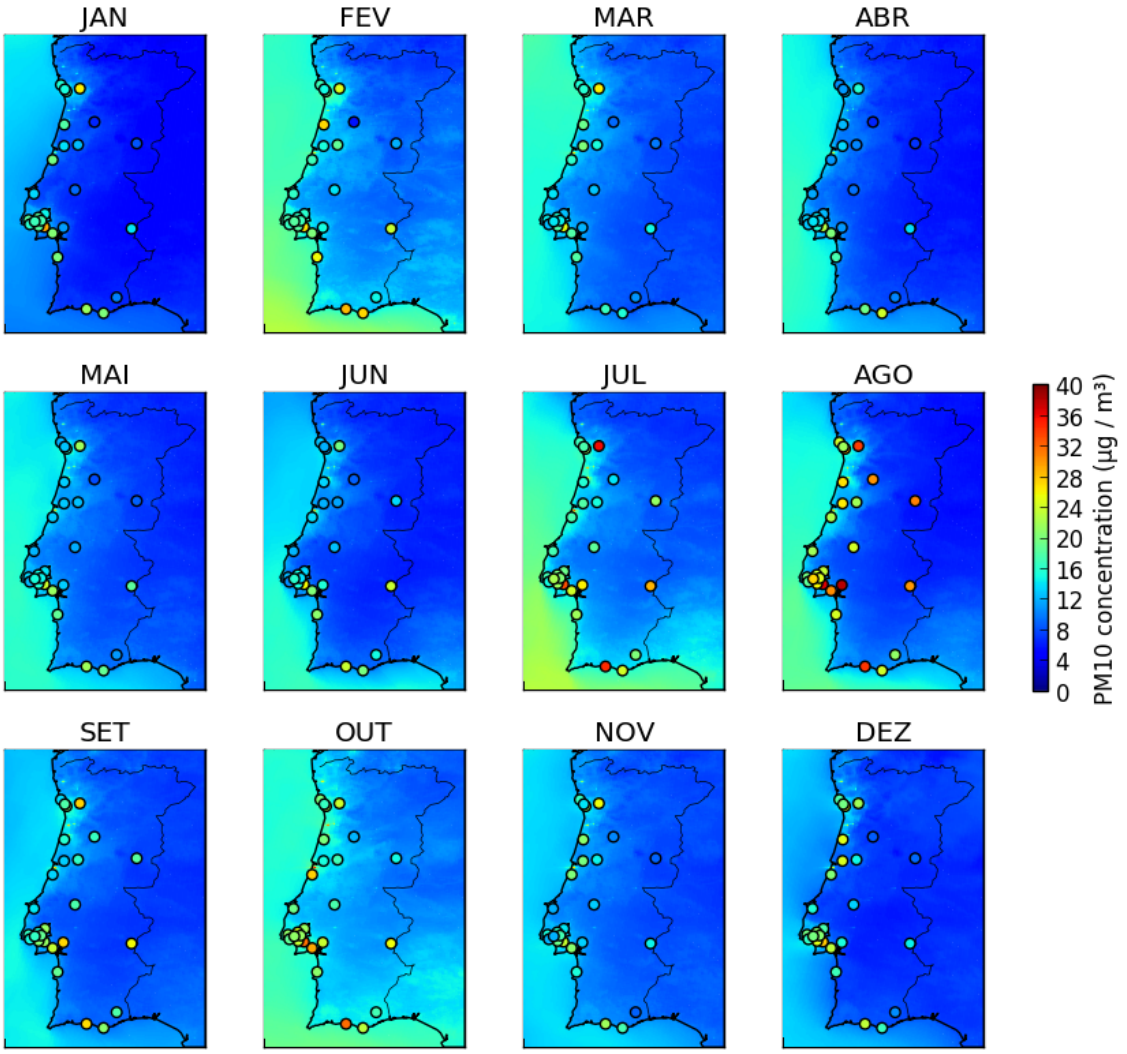

Figure 5.17: Spatial distribution of monthly mean PM10 concentrations, modelled by WRF-CHIMERE exp01, for the year 2016. The monthly mean PM10 concentrations observed in background monitoring sites are shown in circles.

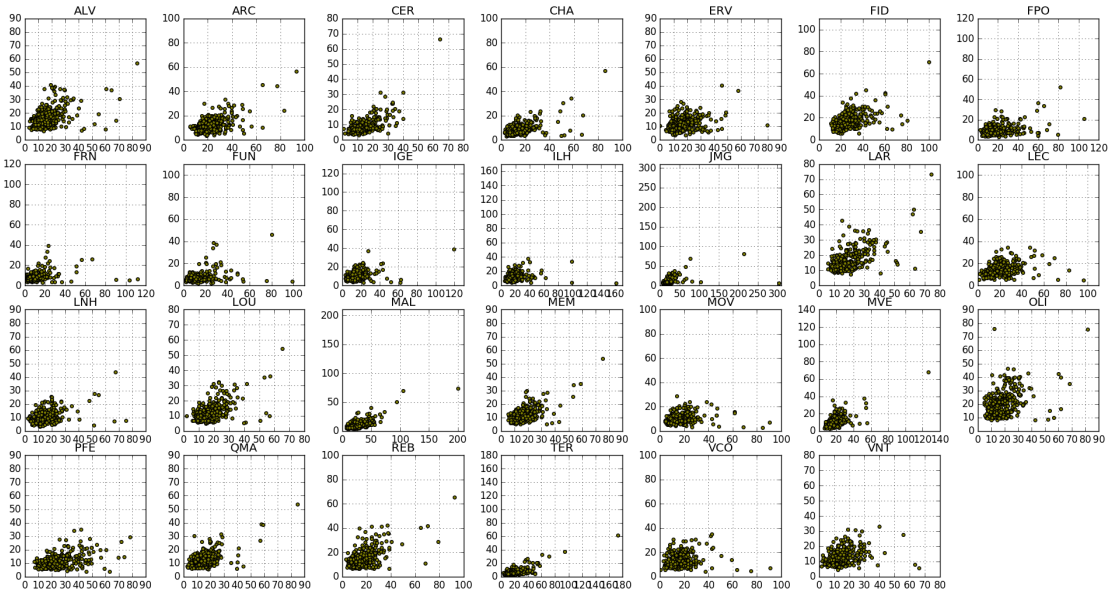

Figure 5.18: Scatter plots of observed (x-axis) and modelled (y-axis) PM10 daily mean concentrations, for the different background monitoring stations, during 2016. Modelled values are the ones simulated by WRF-CHIMERE exp01.

An important feature of a forecast model is its ability to correctly predict peak concentrations, namely PM10 daily concentrations above 50 $\mu g\, m^{-3}$ since this is the limit value for the protection of human health established in the Air Quality Directive. Table 5.5 presents the performance parameters of the different model configurations in forecasting PM10 exceedances, calculated considering the 27 background monitoring stations with more than 75% of valid data recorded during 2016.

Table 5.5: Thresholds exceedance forecast.

	days x sites	Rural 3122	Suburban 1283	Urban 4312
successfully forecasted	oper	7 (11%)	0 (0%)	13 (13%)
	exp01	5 (8%)	0 (0%)	15 (14%)
	exp02	20 (33%)	2 (8%)	38 (36%)
	exp03	0 (0%)	0 (0%)	0 (0%)
false alarms	oper	0 (0%)	0 (0%)	0 (0%)
	exp01	0 (0%)	0 (0%)	1 (0%)
	exp02	58 (2%)	18 (1%)	110 (3%)
	exp03	0 (0%)	0 (0%)	1 (0%)
non predicted	oper	55 (89%)	25 (100%)	94 (88%)
	exp01	57 (92%)	25 (100%)	92 (86%)
	exp02	42 (68%)	23 (92%)	69 (64%)
	exp03	62 (100%)	25 (100%)	107 (100%)

The two simulations which use Alfaro and Gomes (2001) dust production model (oper and exp01) show very similar skills (8-11%, 0% and 13-14% of success in forecasting peak concentrations, for rural, suburban and urban monitoring stations), despite their differences regarding domains and resolution. Although the experimental forecast exp02 shows better scores in successfully forecasting PM10 daily concentrations above $50\,\mu g\,m^{-3}$ (33%, 8% and 36% for rural, suburban and urban monitoring stations, respectively), it has a huge number of false alarms, e.g., days when an event is forecasted but not observed. The number of false alarms is even higher than the successfully forecasted ones, which indicates that probably the model is simulating high PM10 concentrations due to the wrong reasons. The experimental forecast configurations which have the better results are oper and exp01. Despite the lower success in forecasting the observed events than exp02, these set-ups have none or only one false alarm in one location during the year. Results with exp03 show the same false alarm such as exp01; however, simulations with Kok et al. (2014) dust production scheme do not forecast any of the 194 exceedances which were observed.

In order to investigate possible reasons for the model failure to forecast days with PM10 mean concentrations above $50\,\mu g\,m^{-3}$, we select all the days of 2016 when the exp01 simulation (the one using Alfaro and Gomes (2001) dust production scheme and the new domains with higher resolution) does not predict the observed exceedances in more than two monitoring stations. This exercise reveals five PM10 episodes, which are identified and characterized below. To allow a broader view of these five episodes, Figure 5.19 shows the mean modelled and observed PM10 concentrations spatial distribution, for the different periods.

- **February 21-22**: The exceedances observed in these two days are a result of an unusually intense dust outbreak that affected the Iberian Peninsula. The exp01 simulations fail to simulate exceedances in the monitoring stations located in the Centre and North of Portugal.
- **August 08-13**: During this period, Portugal battled numerous wildfires, mostly in the Centre and North of the country. A dust event was reported by the Portuguese Environment Agency during this period, however that event is not simulated by the model (see Figure 5.19). This event will be studied in more detail in the next Chapter.
- **September 05-07**: During this period, Portugal also battled numerous wildfires, mostly in the Centre and North of the country. A dust event is also reported, and simulated by the model.

- **October 27-28**: The PM10 concentrations observed in these two days are a result of a dust outbreak that affected Portugal. The experimental forecast exp01 is able to describe the dust emissions and transport to Portugal. Nevertheless, due to a small bias, the model fails to forecast exceedances to the limit value for the protection of human health.

- **December 21-22**: After December 17, Portugal was under the influence of an intense high synoptic system. The weather was characterized by clear skies and weak wind. From December 17 till the end of the month the temperatures were below the average values and the 20th of December is highlighted in IPMA (2017) as a very cold day in the Centre and North regions. This information suggests that the exceedances observed during these days should be related with (i) an increase in the emissions due to intense domestic heating and (ii) stable atmospheric conditions which favour the accumulation of pollutants close to their sources.

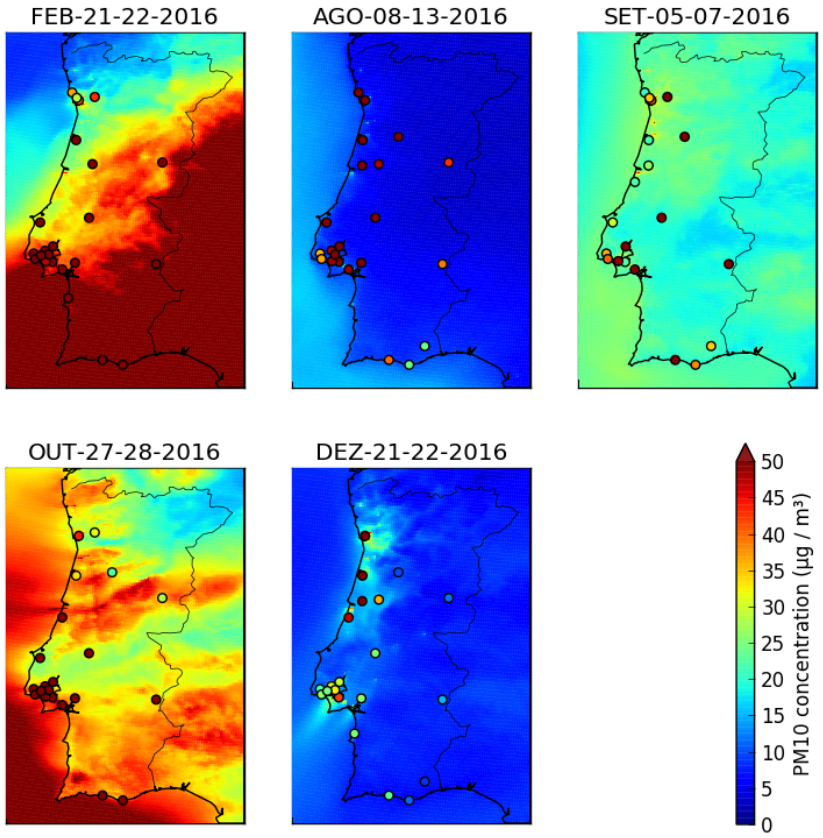

Figure 5.19: Spatial distribution of mean PM10 concentrations, modelled by WRF-CHIMERE exp01, and observed in background monitoring sites (in circles), for the five PM10 episodes identified during 2016, in which in which model failed to forecast excedaance days in more than two monitoring stations.

5.5 Summary and conclusions

In this Chapter, the Portuguese operational forecast system was presented and its aerosol modelling performance assessed. Moreover, "experimental" air quality forecasts were implemented for the whole year 2016, focusing on model resolution and mineral dust production schemes.

Model resolution strongly affects results in the coarser domain. Indeed, the coarser domain is the one in which the increase in resolution between simulations is higher - horizontal resolution increased from 125 x 125 km^2 to 27 x 27 km^2. In terms of the inner domain, the resolution increased from 5 x 5 km^2 to 3 x 3 km^2. Annual mean concentrations seem to have higher details in the higher resolution concentrations (see Figure 5.15). However, statistics computed for the background monitoring sites, which include the ones depicted in the Taylor Diagrams and threshold exceedance skills, do not show such an important increase in the quality of the forecasts with the increase in resolution, for the inner domain.

The forecast system underestimates the variability of the background particulate matter over Portugal. In addition, PM concentrations are in most cases strongly underestimated. The modelling of African dust outbreaks within the Portuguese operational air quality forecasting system is crucial to correctly simulate the PM levels over the country. The operational model configuration slightly under predicts PM levels during strong Saharan dust events.

During 2016, five pollution episodes were identified in which modelling failed to forecast daily PM10 concentrations above 50 $\mu g\, m^{-3}$ - or excedaance days, in more than two monitoring stations. Each of these episodes was analysed in order to identify possible causes for model mismatch. Two of these episodes are linked to dust outbreaks, which are reproduced by the model, however with slightly underestimation. Two other episodes are linked with forest fires - possibly with forest fires and dust storms. Forest fire emissions are not included in the air quality forecast system, and this is a major need for the future, due to the massive influence of forest fires in air quality over Portugal. The last episode which was identified corresponds to very cold and stable atmospheric conditions. The analysis of this episode is planned as future work, focusing on synoptic conditions and on domestic heating emissions.

An anomalous episode of high PM10 concentrations due to a Saharan dust outbreak was observed on February 2016. This episode was firstly characterized based on observations. Then, the same

episode was chosen to evaluate the operational and "experimental" forecast systems. The dust production model by Alfaro and Gomes (2001), already in use in the operational system, proves to be the best of the three parametrisations assessed. The resolution to implement must be decided taking into account computational effort and available resources.

The inclusion of desert dust emissions is very important to consider realistic dust boundary conditions for particulate matter simulations and forecast over Portugal. Regarding anthropogenic emissions, a new official emission inventory was recently launched for Portugal; it includes a better spatial resolution (about 10 x 10 km^2, instead of the previous 50 x 50 km^2). This data will be soon included in the air quality forecast system and better results are expected.

The results presented and discussed through this Chapter were not corrected using post-processing techniques. Bias correction techniques (e.g. Borrego et al., 2011; Mok et al., 2017; Monteiro et al., 2013) must be explored in the future, in order to improve the match between forecasts and observations.

Chapter 6

Saharan dust contribution to PM10 and PM2.5 levels in Portugal

This chapter is based on: Gama, C., Monteiro, A., Borrego, C., Pio, C., Baldasano, J.M., Tchepel, O. Comparison of different methodologies for assessing desert dust contribution to regional PM10 and PM2.5 levels: a one-year study over Portugal. submitted to Aeolian Research.

6.1 Introduction

Particulate matter concentrations in the atmosphere are influenced by several natural and anthropogenic sources. Amongst the natural processes, long-range transport of dust emitted from deserts and other arid areas may affect air quality, severely. Those contributions from natural sources to PM levels can be assessed but cannot be controlled.

Where natural contributions to pollutants in ambient air can be determined with sufficient certainty and when exceedances are due in whole or in part to natural contributions, the European Air Quality Directive (Directive 2008/50/EC) allows to subtract those natural contributions when assessing compliance with air quality limit values.

Currently, one of the official methods (EC, 2011) adopted by the European Commission for evaluating the occurrence of African dust outbreaks and quantifying its contributions, and the one adopted by the Portuguese Environmental Agency, is a statistical approach published by Escudero

et al. (2007) based on the variability of rural background sites. The feasibility of this method was demonstrated by comparing experimentally measured concentrations of mineral matter determined at three Spanish rural background sites (Monagrega and Montseny, both located in the Eastern part of the Iberian Peninsula, and Bellver, located in the Balearic Islands) versus the estimated African dust contributions obtained by this procedure.

In this Chapter, we will apply Escudero's statistical approach to one year of particulate matter concentrations over Portugal (hereafter referred to as P40), and will compare the results to our model estimates. Moreover, the quantification of the exceedances will be performed for the different estimates.

6.2 Methodologies for assessing dust contribution to particulate matter levels

The official method adopted by the Portuguese Environmental Agency to calculate daily African dust contributions to PM10 and PM2.5 is a statistical methodology applied to PM data series. It is based on the application of 30 days moving 40th percentile to the PM10 or PM2.5 data series, after excluding those days impacted by African dust. The days impacted by African dust should be identified based on various data and information, including satellite observations, model back-trajectories and dust forecast models. For each day affected by African dust a percentile value is obtained, which is assumed to be the theoretical background concentration of PM without African dust input. After that, the African dust contribution is obtained by difference between the experimental PM10 or PM2.5 concentration and the calculated 40th percentile value. This methodology was initially published considering the 30th percentile (Escudero et al., 2007). For conservative reasons, the 40th percentile was later adopted instead of the 30th one (EC, 2011).

This calculation is done for regional background sites, in order to obtain a daily contribution of African dust for a specific region. The estimated value may then be subtracted from the daily PM levels observed at other monitoring stations in the same region. Over Portugal, six regional background sites are usually considered for the assessment of African dust contribution to PM levels, which are identified in Table 6.1.

Table 6.1: List of QUALAR rural background stations selected as representative by the Portuguese Environmental Agency (ordered by latitude). PM10 and PM2.5 data completeness is included for the year 2016.

Code	Name	LON	LAT	height (m)	PM10	PM2.5
DRN	Douro Norte	-7.789	41.370	1086	19.1%	20.8%
FUN	Fundão	-7.300	40.232	473	92.1%	69.7%
MOV	Montemor-o-Velho	-8.677	40.183	96	79.2%	-
CHA	Chamusca	-8.468	39.353	143	98.1%	96.7%
TER	Terena	-7.398	38.616	187	98.4%	87.7%
CER	Cerro	-7.680	37.312	300	85.5%	88.5%

Other measurement-based methodologies (non model-based) to detect and quantify African dust contributions to PM levels are found in the literature. The Tel Aviv University, in Israel, developed a method (Ganor et al., 2009) which uses only PM10 and PM2.5 measurements from automatic stations. This method employs an automatic algorithm with three thresholds and does not require any other inputs such as satellite observations, model back-trajectories, dust forecast models, or mineralogical analyses. Viana et al. (2010) compared this method with the one described above, using the 30/40th percentile, and found that the percentile method is more conservative in the detection of episodes, as it is less affected by interferences from local dust sources.

Another procedure for quantifying the wind-blown desert contributions to daily average PM10 concentrations from monitoring sites was proposed by Gomez-Losada et al. (2015). This measurement-based methodology is based on the use of Hidden Markov Models. In that study, the annual average Saharan PM10 contribution in the Canary Islands, Spain, was estimated and compared to the one estimated by the P40 method. The annual contribution of North African episodes to the PM10 mean value in the Canarias Archipelago coincides markedly with the same estimation made with the P40 method.

In this Chapter, the official method adopted by the Portuguese Environmental Agency, the P40 method, is applied to air quality data over Portugal. In addition, a model-based methodology is applied and the results of both approaches compared. In the model-based methodology, the influence of African dust outbreaks on PM levels is quantified using mineral dust concentrations simulated by the WRF-CHIMERE modelling system (see Chapther 5). Numerical models run for three nested domains, applying the dust production model used in the Portuguese operational air quality forecast system (Alfaro and Gomes, 2001). High resolution simulations were performed, using a coarse domain covering Southern Europe and Sahara Desert with a horizontal resolution

of 27x27 km^2; a second domain covering Iberian Peninsula with 9x9 km^2 of horizontal resolution; and a high-resolution domain covering mainland Portugal, with 3x3 km^2.

The impact of mineral dust outbreaks on PM10 and PM2.5 ambient concentrations is calculated by the two different approaches (measurement-based and model-based) for five rural regional background sites across Portugal. Douro Norte data has not been used, due to the low quantity of available observations (see Table 6.1) during the year in analysis, 2016.

6.3 Assessment of dust contribution to PM10 and PM2.5 in Portugal, during 2016

6.3.1 Using the measurement-based methodology

During 2016, the Portuguese Environmental Agency identified in mainland Portugal 93 days (see Figure 6.1) as days impacted by African dust (APA, 2017). This identification was based on the dust forecast models BSC-DREAM8b (Basart et al., 2012b) and SKIRON (Nickovic and Dobricic, 1996), and on the HYSPLIT Trajectory Model (Draxler and Hess, 1998).

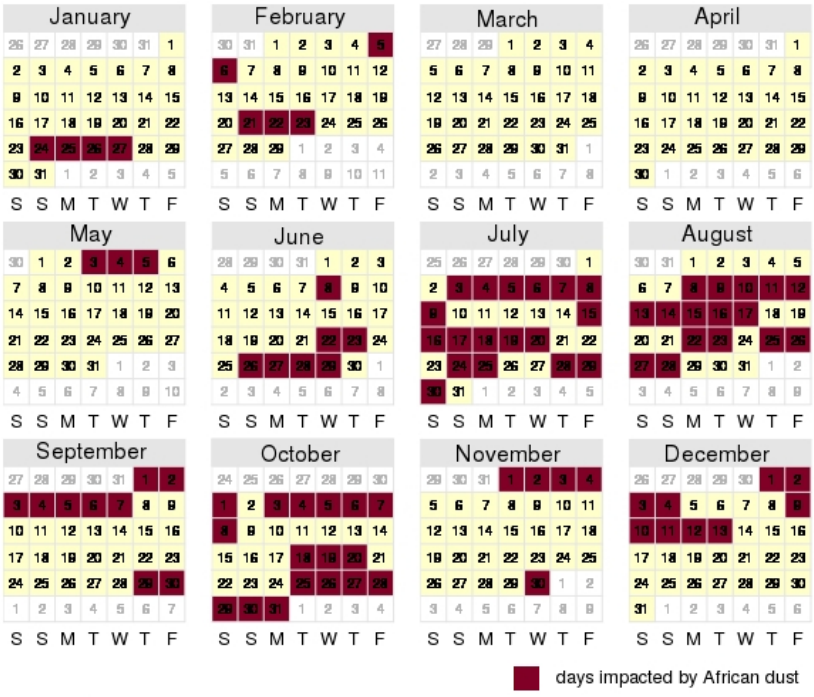

Figure 6.1: Days identified as impacted by African dust by the Portuguese Environmental Agency, during 2016.

For each day identified as impacted by African dust by the Portuguese Environmental Agency, we applied the P40 methodology (described in the previous section) in order to calculate the regional African dust contributions to PM10 and PM2.5 concentrations over Portugal. Results are presented in Figures 6.2 and 6.3, for PM10 and PM2.5, respectively.

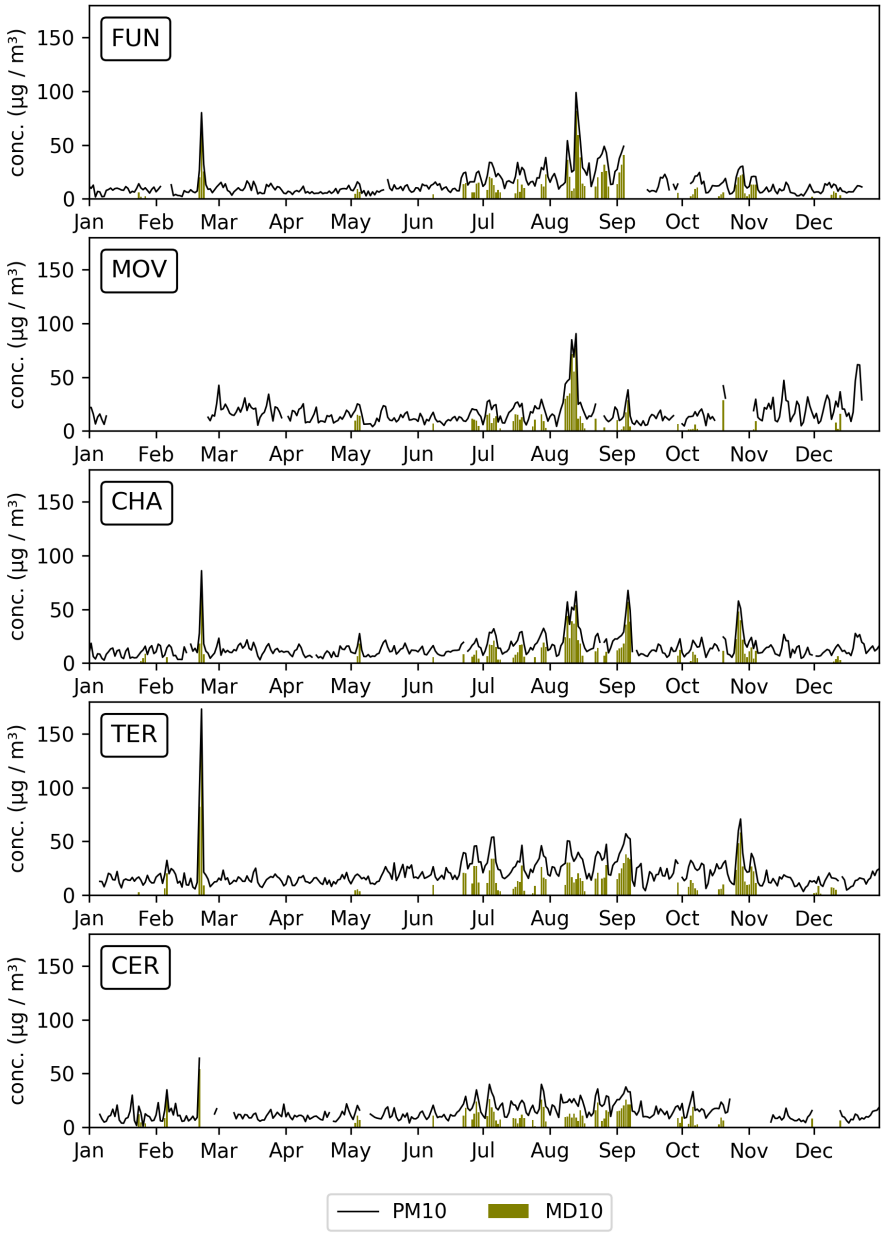

Figure 6.2: PM10 daily concentrations (black line) and natural contribution as estimated by the official method adopted by the Portuguese Environmental Agency (green bars).

African dust contribution to PM levels is evident during a specific episode in February, during several episodes from mid-June to mid-August, and also during October and November. According to the P40 method, the highest daily contribution to PM10 occur during the February episode (at

Feb 22 in TER (161 µg m^{-3}) and CHA (76 µg m^{-3}); at Feb 21 in CER, which has no measurements available during the 22nd) or at August 13 in the Centre region (FUN (82 µg m^{-3}) and MOV (77 µg m^{-3}) monitoring stations). Note that in these days, the contribution of African dust, only, is already sufficient to surpass the PM10 daily limit value (50 µg m^{-3}).

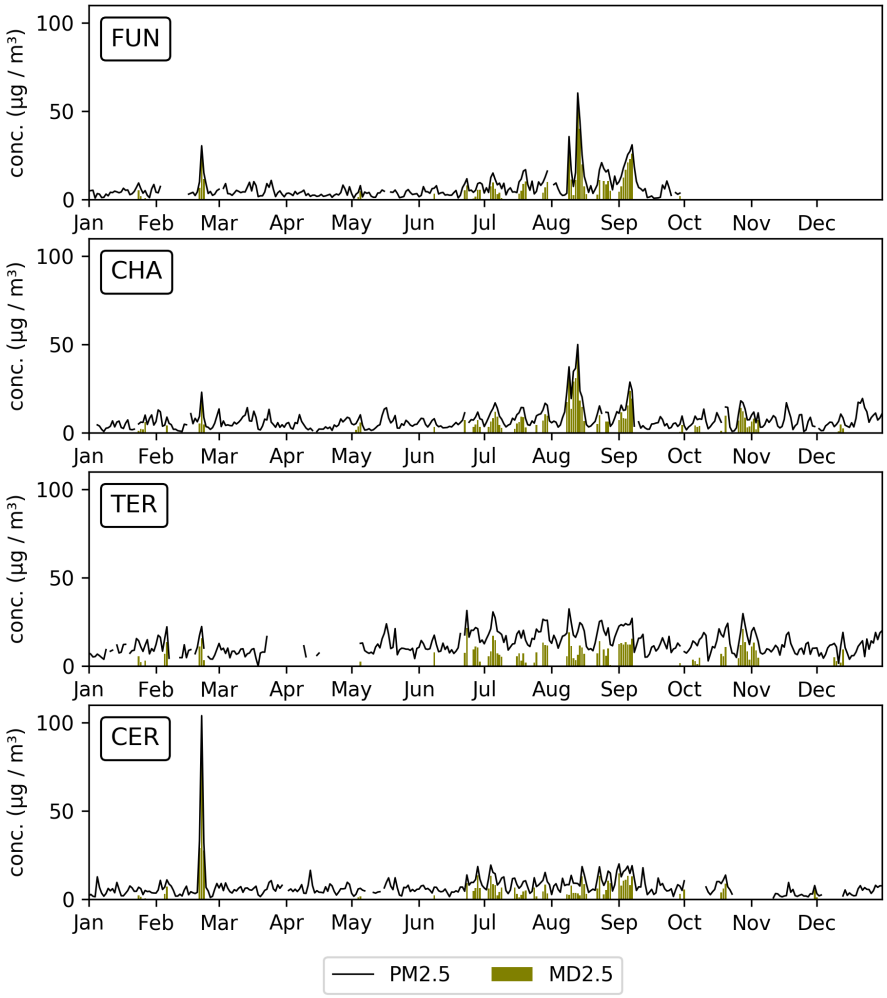

Figure 6.3: PM2.5 daily concentrations (black line) and natural contribution as estimated by the official method adopted by the Portuguese Environmental Agency (green bars).

For each station, the days when the African dust contribution is higher than a certain threshold (2 µg m^{-3} for PM10 and 1 µg m^{-3} for PM2.5) were filtered and a mean daily contribution was estimated, taking into account those days only. Results are presented in Table 6.2 for PM10 and in Table 6.3 for PM2.5.

Table 6.2: Number of days when the African dust contribution of particles with an aerodynamic diameter smaller than 10 µm (AD10) is higher than 2 µg m^{-3}, their mean and maximum daily African dust concentrations (calculated according to the P40 method). The day of the year 2016 with the maximum African dust contribution is also identified.

Monitoring station	No. days AD10>=2 µg m^{-3}	mean daily contribution (µg m^{-3})	max daily contribution (µg m^{-3})	day of occurrence
FUN	71	15.6	81.8	Aug 13
MOV	48	15.5	77.0	Aug 13
CHA	70	16.3	76.1	Feb 22
TER	79	18.9	160.9	Feb 22
CER	68	12.2	54.0	Feb 21

Table 6.3: Number of days when the African dust contribution of particles with an aerodynamic diameter smaller than 2.5 µm (AD2.5) is higher than 1 µg m^{-3}, their mean and maximum daily African dust concentrations (calculated according to the P40 method). The day of the year 2016 with the maximum African dust contribution is also identified.

Monitoring station	No. days AD2.5>=1 µg m^{-3}	mean daily contribution (µg m^{-3})	max daily contribution (µg m^{-3})	day of occurrence
FUN	48	10.7	56.2	Aug 13
CHA	72	8.8	44.4	Aug 13
TER	76	8.5	21.7	Jun 23
CER	63	8.3	99.7	Feb 22

The highest mean daily contribution of African dust to PM10 concentrations occurs in TER, which has also the highest number of days classified as impacted by African dust with a contribution higher than 2 µg m^{-3}. In this station, located in inland Alentejo, according to the P40 methodology, African dust contributes, in average, with nearly 19 µg m^{-3} of particles with an aerodynamic diameter smaller than 10 µm, during the most affected 79 days by desert dust. The fact that the mean daily contribution is lower in CER (located in Algarve) than in TER should be interpreted carefully, since CER has no valid measurements during February 22.

TER monitoring station has also the highest number of days classified as days impacted by African dust when the fraction below 2.5 µm is considered and a contribution higher than 1 µg m^{-3} is imposed. However, it registers the lowest maximum daily contribution (about 22 µg m^{-3}), which occurs on June 23. During February 22, although a contribution of 161 µg m^{-3} is estimated at this station for the particles with an aerodynamic diameter smaller than 10 µm, a contribution of 16 µg m^{-3} only is estimated for the fraction below 2.5 µm.

For the fraction below 2.5 µm (MD2.5), CER monitoring station has the highest maximum daily contribution (100 µg m^{-3}), which is registered during Feb 22. There is no PM10 available data during this day at CER. However, the fraction of MD2.5 estimated for this day is higher than the maximum daily contribution to PM10 estimated at this station during the whole year (54 µg m^{-3}, estimated for Feb 21).

In terms of mean values of African dust contribution to PM2.5 (taking into account days with a contribution higher than 1 µg m^{-3} only), FUN has the highest mean value (about 11 µg m^{-3}). However, this fact must be taken carefully, since FUN has the lowest number of days with AD $>=$ 1 µg m^{-3}, and mean values are calculated for those days only.

Table 6.4 analyses the daily and annual parameters defined in the Directive 2008/50/EC for PM10 and PM2.5 concentrations, before and after the subtraction of the African dust contributions calculated according to the P40 method.

Table 6.4: PM10 and PM2.5 annual mean concentrations, and number of days of exceedance to the PM10 daily limit value, before and after the subtraction of the African dust contributions (calculated according to the P40 method).

Monitoring station	PM10 annual mean (µg m^{-3})		exceedances PM10 (number)		PM2.5 annual mean (µg m^{-3})	
	before	after sub	before	after sub	before	after sub
FUN	13.5	10.2	5	0	6.6	4.6
MOV	17.3	14.7	5	2	–	–
CHA	14.5	11.3	7	0	7.2	5.4
TER	20.7	16.5	11	0	12.7	10.7
CER	14.3	11.7	1	0	7.0	5.4

In terms of terms of annual values, the average contribution of desert dust to the PM10 and PM2.5 concentrations is about to 3 µg m^{-3} (4 µg m^{-3} in TER) and 2 µg m^{-3}, respectively, roughly in the five regions in analysis. Regarding the number of exceedances to the PM10 daily limit value, TER station registers the highest number of days of exceedances attributable to African dust (11 days). This value seems to decrease from South to North, as is expected, with CHA presenting 7 days of exceedances, and the monitoring stations in the Centre presenting between 3 and 5 days of exceedances attributable to African dust. The exception to this behaviour is CER monitoring station, located in the southernmost region of continental Portugal, which has only one day of exceedance attributable to African dust.

6.3.2 Using a model-based methodology

Model results point to an important contribution of natural sources to PM10 and PM2.5 concentrations over Portugal. Figures 6.4 and 6.5 show the monthly mean mineral dust concentrations, modelled with WRF-CHIMERE, for the fractions with aerodynamic diameters below 10 µm and 2.5 µm, respectively. During 2016, WRF-CHIMERE results indicate October, February and July as the months with the highest contributions of desert dust to the PM10 levels over Portugal. During October, African dust contributes, in average, with between 4 and 9 µg m^{-3} to PM10 concentrations. On the contrary, January and April have the lowest contribution, with mean contributions lower than 2 µg m^{-3} through the whole country. For PM2.5, the contribution estimated according to model results, during October, is also higher than during other months. African dust contributes, in average during this month, with between 2 and 4 µg m^{-3} to PM2.5 concentrations. During January, the contribution is the lowest, with mean values lower than 1 µg m^{-3} throughout Portugal.

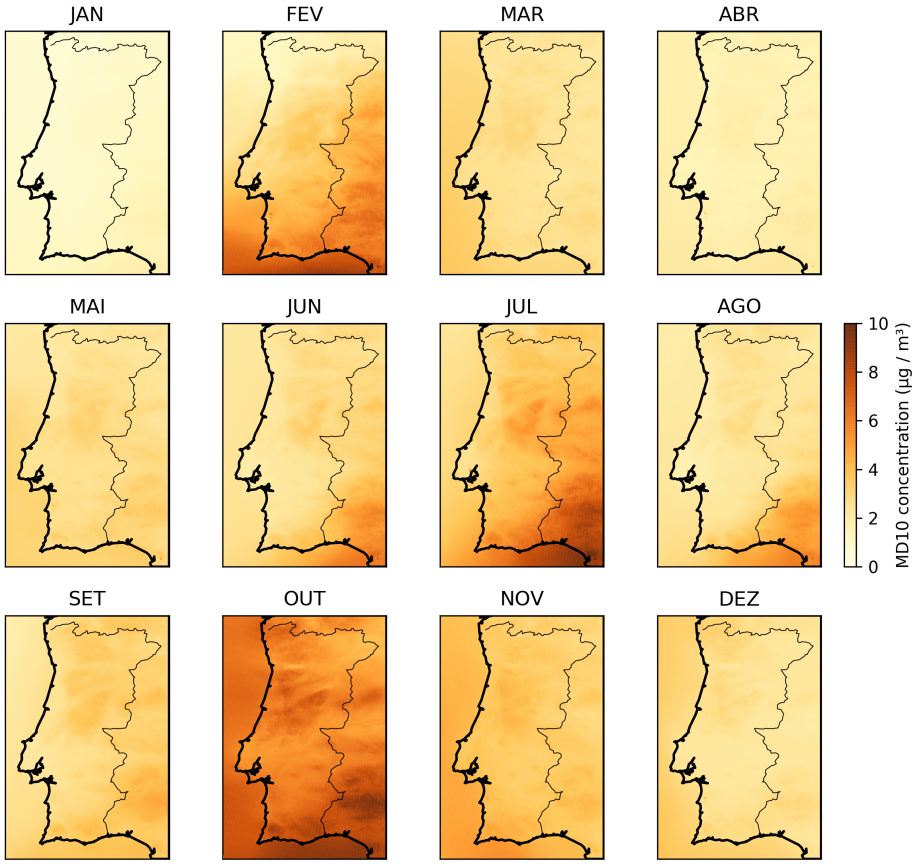

Figure 6.4: Spatial distribution of monthly mean concentrations of mineral dust particles with an aerodynamic diameter smaller than 10 µm, modelled by WRF-CHIMERE, for the year 2016.

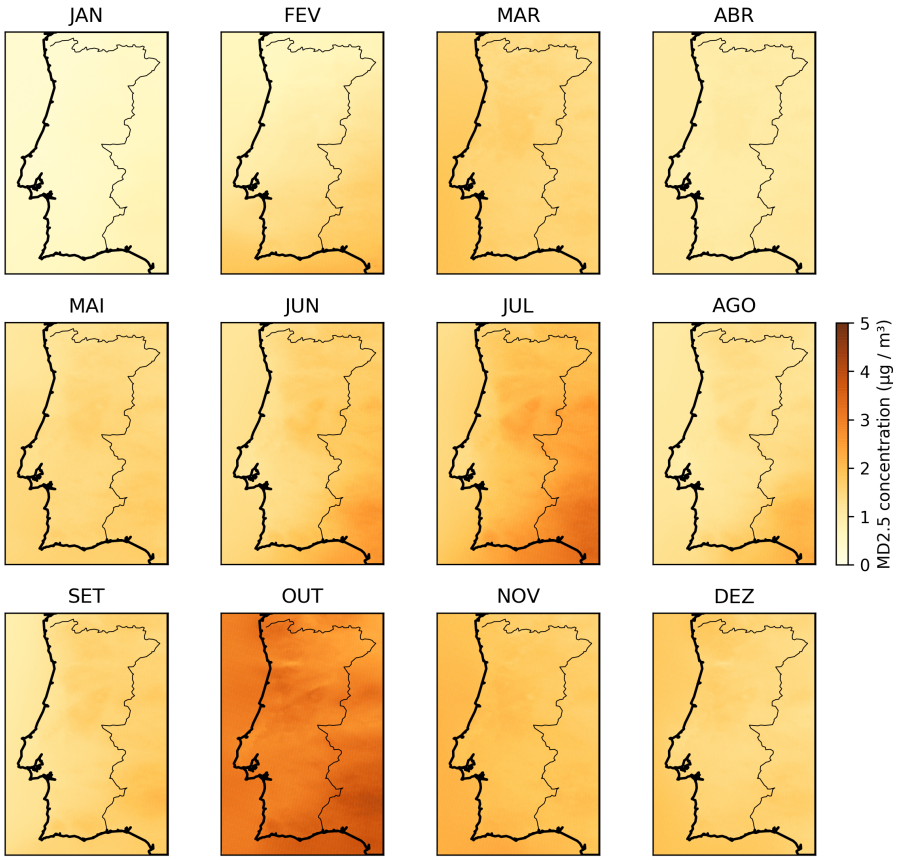

Figure 6.5: Spatial distribution of monthly mean concentrations of mineral dust particles with an aerodynamic diameter smaller than 2.5 µm, modelled by WRF-CHIMERE, for the year 2016.

Modelled mineral dust surface concentrations over Portugal were previously explored by Monteiro et al. (2015), focusing on the year 2011. In that previous study, BSC-DREAM8b model results indicated a strong contribution of dust to the aerosol over Portugal during April and May. However, Basart et al. (2012b) point out the model overestimates dust activity in Northern Algeria when compared to satellite estimates, affecting thus the dust transported towards the Western Mediterranean mainly in spring. Although the year in analysis is distinct, our results do not highlight April and May as months with higher desert dust influence over Portugal. Significant inter-annual variations in African dust events and their contribution to air quality degradation are usually observed, which are correlated with the North Atlantic Oscillation (NAO) index (Pey et al., 2013). In our case, without performing further numerical simulations, it is not possible to know if those differences during spring are linked with the atmospheric models or with real differences in the Earth system, between 2011 and 2016.

To allow the comparison with the P40 estimates, dust contributions to PM10 and PM2.5 are analysed for each of the rural regional background monitoring stations. Time-series are presented in Figures 6.6 and 6.7, for PM10 and PM2.5, respectively. According to model results, the episodes of African dust that influence, the most, PM levels over Portugal occur in February, October and November. Unlike the estimations with the P40 methodology (see Figures 6.2 and 6.3), the model does not show evidence of dust episodes which affect air quality (PM10 and PM2.5) during August.

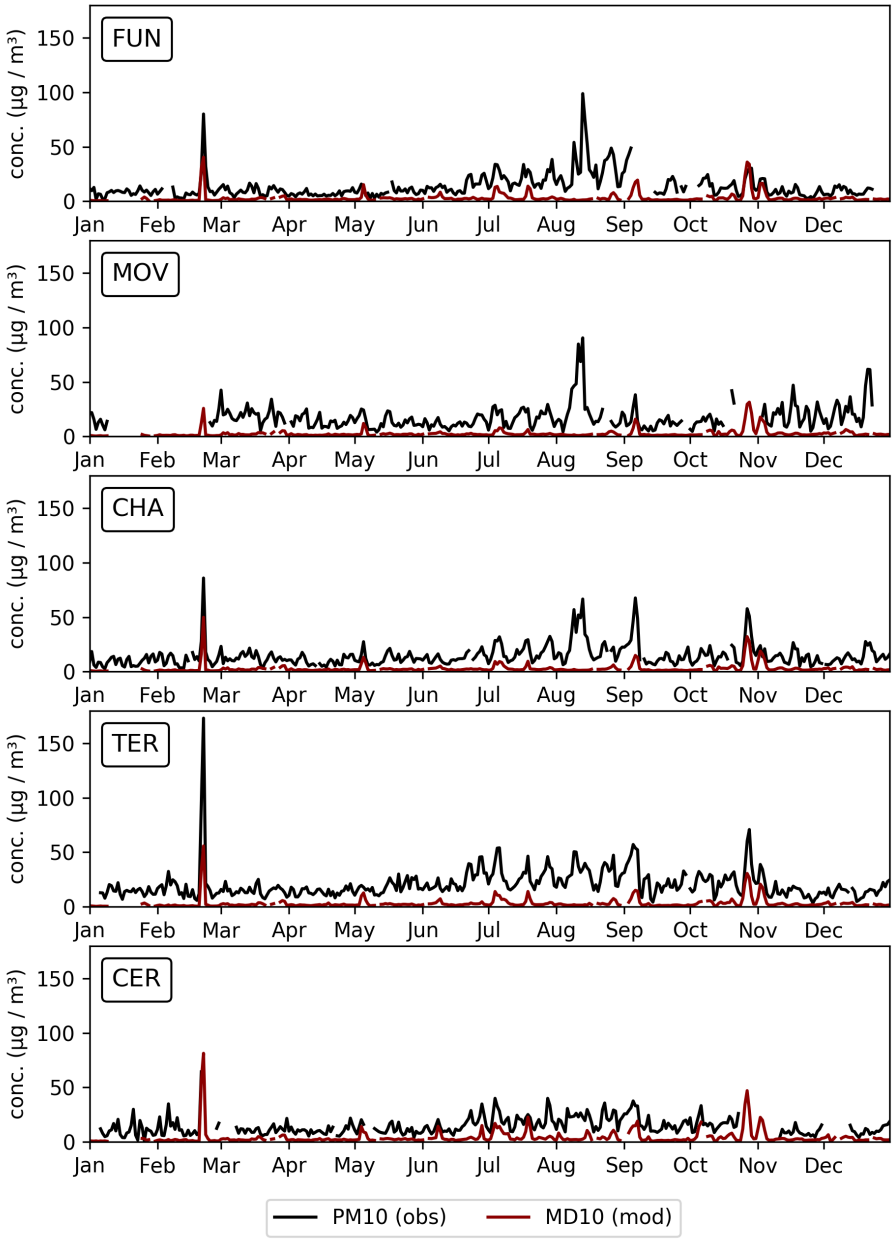

Figure 6.6: PM10 daily concentrations (black line) and contribution from desert dust as estimated by WRF-CHIMERE (brown line).

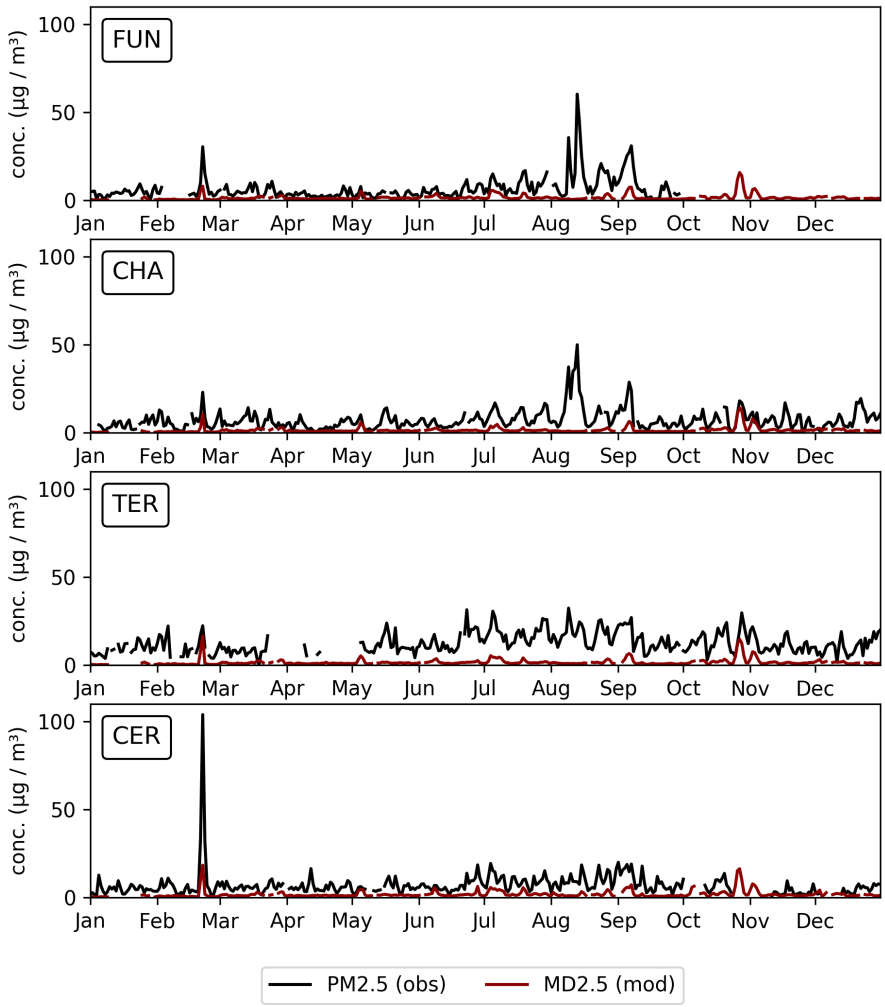

Figure 6.7: PM2.5 daily concentrations (black line) and contribution from desert dust as estimated by WRF-CHIMERE (brown line).

The highest daily contributions to PM10 concentrations (see Table 6.5) occur during the February episode (Feb 22) in all stations, but MOV, where the maximum contribution is estimated at October 28. Maximum values are estimated in CER (81 µg m^{-3}), followed by TER (56 µg m^{-3}), which are the two monitoring stations located in the southernmost region of continental Portugal. The same two episodes register the highest daily contribution of African dust to PM2.5 concentrations (see Table 6.6).

Table 6.5: Number of days when the African dust contribution of particles with an aerodynamic diameter smaller than 10 µm (AD10) is higher than certain thresholds (2 and 4 $\mu g\,m^{-3}$), their mean and maximum daily African dust concentrations (calculated according to the model-based methodology). The day of the year 2016 with the maximum African dust contribution is also identified.

Monitoring station	No. days AD10>=2 $\mu g\,m^{-3}$ (mean conc)	No. days AD10>=4 $\mu g\,m^{-3}$ (mean conc)	max daily contribution ($\mu g\,m^{-3}$)	day of occurrence
FUN	155 (5.0 $\mu g\,m^{-3}$)	39 (11.9 $\mu g\,m^{-3}$)	40.5	Feb 22
MOV	115 (5.0 $\mu g\,m^{-3}$)	41 (9.3 $\mu g\,m^{-3}$)	31.4	Oct 28
CHA	139 (4.9 $\mu g\,m^{-3}$)	39 (10.5 $\mu g\,m^{-3}$)	49.9	Feb 22
TER	141 (5.4 $\mu g\,m^{-3}$)	47 (10.7 $\mu g\,m^{-3}$)	55.8	Feb 22
CER	188 (6.2 $\mu g\,m^{-3}$)	74 (11.5 $\mu g\,m^{-3}$)	81.3	Feb 22

Table 6.6: Number of days when the African dust contribution of particles with an aerodynamic diameter smaller than 2.5 µm (AD2.5) is higher than certain thresholds (1 and 2 $\mu g\,m^{-3}$), their mean and maximum daily African dust concentrations (calculated according to the model-based methodology). The day of the year 2016 with the maximum African dust contribution is also identified.

Monitoring station	No. days AD2.5>=1 $\mu g\,m^{-3}$ (mean conc)	No. days AD2.5>=2 $\mu g\,m^{-3}$ (mean conc)	max daily contribution ($\mu g\,m^{-3}$)	day of occurrence
FUN	213 (2.1 $\mu g\,m^{-3}$)	53 (4.3 $\mu g\,m^{-3}$)	15.8	Oct 27
CHA	191 (2.0 $\mu g\,m^{-3}$)	52 (3.9 $\mu g\,m^{-3}$)	14.2	Oct 27
TER	209 (2.2 $\mu g\,m^{-3}$)	57 (4.3 $\mu g\,m^{-3}$)	16.6	Feb 22
CER	242 (2.3 $\mu g\,m^{-3}$)	74 (4.3 $\mu g\,m^{-3}$)	18.4	Feb 22

Table 6.7 analyses the daily and annual parameters defined in the Directive 2008/50/EC for PM10 and PM2.5 concentrations, before and after the subtraction of the African dust contributions, calculated according to the model estimates. In terms of annual values, the average contribution of desert dust to the PM10 and PM2.5 concentrations is about to 3 $\mu g\,m^{-3}$ and 1.5 $\mu g\,m^{-3}$, respectively, roughly in the five regions in analysis. Regarding the number of exceedances to the PM10 daily limit value, TER station registers the highest number of days of exceedances attributable to African dust (9 days).

Table 6.7: PM10 and PM2.5 annual mean concentrations, and number of days of exceedance to the PM10 daily limit value, before and after the subtraction of the African dust contributions (calculated according to the model-based methodology).

Monitoring station	PM10 annual mean ($\mu g\,m^{-3}$)		exceedances PM10 (number)		PM2.5 annual mean ($\mu g\,m^{-3}$)	
	before	after sub	before	after sub	before	after sub
FUN	13.5	10.8	5	4	6.6	5.3
MOV	17.3	15.1	5	5	–	–
CHA	14.5	11.9	7	4	7.2	5.9
TER	20.7	17.8	11	2	12.7	11.2
CER	14.3	11.2	1	0	7.0	5.5

Unlike what happens when the P40 methodology is considered (see Table 6.4), the number of exceedances registered in the monitoring stations located in the Centre (FUN and MOV) is almost the same before and after the subtraction of the African dust contribution estimated by the model (see Table 6.7). The differences in the number of exceedances after subtraction of the African dust rely on the classification of the event between 09 and 15 of August. Four days during this period, in FUN, and three days, in MOV, registered daily PM10 concentrations higher than $50\,\mu g\,m^{-3}$. The P40 methodology attributes these exceedances to African dust, while according to model simulations there was no significant influence of long-range transport of desert dust on air quality over the Centre of Portugal during those days.

For each monitoring station, a comparison between the desert dust contribution to PM10 and PM2.5 concentrations, calculated according to the P40 methodology and according to the WRF-CHIMERE simulations, is shown in the scatter plots of Figures 6.8 and 6.9, respectively. The data points that correspond to the period between August 08 and 15 are plotted in red.

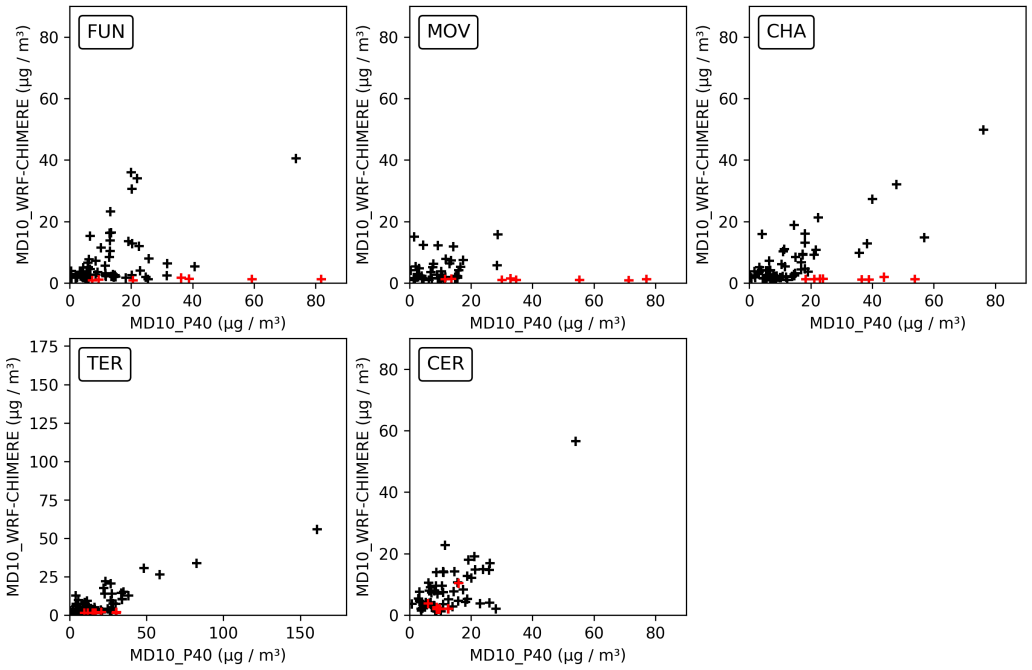

Figure 6.8: Comparison between the African dust contributions to PM10 obtained by the two different methodologies during 2016. Red points correspond to the period between August 08 and 15.

Excluding those points in red colour, the estimates from both methodologies are quite in accordance for the fraction of African dust with an aerodynamic diameter smaller than 10 µm (Figure 6.8). Nevertheless, the model-base methodology estimates are, in general, lower than the P40 ones, especially for TER and CHA. CER has the best agreement between the two methodologies.

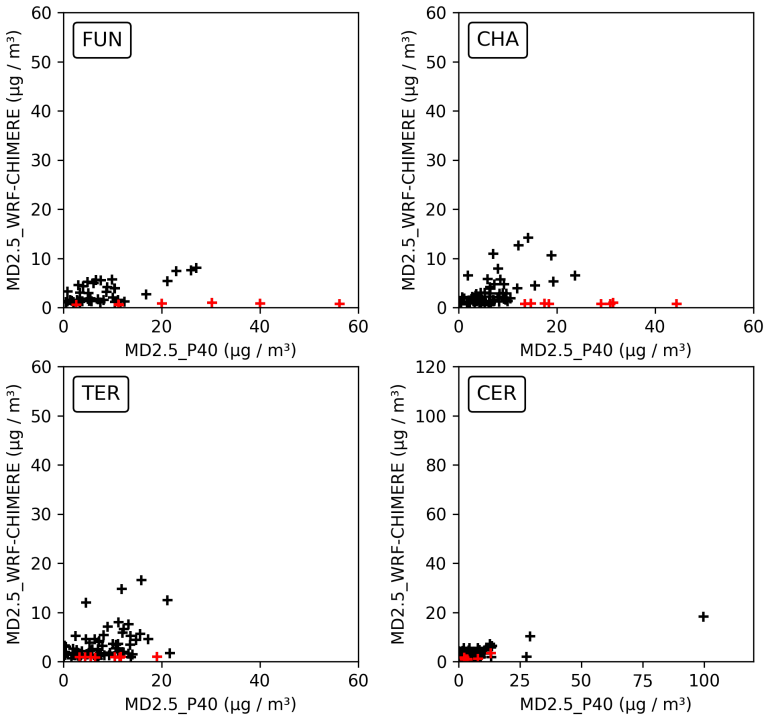

Figure 6.9: Comparison between the African dust contributions to PM2.5 obtained by the two different methodologies during 2016. Red points correspond to the period between August 08 and 15.

Notice, however, that this station has no available data during Feb 22, when PM10 concentrations were very high (a daily mean concentration value of 104 µg m^{-3} was observed in this station for PM2.5, and a contribution of nearly 100 µg m^{-3} of African dust was attributed to desert dust, for the fraction of particles below 2.5 µm only).

When the fraction of particles with an aerodynamic diameter smaller than 2.5 µm is considered (Figure 6.9), it seems that model estimates for African dust contribution are much lower than P40 ones, especially for FUN and CER remote regions.

The main differences in the results obtained with the two methodologies happen in the first half of August. During this period, a high contribution of African dust to the particulate matter over Portugal is estimated by the P40 methodology. Indeed, in the monitoring stations FUN and MOV, in the Centre of Portugal, the maximum daily contribution of African dust to PM10 levels over the whole year 2016, is estimated during this period (82 and 77 µg m^{-3} during August 13, see Table 6.2). The same happens regarding the contribution of desert dust to PM2.5 concentrations, with a contribution of 56 and 44 µg m^{-3} estimated by the P40 method (see Table 6.3). During these days, model results indicate, however, a small influence of long-range transport in the PM10 levels,

in the south of Portugal only (CER monitoring station, where a contribution of about 10 $\mu g\,m^{-3}$ was estimated by the model on August 15). In the rest of the regions and rest of the days, the contribution of African dust to PM levels over Portugal is almost negligible.

In fact, during the first half of August, Portugal battled numerous wildfires, mostly in the Centre and North of the country. Satellites began to detect those large numbers of fires on August 6. In the following days, the fires grew more numerous and the amount of smoke increased dramatically (Figure 6.10), affecting severely air quality.

When extreme events, such as forest fires, occur simultaneously with the long-range transport of desert dust, the P40 methodology may lead to an overestimation of the contribution of African dust to PM levels. Moreover, the combination of desert dust episodes and forest fires is quite common during summer in Portugal. During desert dust episodes, warm and dry air masses are transported over Portugal, which favour the occurrence and grow of wild fires. That situation occurred during August 2016, and recently during October 2017 during the severe forest fires in the Centre and North of Portugal linked with the Hurricane Ophelia.

6.4 Summary and conclusions

The importance of mineral dust contribution for the total aerosol mass observed in Portugal during 2016 was estimated by two different approaches: the official method adopted by the Portuguese Environmental Agency (the P40 method), based on the work by Escudero et al. (2007), and a model-based methodology based on WRF-CHIMERE simulations. The results obtained by both methods for remote areas of Portugal were compared.

Although the P40 method is based on measurements, it relies on dust models for the selection of days identified as impacted by African dust. In Portugal, the Portuguese Environmental Agency bases this selection in two dust models: the BSC-DREAM8b and the SKIRON. Then, the quantification of the desert dust contribution in terms of particles with aerodynamic diameters smaller than 10 and 2.5 µm is based on measured data only.

(a) Aug 07, 2016 13:10 UTC

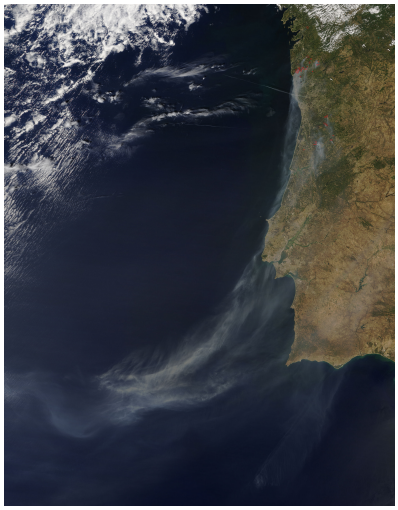

(b) Aug 09, 2016 11:20 UTC

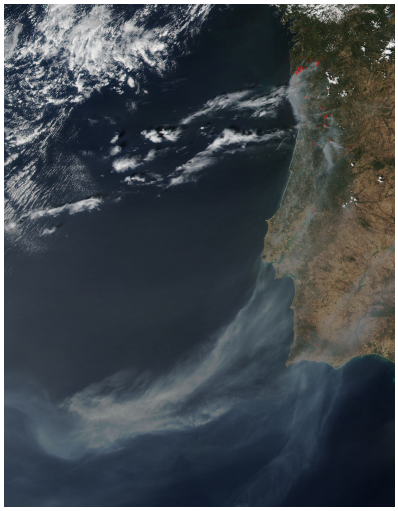

(c) Aug 09, 2016 12:55 UTC

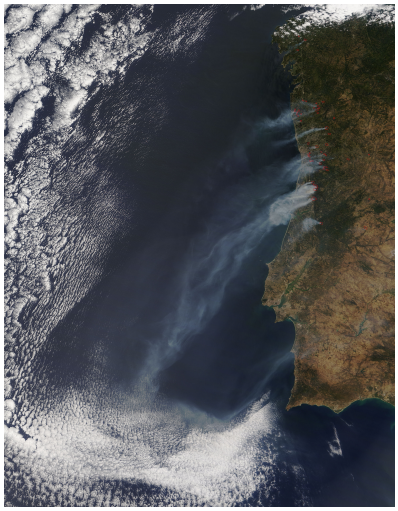

(d) Aug 10, 2016 12:00 UTC

(e) Aug 12, 2016 11:50 UTC

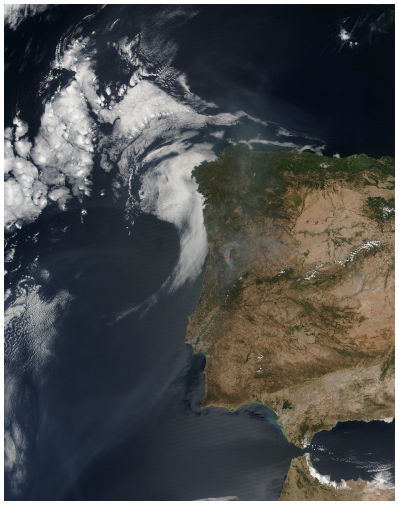

(f) Aug 13, 2016 13:25 UTC

Figure 6.10: Satellite images captured from 6 to 13 August 2016 by Terra/MODIS and SNPP/VIIRS, showing actively burning areas (outlined in red) and associated smoke plumes.

In general, African dust contributions obtained with the P40 methodology are higher than the ones simulated by WRF-CHIMERE. Contributions to PM10 concentrations range from 0 to 90 $\mu g\,m^{-3}$ in most of the regions and days (TER is exception, as a contribution higher than 150 $\mu g\,m^{-3}$ is estimated for February 22. CER, located in the southernmost region of Portugal, has no measurements available during this day). Excluding February 22 (in CER), African dust contributions up to 30 $\mu g\,m^{-3}$ are found for PM2.5 levels.

When other extreme events, such as forest fires, occur simultaneously with the long-range transport of desert dust, this methodology may classify the event as a desert dust event when that is not the main factor affecting PM concentrations. Indeed, the combination of desert dust episodes and forest fires is quite common during summer in Portugal. During desert dust episodes, warm and dry air masses are transported over Portugal, which favour the occurrence and grow of wild fires, as happened in August 2016 or, more recently, in the severe forest fires of October 2017. Therefore, we do not recommend the usage of the P40 methodology during those events (combination of African dust with forest fires), as it increases the contribution of African dust to the PM levels over Portugal.

The results presented in this Chapter confirm that dust is an abundant type of natural atmospheric aerosol in the planetary boundary layer in Portugal. According to our results, desert dust episodes were quite frequent during 2016. Their intensity was variable, with at least two events contributing to exceedances to the PM10 daily limit value defined in the Air Quality Directive. Those severe episodes took place in February (21 and 22) and in October (27 and 28) 2016, and have affected the air quality in all the remote regions studied in this Chapter.

Part Four. Conclusions

Chapter 7

Conclusions and future work

7.1 Main findings

The main objective of this Thesis was to improve the assessment of long-range transport of African dust, focusing on two different regions: Cape Verde, located in an area of massive transport of dust from land to ocean, and Portugal, also affected by desert dust outbreaks.

To achieve this objective, available observations have been collected, which provide information about aerosol levels and its variability, both at surface level and using column integrated data. For Cape Verde region, one year of particulate matter surface concentration measurements obtained through the CV-DUST project has been studied, as well as optical column data from the AERONET network. For Portugal, ten years of particulate matter (PM10 and PM2.5) concentrations observed within the Portuguese air quality monitoring network have been studied. Moreover, LIDAR data and satellite images acquired during specific dust events were analysed.

Dust models have been applied for a complete year cycle, in order to study the spatial and temporal variability of dust emissions and transport to our regions of interest. For Cape Verde region, the BSC-DREAM8b and the NMMB/BSC-Dust models have been applied. Models run for the year 2011, the same period of the experimental campaign. For Portugal, CHIMERE model was applied, driven by meteorological outputs from WRF model. The year in analysis in this region was 2016 - the most recent year at the time simulations were performed.

Model outputs have been compared with available observations. This comparison, on the one hand, contributes for model validation. On the other hand, it allows the identification of issues where model improvements are needed. Experimental campaigns such as CV-DUST provide valuable data for model assessment and development. Moreover, model results are useful to complement and understand observations.

New parametrizations and numerical schemes were implemented in the numerical models and results were assessed, with the specific aim of achieving better agreement between model results and observations, in our case studies, and a general aim of contributing for dust models improvement.

This Thesis contributes to the characterization of the processes and sources responsible for aerosol loading in the regions of Cape Verde and Portugal. The work developed allows to answer each of the formulated research questions:

Which are the processes and sources responsible for desert dust loading in the Cape Verde region?

Seasonal differences simulated by the models in terms of dust emissions, air mass circulations and PM concentrations are important for the analyses of observed episodes in Cape Verde. From October till March, significant seasonal intrusions of dust from North West Africa affect Cape Verde at surface levels when atmospheric concentration levels in Praia exhibit very high levels (PM10 observed concentrations reach hourly values up to 710 $\mu g\, m^{-3}$). High aerosol optical depth (AOD) values were observed for Sal Island on the same days as the peaks observed for surface concentration on Santiago Island, highlighting the extent of episodes of long-range transport of desert dust from the African continent. While surface concentrations were higher during winter, AOD were higher during summer, indicating that during this period dust is transported from North Africa at higher altitudes.

Possible dust-source areas that may affect the Cape Verde region were analysed and found to have distinct seasonal patterns. The most active source in terms of dust emission was the Bodélé region, mainly between December and May. Other significant sources include the Algeria-Morocco region, West Sahara-Mauritania, the Libya desert, Algeria-Tunisia and Algeria-Mali. According to the backward trajectories analysis, the air masses responsible for the highest aerosol concentrations

in Cape Verde describe a path over the central Saharan desert area in Algeria, Mali and Mauritania before reaching the Atlantic Ocean.

The comparison between model results and observations allow rough estimation that on a yearly basis, 42% of the PM10 mass observed in Cape Verde is associated with dust transported from North African deserts.

How accurately dust models reproduce the dust cycle in a strategic site such as Cape Verde? Can we improve models performance?

The BSC-DREAM8b and the NMMB/BSC-Dust models have been used to evaluate, for the first time, particulate matter surface concentration and size distribution in Cape Verde over a one-year period (Chapter 2). Both models are able to reproduce the majority of the dust episodes, although the magnitude of the predicted concentrations was lower than those observed. While the dust models take into account only aeolian mineral particles emitted from the deserts, the measurement data set may also reflect non-dust aerosols like sea-salt or biomass burning particles, secondary pollutants and local anthropogenic sources.

Results from NMMB/BSC-Dust are in better agreement with observed PM concentrations and AOD through the year, than results from BSC-DREAM8b. For that model, the comparison between observed and modelled PM10 daily averaged concentrations yields a correlation coefficient of 0.77, denoting the importance of mineral dust contribution for the total aerosol mass, and a 29.0 $\mu g\,m^{-3}$ "bias", of which 12-14 $\mu g\,m^{-3}$ are explained by the observed sea salt contribution to PM10 during 2011. PM size distribution modelled with BSC-DREAM8b seems to be in better agreement with observations than NMMB/BSC-Dust, since the estimated contribution of the larger particles for the total dust mass was higher. Based on these results, further improvements were needed in terms of modelling particle size distribution within NMMB/BSC-Dust model.

A new methodology to distribute the total vertical dust flux by each model size bin was derived from Kok's brittle fragmentation theory (Kok, 2011a) and implemented in the model, without changing the computation of the total dust emission flux nor the number and range of the size transport bins considered (Chapter 3). Kok's size distribution function leads to a decrease in the fine model bins mass emissions and an increase in the coarser ones, which has impact in the modelled downwind concentrations and optical parameters.

Model outputs obtained with the new emission scheme exhibit mass dominance of particles with equivalent aerodynamic diameter between 3.6 and 6.0 µm, which is in agreement with observations in Cape Verde. However, PM10 concentrations are underestimated, which is probably related with an increase in the deposition phenomena along transport, which remove the coarser fractions of the dust from the load-column, since with the new size distribution scheme the mass fraction flux of the coarser bins is higher. Model results were also compared with AOD observations from AERONET sites located within the domain. Modelled AOD fine fraction is generally in better agreement with observations when the new size emission scheme is considered, however total AOD is in some sites underestimated. This tentative of improvement of model results should be complemented with a more exhaustive evaluation of the impact of Kok's size distribution on the dust deposition rates over the domain. Moreover, tunning the model may be necessary.

How do particulate matter concentrations vary through time over Portugal?

The aerosol background levels in Portugal have been analysed (Chapter 4) based on data gathered from 2007 to 2016. PM10 and PM2.5 concentrations are characterized by typical temporal patterns. Along the day, concentrations follow the expected patterns with rural sites exhibiting less variability through the day and urban and suburban sites characterized by two main peaks during the day: one during the morning, and the largest one at late evening.

It is on suburban sites that the larger differences between the PM10 characteristic daily cycle of each season are found. In this group of stations, the highest daily concentrations (observed at late evening / during the night) during winter are in average 20 $\mu g\,m^{-3}$ higher than during summer. PM2.5 concentrations could not be assessed at suburban stations, since this specie is not measured at those monitoring stations.

A decreasing trend is observed in PM10 concentrations through the last decade, mainly for the urban and suburban stations. Our analysis shows that the main factor contributing to the PM10 decrease in urban areas is the decrease in the coarse (2.5-10 µm) concentrations. While in January 2007 there was a large difference between PM10 levels observed at suburban, urban and rural stations (33.4, 29.6 and 22.3 $\mu g\,m^{-3}$), ten years later, values are 17.8, 19.1 and 18.2 $\mu g\,m^{-3}$, respectively.

Compliance with the Directive 2008/50/EC has been assessed and a decreasing tendency was found within the number of non-compliance situations. While between 2007 and 2012 we had at least one background station each year with more than 35 exceedances to the PM10 daily limit value, between 2013 and 2016 all the background stations analysed, despite their type, have accomplished the values established for the protection of human health.

The results of this work point out the importance of coarse particles of anthropogenic origin in Portugal. This conclusion is supported by the larger differences between weekdays and Sundays in PM10 than PM2.5. The aerosol coarse fraction is about to 3 $\mu g\,m^{-3}$ higher during week-days than during Sundays, at urban sites.

What is the contribution from the North African deserts to the atmospheric aerosol in Portugal?

The contribution from North African deserts to the aerosol mass observed in Portugal was studied at surface level only, and for a one-year period (2016). Two different methodologies were applied in order to estimate mineral dust contribution to PM10 and PM2.5 concentrations over Portugal: a measurement-based approach (P40 methodology) and a model-based methodology (based on WRF-CHIMERE simulations).

According to our results, desert dust episodes were frequent during 2016. The WRF-CHIMERE outputs indicate October as the month with the highest mean contribution of desert dust to the PM10 (between 4 to 9 $\mu g\,m^{-3}$) and PM2.5 (between 2 to 4 $\mu g\,m^{-3}$) concentrations over Portugal. On the contrary, January has the lowest contribution, with mean values lower than 2 $\mu g\,m^{-3}$ and 1 $\mu g\,m^{-3}$, for the fractions of particles with aerodynamic diameters smaller than 10 µm and 2.5 µm, respectively.

The intensity of dust events that affected Portugal and their impact on air quality varied from one episode to another. During 2016, at least two events contributed to exceedances to the PM10 daily limit value defined in the Air Quality Directive (50 $\mu g\,m^{-3}$). Those severe episodes took place in February (21 and 22) and in October (27 and 28), and have affected the air quality over the whole mainland Portugal. During these two events, the contribution of African dust, only, was already sufficient to promote the surpassing of the PM10 daily limit value.

In general, during episodes, African dust contributions obtained with the P40 methodology are higher than the ones simulated by WRF-CHIMERE. Contributions to PM10 concentrations range from 0 to 90 $\mu g\,m^{-3}$ in most of the regions and episode days (TER is exception, with a contribution higher than 150 $\mu g\,m^{-3}$ estimated by the P40 method for February 22). Excluding February 22 (in CER) and the period between 8 and 15 of August, when we believe the P40 results were affected by severe forest fires, African dust contributions of up to 30 $\mu g\,m^{-3}$ are found for PM2.5 levels.

When other extreme events, such as forest fires, occur simultaneously with the long-range transport of desert dust, the P40 methodology may lead to an overestimation of the contribution of African dust to the PM levels over Portugal. Therefore, we do not recommend the usage of the P40 methodology when days influenced by African dust happen together with forest fires, which is quite common during summer in Portugal.

How is the operational air quality forecasting system performing over Portugal? Can we improve its performance?

The modelling of African dust outbreaks within the Portuguese operational air quality forecasting system is crucial to correctly simulate the PM levels and variability over the country, since the inclusion of desert dust emissions provide more realistic dust boundary conditions for particulate matter simulations and forecast over Portugal. The air quality forecasts, namely PM10 concentrations predicted by the numerical system during a whole year, 2016, have been compared with the observations recorded in all the background stations within the Portuguese air quality monitoring network. Moreover, "experimental" air quality forecasts were implemented for the whole year 2016, focusing on model resolution and mineral dust production schemes, with the goal of improving system's performance.

Model resolution strongly affects results in the outermost domain. Indeed, that domain is the one in which the increase in resolution between simulations is highest - horizontal resolution increased from 125 x 125 km^2 to 27 x 27 km^2. In terms of the inner domain, its resolution increased from 5 x 5 km^2 to 3 x 3 km^2. Although annual mean concentrations seem to have higher spatial details in the higher resolution concentrations, statistics computed for the background monitoring sites do not show such an important increase in the quality of the forecasts with the increase in resolution, for the inner domain. The resolution to implement must be decided taking into account computational effort and available resources.

Regarding dust production models, the one already in use in the operational system proves to be the best of the three parametrisations assessed in Chapter 5.

During 2016, five pollution episodes were identified in which model failed to forecast daily PM10 concentrations above 50 $\mu g\, m^{-3}$ – or excedaance days, in at least two background monitoring stations. Each of these episodes was analysed in order to identify possible causes for model mismatch. Two of these episodes are linked to dust storms, which are reproduced by the model, however slightly underestimated. Two other episodes are linked with forest fires – possibly with forest fires and dust storms. Forest fire emissions are not included yet in the Portuguese air quality forecast system. The last pollution episode corresponds to very cold and stable atmospheric conditions. Future research tasks are suggested in the next Section, in order to improve model's performance during forest fire episodes and also regarding pollution episodes linked with anthropogenic sources.

7.2 Future research tasks

The inclusion of a non-climatic representation of African dust emission and transport in the Portuguese operational air quality forecasting system was already a step forward. However, future work is needed in order to improve particulate matter forecasts.

Regarding anthropogenic emissions, a new official emission inventory was recently launched for Portugal and includes a better spatial resolution (about 10 x 10 km^2, instead of the previous 50 x 50 km^2). This data will be soon included in the air quality forecast system and better results are expected. Furthermore, a dynamic emission model to downscale annual emissions to hourly estimates could be developed. The idea behind a dynamic emission model is to base the temporal disaggregation not only on average diurnal, weekly and seasonal time profiles per sector, as it is currently done, but also on meteorological conditions which affect the variation of emission strength with activity patterns.

The inclusion of forest fire emissions in the Portuguese operational air quality forecasting is a major need, due to the impact these events have in air quality and due to their frequency in our region. Such inclusion could be based on satellite observations that measure the radiative energy released by fires (the Fire Radiative Power, which is closely related to the amount of biomass burned) combined with detailed knowledge of the surface emission fluxes from biomass burning.

The results presented and discussed through this Thesis were not corrected using post-processing techniques. Bias correction techniques (e.g. Borrego et al., 2011; Mok et al., 2017; Monteiro et al., 2013) must be explored in the future, in order to improve the match between forecasts and observations.

References

Albani, S., Mahowald, N. M., Perry, A. T., Scanza, R. A., Zender, C. S., Heavens, N. G., Maggi, V., Kok, J. F., and Otto-Bliesner, B. L. (2014). Improved dust representation in the community atmosphere model. *Journal of Advances in Modeling Earth Systems*, 6(3):541–570.

Alfaro, S. C. and Gomes, L. (2001). Modeling mineral aerosol production by wind erosion: Emission intensities and aerosol size distributions in source areas. *Journal of Geophysical Research: Atmospheres*, 106(D16):18075–18084.

Almeida, S., Pio, C., Freitas, M., Reis, M., and Trancoso, M. (2006). Source apportionment of atmospheric urban aerosol based on weekdays/weekend variability: evaluation of road resuspended dust contribution. *Atmospheric Environment*, 40(11):2058–2067.

Almeida, S. M., Almeida-Silva, M., Pio, C., Nunes, T., and Cardoso, J. (2013a). Source apportionment of particulate matter sampled in Cape Verde. EGU General Assembly 2013. Vienna, Austria.

Almeida, S. M., Freitas, M. C., Repolho, C., Dionísio, I., Dung, H. M., Caseiro, A., Alves, C., Pio, C. A., and Pacheco, A. M. G. (2009). Characterizing air particulate matter composition and sources in Lisbon, Portugal. *Journal of Radioanalytical and Nuclear Chemistry*, 281(2):215–218.

Almeida, S. M., Silva, A. I., Freitas, M. C., Dzung, H. M., Caseiro, A., and Pio, C. A. (2013b). Impact of maritime air mass trajectories on the western european coast urban aerosol. *Journal of Toxicology and Environmental Health, Part A*, 76(4-5):252–262.

Almeida-Silva, M., Almeida, S. M., Freitas, M. C., Pio, C. A., Nunes, T., and Cardoso, J. (2013). Impact of Sahara Dust Transport on Cape Verde Atmospheric Element Particles. *Journal of Toxicology and Environmental Health - Part A - Current Issues*, 76(4-5, SI):240–251.

Alonso-Perez, S., Cuevas, E., Perez, C., Querol, X., Baldasano, J. M., Draxler, R., and De Bustos, J. J. (2011). Trend changes of African airmass intrusions in the marine boundary layer over the subtropical Eastern North Atlantic region in winter. *Tellus Series B-Chemical and Physical Meteorology*, 63(2):255–265.

Alves, C., Pio, C., and Duarte, A. (2001). Composition of extractable organic matter of air particles from rural and urban Portuguese areas. *Atmospheric Environment*, 35(32):5485–5496.

Amiridis, V., Kafatos, M., Perez, C., Kazadzis, S., Gerasopoulos, E., Mamouri, R. E., Papayannis, A., Kokkalis, P., Giannakaki, E., Basart, S., Daglis, I., and Zerefos, C. (2009). The potential of the synergistic use of passive and active remote sensing measurements for the validation of a regional dust model. *Annales Geophysicae*, 27(8):3155–3164. 12th International Symposium on Equatorial Aeronomy (ISEA-12), Crete, Greece, May 18-24, 2008.

Amiridis, V., Wandinger, U., Marinou, E., Giannakaki, E., Tsekeri, A., Basart, S., Kazadzis, S., Gkikas, A., Taylor, M., Baldasano, J., and Ansmann, A. (2013). Optimizing CALIPSO Saharan dust retrievals. *Atmospheric Chemistry and Physics*, 13(23):12089–12106.

Andreae, M. and Rosenfeld, D. (2008). Aerosol–cloud–precipitation interactions. part 1. the nature and sources of cloud-active aerosols. *Earth-Science Reviews*, 89(1):13 – 41.

Ansmann, A., Baars, H., Tesche, M., Mueller, D., Althausen, D., Engelmann, R., Pauliquevis, T., and Artaxo, P. (2009). Dust and smoke transport from Africa to South America: Lidar profiling over Cape Verde and the Amazon rainforest. *Geophysical Research Letters*, 36.

Ansmann, A., Petzold, A., Kandler, K., Tegen, I., Wendisch, M., Mueller, D., Weinzierl, B., Mueller, T., and Heintzenberg, J. (2011). Saharan Mineral Dust Experiments SAMUM-1 and SAMUM-2: what have we learned? *Tellus Series B-Chemical and Physical Meteorology*, 63(4, SI):403–429.

APA (2017). Identificação e avaliação da ocorrência de eventos de âmbito natural em Portugal em 2016, Relatório Anual. Available here: https://www.apambiente.pt/index.php?ref=16&subref=82&sub2ref=316&sub3ref=383.

Ashpole, I. and Washington, R. (2013). Intraseasonal variability and atmospheric controls on daily dust occurrence frequency over the central and western Sahara during the boreal summer. *Journal of Geophysical Research-Atmospheres*, 118(23):12915–12926.

Badia, A. and Jorba, O. (2015). Gas-phase evaluation of the online NMMB/BSC-CTM model over Europe for 2010 in the framework of the AQMEII-Phase2 project. *Atmospheric Environment*, 115:657–669.

Basart, S., Pay, M. T., Jorba, O., Perez, C., Jimenez-Guerrero, P., Schulz, M., and Baldasano, J. M. (2012a). Aerosols in the CALIOPE air quality modelling system: evaluation and analysis of PM levels, optical depths and chemical composition over Europe. *Atmospheric Chemistry and Physics*, 12(7):3363–3392.

Basart, S., Perez, C., Cuevas, E., Baldasano, J. M., and Gobbi, G. P. (2009). Aerosol characterization in Northern Africa, Northeastern Atlantic, Mediterranean Basin and Middle East from direct-sun AERONET observations. *Atmospheric Chemistry and Physics*, 9(21):8265–8282.

Basart, S., Perez, C., Nickovic, S., Cuevas, E., and Baldasano, J. M. (2012b). Development and evaluation of the BSC-DREAM8b dust regional model over Northern Africa, the Mediterranean and the Middle East. *Tellus Series B-Chemical and Physical Meteorology*, 64.

Basart, S., Vendrell, L., and Baldasano, J. (2016). High-resolution dust modelling over complex terrains in west asia. *Aeolian Research*, 23:37–50.

Betts, A. (1986). A new convective adjustment scheme. 1.Observational and theoretical basis. *Quarterly Journal of the Royal Meteorological Society*, 112(473):677–691.

Betts, A. and Miller, M. (1986). A new convective adjustment scheme. 2. Single column tests using gate wave, bomex, atex and Arctic air-mass data sets. *Quarterly Journal of the Royal Meteorological Society*, 112(473):693–709.

Borrego, C., Monteiro, A., Pay, M., Ribeiro, I., Miranda, A., Basart, S., and Baldasano, J. (2011). How bias-correction can improve air quality forecasts over Portugal. *Atmospheric Environment*, 45(37):6629 – 6641.

Borrego, C., Valente, J., Carvalho, A., Sa, E., Lopes, M., and Miranda, A. I. (2010). Contribution of residential wood combustion to PM10 levels in Portugal. *Atmospheric Environment*, 44(5):642–651.

Bouchlaghem, K., Nsom, B., Latrache, N., and Kacem, H. H. (2009). Impact of Saharan dust on PM10 concentration in the Mediterranean Tunisian coasts. *Atmospheric Research*, 92(4):531–539.

Cabello, M., Orza, J. A. G., Barrero, M. A., Gordo, E., Berasaluce, A., Cantón, L., Dueñas, C., Fernández, M. C., and Pérez, M. (2012). Spatial and temporal variation of the impact of an extreme Saharan dust event. *Journal of Geophysical Research: Atmospheres*, 117(D11):n/a–n/a. D11204.

Calvo, A., Alves, C., Castro, A., Pont, V., Vicente, A., and Fraile, R. (2013). Research on aerosol sources and chemical composition: Past, current and emerging issues. *Atmospheric Research*, 120–121:1–28.

Carslaw, D. C., Beevers, S. D., and Tate, J. E. (2007). Modelling and assessing trends in traffic-related emissions using a generalised additive modelling approach. *Atmospheric Environment*, 41(26):5289–5299.

Carslaw, D. C. and Ropkins, K. (2012). openair - An R package for air quality data analysis. *Environmental Modelling & Software*, 27-28:52–61.

Cazorla, A., Casquero-Vera, J. A., Román, R., Guerrero-Rascado, J. L., Toledano, C., Cachorro, V. E., Orza, J. A. G., Cancillo, M. L., Serrano, A., Titos, G., Pandolfi, M., Alastuey, A., Hanrieder, N., and Alados-Arboledas, L. (2017). Near-real-time processing of a ceilometer network assisted with sun-photometer data: monitoring a dust outbreak over the Iberian Peninsula. *Atmospheric Chemistry and Physics*, 17(19):11861–11876.

Cesari, D., Benedetto, G. D., Bonasoni, P., Busetto, M., Dinoi, A., Merico, E., Chirizzi, D., Cristofanelli, P., Donateo, A., Grasso, F., Marinoni, A., Pennetta, A., and Contini, D. (2018). Seasonal variability of PM2.5 and PM10 composition and sources in an urban background site in Southern Italy. *Science of The Total Environment*, 612(Supplement C):202–213.

Chen, G., Ziemba, L. D., Chu, D. A., Thornhill, K. L., Schuster, G. L., Winstead, E. L., Diskin, G. S., Ferrare, R. A., Burton, S. P., Ismail, S., Kooi, S. A., Omar, A. H., Slusher, D. L., Kleb, M. M., Reid, J. S., Twohy, C. H., Zhang, H., and Anderson, B. E. (2011). Observations of Saharan dust microphysical and optical properties from the Eastern Atlantic during NAMMA airborne field campaign. *Atmospheric Chemistry and Physics*, 11(2):723–740.

Chiapello, I., Bergametti, G., Chatenet, B., Bousquet, P., Dulac, F., and Soares, E. (1997). Origins of African dust transported over the northeastern tropical Atlantic. *Journal of Geophysical Research-Atmospheres*, 102(D12):13701–13709.

Chiapello, I., Bergametti, G., Gomes, L., Chatenet, B., Dulac, F., Pimenta, J., and Suares, E. (1995). An additional low layer transport of Sahelian and Saharan dust over the North-Eastern tropical Atlantic. *Geophysical Research Letters*, 22(23):3191–3194.

Cleveland, R. B., Cleveland, W. S., McRae, J. E., and Terpenning, I. (1990). STL: A Seasonal-Trend Decomposition Procedure Based on Loess. *Journal of Official Statistics*, 6(1):3–73.

Colette, A., Andersson, C., Manders, A., Mar, K., Mircea, M., Pay, M.-T., Raffort, V., Tsyro, S., Cuvelier, C., Adani, M., Bessagnet, B., Bergström, R., Briganti, G., Butler, T., Cappelletti, A., Couvidat, F., D'Isidoro, M., Doumbia, T., Fagerli, H., Granier, C., Heyes, C., Klimont, Z., Ojha, N., Otero, N., Schaap, M., Sindelarova, K., Stegehuis, A. I., Roustan, Y., Vautard, R., van Meijgaard, E., Vivanco, M. G., and Wind, P. (2017). EURODELTA-Trends, a multi-model experiment of air quality hindcast in Europe over 1990–2010. *Geoscientific Model Development*, 10(9):3255–3276.

Creamean, J. M., Suski, K. J., Rosenfeld, D., Cazorla, A., DeMott, P. J., Sullivan, R. C., White, A. B., Ralph, F. M., Minnis, P., Comstock, J. M., Tomlinson, J. M., and Prather, K. A. (2013). Dust and Biological Aerosols from the Sahara and Asia Influence Precipitation in the Western U.S. *Science*, 339(6127):1572–1578.

Cruz, A. M. J., Alves, C., Gouveia, S., Scotto, M. G., Freitas, M. d. C., and Wolterbeek, H. T. (2016). A wavelet-based approach applied to suspended particulate matter time series in Portugal. *Air Quality, Atmosphere & Health*, 9(8):847–859.

Cuesta, J., Eremenko, M., Flamant, C., Dufour, G., Laurent, B., Bergametti, G., Hoepfner, M., Orphal, J., and Zhou, D. (2015). Three-dimensional distribution of a major desert dust outbreak over East Asia in March 2008 derived from IASI satellite observations. *Journal of Geophysical Research: Atmospheres*, 120(14):7099–7127.

Custódio, D., Cerqueira, M., Alves, C., Nunes, T., Pio, C., Esteves, V., Frosini, D., Lucarelli, F., and Querol, X. (2016). A one-year record of carbonaceous components and major ions in aerosols from an urban kerbside location in Oporto, Portugal. *Science of The Total Environment*, 562:822–833.

Dall'Osto, M., Harrison, R. M., Highwood, E. J., O'Dowd, C., Ceburnis, D., Querol, X., and Achterberg, E. P. (2010). Variation of the mixing state of Saharan dust particles with atmospheric transport. *Atmospheric Environment*, 44(26):3135–3146.

D'Almeida, G. (1987). On the variability of desert aerosol radiative characteristics. *Journal of Geophysical Research-Atmospheres*, 92(D3):3017–3026.

Delcloo, A. W. and De Backer, H. (2008). Five day 3D back trajectory clusters and trends analysis of the Uccle ozone sounding time series in the lower troposphere (1969-2001). *Atmospheric Environment*, 42(19):4419–4432.

Diapouli, E., Manousakas, M. I., Vratolis, S., Vasilatou, V., Pateraki, S., Bairachtari, K. A., Querol, X., Amato, F., Alastuey, A., Karanasiou, A. A., Lucarelli, F., Nava, S., Calzolai, G., Gianelle, V. L., Colombi, C., Alves, C., Custódio, D., Pio, C., Spyrou, C., Kallos, G. B., and Eleftheriadis, K. (2017). AIRUSE-LIFE+: estimation of natural source contributions to urban ambient air PM10 and PM2.5 concentrations in southern Europe – implications to compliance with limit values. *Atmospheric Chemistry and Physics*, 17(5):3673–3685.

Dingenen, R. V., Raes, F., Putaud, J.-P., Baltensperger, U., Charron, A., Facchini, M.-C., Decesari, S., Fuzzi, S., Gehrig, R., Hansson, H.-C., Harrison, R. M., Hüglin, C., Jones, A. M., Laj, P., Lorbeer, G., Maenhaut, W., Palmgren, F., Querol, X., Rodriguez, S., Schneider, J., ten Brink, H., Tunved, P., Tørseth, K., Wehner, B., Weingartner, E., Wiedensohler, A., and Wåh-

lin, P. (2004). A European aerosol phenomenology — 1: Physical characteristics of particulate matter at kerbside, urban, rural and background sites in Europe. *Atmospheric Environment*, 38(16):2561–2577.

Draxler, R. and Hess, G. (1998). An overview of the HYSPLIT_4 modelling system for trajectories, dispersion and deposition. *Australian Meteorological Magazine*, 47(4):295–308.

EC (2011). Commission staff working paper establishing guidelines for demonstration and subtraction of exceedances attributable to natural sources under the Directive 2008/50/EC on ambient air quality and cleaner air for Europe. Brussels, 15.02.2011, SEC(2011) 208 final. Available here: http://ec.europa.eu/environment/air/quality/legislation/pdf/sec_2011_0208.pdf.

Eck, T. F., Holben, B. N., Sinyuk, A., Pinker, R. T., Goloub, P., Chen, H., Chatenet, B., Li, Z., Singh, R. P., Tripathi, S. N., Reid, J. S., Giles, D. M., Dubovik, O., O'Neill, N. T., Smirnov, A., Wang, P., and Xia, X. (2010). Climatological aspects of the optical properties of fine/coarse mode aerosol mixtures. *Journal of Geophysical Research: Atmospheres*, 115(D19):n/a–n/a.

Engelstaedter, S., Tegen, I., and Washington, R. (2006). North African dust emissions and transport. *Earth-Science Reviews*, 79(1-2):73–100.

Escudero, M., Castillo, S., Querol, X., Avila, A., Alarcón, M., Viana, M. M., Alastuey, A., Cuevas, E., and Rodríguez, S. (2005). Wet and dry african dust episodes over eastern spain. *Journal of Geophysical Research: Atmospheres*, 110(D18). D18S08.

Escudero, M., Querol, X., Pey, J., Alastuey, A., Perez, N., Ferreira, F., Alonso, S., Rodriguez, S., and Cuevas, E. (2007). A methodology for the quantification of the net African dust load in air quality monitoring networks. *Atmospheric Environment*, 41(26):5516–5524.

EU (2008). Directive 2008/50/EC of the European Parliament and of the Council of 21 May 2008 on Ambient Air Quality and Cleaner Air for Europe. OJ L 152, 11.6.2008.

Fairlie, T. D., Jacob, D. J., and Park, R. J. (2007). The impact of transpacific transport of mineral dust in the United States. *Atmospheric Environment*, 41(6):1251–1266.

Fan, J., Leung, L. R., DeMott, P. J., Comstock, J. M., Singh, B., Rosenfeld, D., Tomlinson, J. M., White, A., Prather, K. A., Minnis, P., Ayers, J. K., and Min, Q. (2014). Aerosol impacts on California winter clouds and precipitation during CalWater 2011: local pollution versus long-range transported dust. *Atmospheric Chemistry and Physics*, 14(1):81–101.

Ferrier, B. S., Jin, Y., Lin, Y., Black, T., Rogers, E., and DiMego, G. (2002). Implementation of a new grid-scale cloud and precipitation scheme in the NCEP Eta Model. 19th Conf. on Weather Analysis and Forecasting/15th Conf. on Numerical Weather Prediction, pages 280–283.

Fischer, E. V., Hsu, N. C., Jaffe, D. A., Jeong, M.-J., and Gong, S. L. (2009). A decade of dust: Asian dust and springtime aerosol load in the U.S. Pacific Northwest. *Geophysical Research Letters*, 36(3). L03821.

Fomba, K. W., Mueller, K., van Pinxteren, D., Poulain, L., van Pinxteren, M., and Herrmann, H. (2014). Long-term chemical characterization of tropical and marine aerosols at the Cape Verde Atmospheric Observatory (CVAO) from 2007 to 2011. *Atmospheric Chemistry and Physics*, 14(17):8883–8904.

Formenti, P., Elbert, W., Maenhaut, W., Haywood, J., and Andreae, M. (2003). Chemical composition of mineral dust aerosol during the Saharan Dust Experiment (SHADE) airborne campaign in the Cape Verde region, September 2000. *Journal of Geophysical Research-Atmospheres*, 108(D18).

Fuller, G. W., Tremper, A. H., Baker, T. D., Yttri, K. E., and Butterfield, D. (2014). Contribution of wood burning to PM10 in London. *Atmospheric Environment*, 87:87–94.

Fuzzi, S., Baltensperger, U., Carslaw, K., Decesari, S., Denier van der Gon, H., Facchini, M. C., Fowler, D., Koren, I., Langford, B., Lohmann, U., Nemitz, E., Pandis, S., Riipinen, I., Rudich, Y., Schaap, M., Slowik, J. G., Spracklen, D. V., Vignati, E., Wild, M., Williams, M., and Gilardoni, S. (2015). Particulate matter, air quality and climate: lessons learned and future needs. *Atmospheric Chemistry and Physics*, 15(14):8217–8299.

Gallisai, R., Peters, F., Volpe, G., Basart, S., and Baldasano, J. M. (2014). Saharan Dust Deposition May Affect Phytoplankton Growth in the Mediterranean Sea at Ecological Time Scales. *PLOS ONE*, 9(10).

Ganor, E., Stupp, A., and Alpert, P. (2009). A method to determine the effect of mineral dust aerosols on air quality. *Atmospheric Environment*, 43(34):5463–5468.

Garcia-Pando, C. P., Stanton, M. C., Diggle, P. J., Trzaska, S., Miller, R. L., Perlwitz, J. P., Baldasano, J. M., Cuevas, E., Ceccato, P., Yaka, P., and Thomson, M. C. (2014). Soil Dust Aerosols and Wind as Predictors of Seasonal Meningitis Incidence in Niger. *Environmental Health Perspectives*, 122(7):679–686.

Gimeno, L., Trigo, R. M., Ribera, P., and García, J. A. (2007). Editorial: Special issue on cut-off low systems. *Meteorology and Atmospheric Physics*, 96(1):1–2.

Ginoux, P., Chin, M., Tegen, I., Prospero, J., Holben, B., Dubovik, O., and Lin, S. (2001). Sources and distributions of dust aerosols simulated with the GOCART model. *Journal of Geophysical Research-Atmospheres*, 106(D17):20255–20273.

Ginoux, P., Prospero, J., Torres, O., and Chin, M. (2004). Long-term simulation of global dust distribution with the GOCART model: correlation with North Atlantic Oscillation. *Environmental Modelling & Software*, 19(2):113–128.

Ginoux, P., Prospero, J. M., Gill, T. E., Hsu, N. C., and Zhao, M. (2012). Global-scale attribution of anthropogenic and natural dust sources and their emission rates based on MODIS Deep Blue aerosol products. *Reviews of Geophysics*, 50.

Giorgi, F. (1986). A particle dry-deposition parameterization scheme for use in tracer transport models. *Journal of Geophysical Research-Atmospheres*, 91(D9):9794–9806.

Gkikas, A., Hatzianastassiou, N., Mihalopoulos, N., Katsoulis, V., Kazadzis, S., Pey, J., Querol, X., and Torres, O. (2013). The regime of intense desert dust episodes in the mediterranean based on contemporary satellite observations and ground measurements. *Atmospheric Chemistry and Physics*, 13(23):12135–12154.

Gobbi, G. P., Kaufman, Y. J., Koren, I., and Eck, T. F. (2007). Classification of aerosol properties derived from AERONET direct sun data. *Atmospheric Chemistry and Physics*, 7:453–458.

Gomez-Losada, A., Pires, J. C. M., and Pino-Mejias, R. (2015). Time series clustering for estimating particulate matter contributions and its use in quantifying impacts from deserts. *Atmospheric Environment*, 117:271–281.

Gonçalves, C., Alves, C., and Pio, C. (2012). Inventory of fine particulate organic compound emissions from residential wood combustion in Portugal. *Atmospheric Environment*, 50:297–306.

Goudie, A. and Middleton, N. (2001). Saharan dust storms: nature and consequences. *Earth-Science Reviews*, 56(1-4):179–204.

Grimm, H. and Eatough, D. J. (2009). Aerosol Measurement: The Use of Optical Light Scattering for the Determination of Particulate Size Distribution, and Particulate Mass, Including the Semi-Volatile Fraction. *Journal of the Air & Waste Management Association*, 59(1):101–107.

Gross, A., Goren, T., Pio, C., Cardoso, J., Tirosh, O., Todd, M. C., Rosenfeld, D., Weiner, T., Custódio, D., and Angert, A. (2015). Variability in sources and concentrations of saharan dust phosphorus over the atlantic ocean. *Environmental Science & Technology Letters*, 2(2):31–37.

Guenther, A., Karl, T., Harley, P., Wiedinmyer, C., Palmer, P. I., and Geron, C. (2006). Estimates of global terrestrial isoprene emissions using MEGAN (Model of Emissions of Gases and Aerosols from Nature). *Atmospheric Chemistry and Physics*, 6:3181–3210.

Gutman, G. and Ignatov, A. (1998). The derivation of the green vegetation fraction from NOAA/AVHRR data for use in numerical weather prediction models. *International Journal of Remote Sensing*, 19(8):1533–1543.

Harrison, R. M., Laxen, D., Moorcroft, S., and Laxen, K. (2012). Processes affecting concentrations of fine particulate matter (PM2.5) in the UK atmosphere. *Atmospheric Environment*, 46:115–124.

Haustein, K., Perez, C., Baldasano, J. M., Jorba, O., Basart, S., Miller, R. L., Janjic, Z., Black, T., Nickovic, S., Todd, M. C., Washington, R., Mueller, D., Tesche, M., Weinzierl, B., Esselborn, M., and Schladitz, A. (2012). Atmospheric dust modeling from meso to global scales with the online NMMB/BSC-Dust model - Part 2: Experimental campaigns in Northern Africa. *Atmospheric Chemistry and Physics*, 12(6):2933–2958.

Haustein, K., Perez, C., Baldasano, J. M., Mueller, D., Tesche, M., Schladitz, A., Esselborn, M., Weinzierl, B., Kandler, K., and von Hoyningen-Huene, W. (2009). Regional dust model performance during SAMUM 2006. *Geophysical Research Letters*, 36.

Haywood, J., Francis, P., Glew, M., and Taylor, J. (2001). Optical properties and direct radiative effect of Saharan dust: A case study of two Saharan dust outbreaks using aircraft data. *Journal of Geophysical Research-Atmospheres*, 106(D16):18417–18430.

Heinold, B., Helmert, J., Hellmuth, O., Wolke, R., Ansmann, A., Marticorena, B., Laurent, B., and Tegen, I. (2007). Regional modeling of Saharan dust events using LM-MUSCAT: Model description and case studies. *Journal of Geophysical Research-Atmospheres*, 112(D11).

Heinold, B., Knippertz, P., Marsham, J. H., Fiedler, S., Dixon, N. S., Schepanski, K., Laurent, B., and Tegen, I. (2013). The role of deep convection and nocturnal low-level jets for dust

emission in summertime west africa: Estimates from convection-permitting simulations. *Journal of Geophysical Research: Atmospheres*, 118(10):4385–4400.

Heinold, B., Tegen, I., Schepanski, K., Tesche, M., Esselborn, M., Freudenthaler, V., Gross, S., Kandler, K., Knippertz, P., Mueller, D., Schladitz, A., Toledano, C., Weinzierl, B., Ansmann, A., Althausen, D., Mueller, T., Petzold, A., and Wiedensohler, A. (2011). Regional modelling of Saharan dust and biomass-burning smoke Part I: Model description and evaluation. *Tellus Series B-Chemical and Physical Meteorology*, 63(4, SI):781–799.

Hodzic, A., Jimenez, J. L., Madronich, S., Aiken, A. C., Bessagnet, B., Curci, G., Fast, J., Lamarque, J. F., Onasch, T. B., Roux, G., Schauer, J. J., Stone, E. A., and Ulbrich, I. M. (2009). Modeling organic aerosols during MILAGRO: importance of biogenic secondary organic aerosols. *Atmospheric Chemistry and Physics*, 9(18):6949–6981.

Holben, B., Eck, T., Slutsker, I., Tanre, D., Buis, J., Setzer, A., Vermote, E., Reagan, J., Kaufman, Y., Nakajima, T., Lavenu, F., Jankowiak, I., and Smirnov, A. (1998). AERONET - A federated instrument network and data archive for aerosol characterization. *Remote Sensing of Environment*, 66(1):1–16.

Hong, S.-Y. and Lim, J.-O. J. (2006). The WRF single-moment 6-class microphysics scheme (WSM6). *Journal of Korean Meteorological Society*, 42:129–151.

Iacono, M. J., Delamere, J. S., Mlawer, E. J., Shephard, M. W., Clough, S. A., and Collins, W. D. (2008). Radiative forcing by long-lived greenhouse gases: Calculations with the AER radiative transfer models. *Journal of Geophysical Research: Atmospheres*, 113(D13). D13103.

IPMA (2017). Boletim climatológico, Dezembro 2016, Portugal Continental. Available here: https://www.ipma.pt/pt/oclima/boletins.

Israelevich, P., Ganor, E., Alpert, P., Kishcha, P., and Stupp, A. (2012). Predominant transport paths of Saharan dust over the Mediterranean Sea to Europe. *Journal of Geophysical Research: Atmospheres*, 117(D2). D02205.

Janjic, Z. (1994). The step-mountain ETA coordinate model - further developments of the convection, viscous sublayer, and turbulence closure schemes. *Monthly Weather Review*, 122(5):927–945.

Janjic, Z., Huang, H., and Lu, S. (2009). A Unified Atmospheric Model Suitable for Studying Transport of Mineral Aerosols From Meso to Global Scales. In Perez, JC and Baldasano, JM, editor, *WMO/GEO Expert Meeting on an International Sand and Dust Storm Warning System*, volume 7 of *IOP Conference Series Earth and Environmental Science*. WMO/GEO Expert Meeting on an International Sand and Dust Storm Warning System, Barcelona, Spain, Nov 07-09, 2007.

Jeong, G.-R. and Sokolik, I. N. (2007). Effect of mineral dust aerosols on the photolysis rates in the clean and polluted marine environments. *Journal of Geophysical Research-Atmospheres*, 112(D21).

Jeong, M.-J., Tsay, S.-C., Ji, Q., Hsu, N. C., Hansell, R. A., and Lee, J. (2008). Ground-based measurements of airborne Saharan dust in marine environment during the NAMMA field experiment. *Geophysical Research Letters*, 35(20).

Jimenez-Guerrero, P., Perez, C., Jorba, O., and Baldasano, J. M. (2008). Contribution of Saharan dust in an integrated air quality system and its on-line assessment. *Geophysical Research Letters*, 35(3).

Johnson, M. S., Meskhidze, N., and Kiliyanpilakkil, V. P. (2012). A global comparison of GEOS-Chem-predicted and remotely-sensed mineral dust aerosol optical depth and extinction profiles. *Journal of Advances in Modeling Earth Systems*, 4.

Jorba, O., Dabdub, D., Blaszczak-Boxe, C., Perez, C., Janjic, Z., Baldasano, J. M., Spada, M., Badia, A., and Goncalves, M. (2012). Potential significance of photoexcited NO2 on global air quality with the NMMB/BSC chemical transport model. *Journal of Geophysical Research-Atmospheres*, 117.

Kaaden, N., Massling, A., Schladitz, A., Mueller, T., Kandler, K., Schuetz, L., Weinzierl, B., Petzold, A., Tesche, M., Leinert, S., Deutscher, C., Ebert, M., Weinbruch, S., and Wiedensohler, A. (2009). State of mixing, shape factor, number size distribution, and hygroscopic growth of the Saharan anthropogenic and mineral dust aerosol at Tinfou, Morocco. *Tellus Series B-Chemical and Physical Meteorology*, 61(1):51–63.

Kain, J. S. (2004). The Kain-Fritsch convective parameterization: an update. *Journal of Applied Meteorology*, 43:170–181.

Kandler, K., Schuetz, L., Jaeckel, S., Lieke, K., Emmel, C., Mueller-Ebert, D., Ebert, M., Scheuvens, D., Schladitz, A., Segvic, B., Wiedensohler, A., and Weinbruch, S. (2011). Ground-based off-line aerosol measurements at Praia, Cape Verde, during the Saharan Mineral Dust Experiment: microphysical properties and mineralogy. *Tellus Series B-Chemical and Physical Meteorology*, 63(4, SI):459–474.

Kaufman, Y., Koren, I., Remer, L., Tanre, D., Ginoux, P., and Fan, S. (2005). Dust transport and deposition observed from the Terra-Moderate Resolution Imaging Spectroradiometer (MODIS) spacecraft over the Atlantic ocean. *Journal of Geophysical Research-Atmospheres*, 110(D10).

Klein, H., Nickovic, S., Haunold, W., Bundke, U., Nillius, B., Ebert, M., Weinbruch, S., Schuetz, L., Levin, Z., Barrie, L. A., and Bingemer, H. (2010). Saharan dust and ice nuclei over Central Europe. *Atmospheric Chemistry and Physics*, 10(21):10211–10221.

Knippertz, P., Tesche, M., Heinold, B., Kandler, K., Toledano, C., and Esselborn, M. (2011). Dust mobilization and aerosol transport from West Africa to Cape Verde-a meteorological overview of SAMUM-2. *Tellus Series B-Chemical and Physical Meteorology*, 63(4, SI):430–447.

Kok, J. F. (2011a). A scaling theory for the size distribution of emitted dust aerosols suggests climate models underestimate the size of the global dust cycle. *Proceedings of the National Academy of Sciences of the United States of America*, 108(3):1016–1021.

Kok, J. F. (2011b). Does the size distribution of mineral dust aerosols depend on the wind speed at emission? *Atmospheric Chemistry and Physics*, 11(19):10149–10156.

Kok, J. F., Mahowald, N. M., Fratini, G., Gillies, J. A., Ishizuka, M., Leys, J. F., Mikami, M., Park, M. S., Park, S. U., Van Pelt, R. S., and Zobeck, T. M. (2014). An improved dust emission model - Part 1: Model description and comparison against measurements. *Atmospheric Chemistry and Physics*, 14(23):13023–13041.

Kokkalis, P., Mamouri, R. E., Todua, M., Didebulidze, G. G., Papayannis, A., Amiridis, V., Basart, S., Perez, C., and Baldasano, J. M. (2012). Ground-, satellite- and simulation-based analysis of a strong dust event over Abastumani, Georgia, during May 2009. *International Journal of Remote Sensing*, 33(16):4886–4901.

Li, D., Bian, J., and Fan, Q. (2015). A deep stratospheric intrusion associated with an intense cut-off low event over East Asia. *Science China Earth Sciences*, 58(1):116–128.

Liao, H. and Seinfeld, J. (1998). Radiative forcing by mineral dust aerosols: sensitivity to key variables. *Journal of Geophysical Research-Atmospheres*, 103(D24):31637–31645.

Liu, M. and Westphal, D. (2001). A study of the sensitivity of simulated mineral dust production to model resolution. *Journal of Geophysical Research-Atmospheres*, 106(D16):18099–18112.

López-Villarrubia, E., Iñiguez, C., Costa, O., and Ballester, F. (2016). Acute effects of urban air pollution on respiratory emergency hospital admissions in the Canary Islands. *Air Quality, Atmosphere & Health*, 9(7):713–722.

Mahowald, N., Albani, S., Kok, J. F., Engelstaeder, S., Scanza, R., Ward, D. S., and Flanner, M. G. (2014). The size distribution of desert dust aerosols and its impact on the Earth system. *Aeolian Research*, 15:53–71.

Mahowald, N., Baker, A., Bergametti, G., Brooks, N., Duce, R., Jickells, T., Kubilay, N., Prospero, J., and Tegen, I. (2005). Atmospheric global dust cycle and iron inputs to the ocean. *Global Biogeochemical Cycles*, 19(4).

Mailler, S., Menut, L., Khvorostyanov, D., Valari, M., Couvidat, F., Siour, G., Turquety, S., Briant, R., Tuccella, P., Bessagnet, B., Colette, A., Létinois, L., Markakis, K., and Meleux, F. (2017). Chimere-2017: from urban to hemispheric chemistry-transport modeling. *Geoscientific Model Development*, 10(6):2397–2423.

Marsham, J. H., Hobby, M., Allen, C. J. T., Banks, J. R., Bart, M., Brooks, B. J., Cavazos-Guerra, C., Engelstaedter, S., Gascoyne, M., Lima, A. R., Martins, J. V., McQuaid, J. B., O'Leary, A., Ouchene, B., Ouladichir, A., Parker, D. J., Saci, A., Salah-Ferroudj, M., Todd, M. C., and Washington, R. (2013). Meteorology and dust in the central Sahara: Observations from Fennec supersite-1 during the June 2011 Intensive Observation Period. *Journal of Geophysical Research-Atmospheres*, 118(10):4069–4089.

Marsham, J. H., Knippertz, P., Dixon, N. S., Parker, D. J., and Lister, G. M. S. (2011). The importance of the representation of deep convection for modeled dust-generating winds over West Africa during summer. *Geophysical Research Letters*, 38.

Martet, M. and Peuch, V.-H. (2009). Aerosol modelling in MOCAGE and operational dust forecasting at Meteo-France. In Perez, JC and Baldasano, JM, editor, *WMO/GEO Expert Meeting on an International Sand and Dust Storm Warning System*, volume 7 of *IOP Conference Series Earth and Environmental Science*. WMO/GEO Expert Meeting on an International Sand and Dust Storm Warning System, Barcelona, Spain, Nov 07-09, 2007.

Marticorena, B. and Bergametti, G. (1995). Modeling the atmospheric dust cycle. 1.Design of a soil-derived dust emission scheme. *Journal of Geophysical Research-Atmospheres*, 100(D8):16415–16430.

Marticorena, B., Bergametti, G., Aumont, B., Callot, Y., NDoume, C., and Legrand, M. (1997). Modeling the atmospheric dust cycle .2. Simulation of Saharan dust sources. *Journal of Geophysical Research-Atmospheres*, 102(D4):4387–4404.

Matthias, V. (2008). The aerosol distribution in Europe derived with the Community Multiscale Air Quality (CMAQ) model: comparison to near surface in situ and sunphotometer measurements. *Atmospheric Chemistry and Physics*, 8(17):5077–5097.

Menut, L., Bessagnet, B., Khvorostyanov, D., Beekmann, M., Blond, N., Colette, A., Coll, I., Curci, G., Foret, G., Hodzic, A., Mailler, S., Meleux, F., Monge, J. L., Pison, I., Siour, G., Turquety, S., Valari, M., Vautard, R., and Vivanco, M. G. (2013). CHIMERE 2013: a model for regional atmospheric composition modelling. *Geoscientific Model Development*, 6(4):981–1028.

Menut, L., Chiapello, I., and Moulin, C. (2009). Previsibility of Saharan dust events using the CHIMERE-DUST transport model. In Perez, JC and Baldasano, JM, editor, *WMO/GEO Expert Meeting on an International Sand and Dust Storm Warning System*, volume 7 of *IOP Conference Series Earth and Environmental Science*. WMO/GEO Expert Meeting on an International Sand and Dust Storm Warning System, Barcelona, Spain, Nov 07-09, 2007.

Menut, L., Schmechtig, C., and Marticorena, B. (2005). Sensitivity of the sandblasting flux calculations to the soil size distribution accuracy. *Journal of Atmospheric and Oceanic Technology*, 22(12):1875–1884.

Mlawer, E., Taubman, S., Brown, P., Iacono, M., and Clough, S. (1997). Radiative transfer for inhomogeneous atmospheres: RRTM, a validated correlated-k model for the longwave. *Journal of Geophysical Research-Atmospheres*, 102(D14):16663–16682.

Mok, K., Miranda, A., Yuen, K., Hoi, K., Monteiro, A., and Ribeiro, I. (2017). Selection of bias correction models for improving the daily PM10 forecasts of WRF-EURAD in Porto, Portugal. *Atmospheric Pollution Research*, 8(4):628–639.

Monahan, E. C. (1986). *The Ocean as a Source for Atmospheric Particles*, pages 129–163. Springer Netherlands, Dordrecht.

Monteiro, A., Fernandes, A. P., Gama, C., Borrego, C., and Tchepel, O. (2015). Assessing the mineral dust from North Africa over Portugal region using BSC-DREAM8b model. *Atmospheric Pollution Research*, 6(1):70–81.

Monteiro, A., Lopes, M., Miranda, A., Borrego, C., and Vautard, R. (2005). Air pollution forecast in Portugal: a demand from the new air quality framework directive. *International Journal of Environment and Pollution*, 25(1-4):4–15.

Monteiro, A., Ribeiro, I., Tchepel, O., Sá, E., Ferreira, J., Carvalho, A., Martins, V., Strunk, A., Galmarini, S., Elbern, H., Schaap, M., Builtjes, P., Miranda, A. I., and Borrego, C. (2013). Bias correction techniques to improve air quality ensemble predictions: Focus on O3 and PM over portugal. *Environmental Modeling & Assessment*, 18(5):533–546.

Monteiro, A., Russo, M., Gama, C., Lopes, M., and C., B. (2017a). How economic crisis influence air quality over portugal. Paper presented at the 4th Meeting on Energy and Environmental Economics, University of Aveiro, Portugal.

Monteiro, A., Sá, E., Fernandes, A., Gama, C., Sorte, S., Borrego, C., Lopes, M., and Russo, M. A. (2017b). How healthy will be the air quality in 2050? *Air Quality, Atmosphere & Health*, pages 1–10.

Moxim, W. J., Fan, S.-M., and Levy, II, H. (2011). The meteorological nature of variable soluble iron transport and deposition within the North Atlantic Ocean basin. *Journal of Geophysical Research-Atmospheres*, 116.

Mueller, K., Lehmann, S., van Pinxteren, D., Gnauk, T., Niedermeier, N., Wiedensohler, A., and Herrmann, H. (2010). Particle characterization at the Cape Verde atmospheric observatory during the 2007 RHaMBLe intensive. *Atmospheric Chemistry and Physics*, 10(6):2709–2721.

Nabat, P., Solmon, F., Mallet, M., Kok, J. F., and Somot, S. (2012). Dust emission size distribution impact on aerosol budget and radiative forcing over the Mediterranean region: a regional climate model approach. *Atmospheric Chemistry and Physics*, 12(21):10545–10567.

Nickovic, S. and Dobricic, S. (1996). A model for long-range transport of desert dust. *Monthly Weather Review*, 124(11):2537–2544.

Nickovic, S., Kallos, G., Papadopoulos, A., and Kakaliagou, O. (2001). A model for prediction of desert dust cycle in the atmosphere. *Journal of Geophysical Research-Atmospheres*, 106(D16):18113–18129.

Nunes, T., Cardoso, J., Custódio, D., Cerqueira, M., Almeida, S. M., and co authors (2012). Carbonaceous and inorganic water soluble species in PM in Cape Verde atmosphere. European Aerosol Conference. Granada, Spain,.

O'Neill, N., Eck, T., Smirnov, A., Holben, B., and Thulasiraman, S. (2003). Spectral discrimination of coarse and fine mode optical depth. *Journal of Geophysical Research-Atmospheres*, 108(D17).

Ots, R., Vieno, M., Allan, J. D., Reis, S., Nemitz, E., Young, D. E., Coe, H., Di Marco, C., Detournay, A., Mackenzie, I. A., Green, D. C., and Heal, M. R. (2016). Model simulations of cooking organic aerosol (COA) over the UK using estimates of emissions based on measurements at two sites in London. *Atmospheric Chemistry and Physics*, 16(21):13773–13789.

Pay, M. T., Jimenez-Guerrero, P., Jorba, O., Basart, S., Querol, X., Pandolfi, M., and Baldasano, J. M. (2012). Spatio-temporal variability of concentrations and speciation of particulate matter across Spain in the CALIOPE modeling system. *Atmospheric Environment*, 46:376–396.

Pay, M. T., Piot, M., Jorba, O., Gasso, S., Goncalves, M., Basart, S., Dabdub, D., Jimenez-Guerrero, P., and Baldasano, J. M. (2010). A full year evaluation of the CALIOPE-EU air quality modeling system over Europe for 2004. *Atmospheric Environment*, 44(27):3322–3342.

Perez, C., Haustein, K., Janjic, Z., Jorba, O., Huneeus, N., Baldasano, J. M., Black, T., Basart, S., Nickovic, S., Miller, R. L., Perlwitz, J. P., Schulz, M., and Thomson, M. (2011). Atmospheric dust modeling from meso to global scales with the online NMMB/BSC-Dust model - Part 1: Model description, annual simulations and evaluation. *Atmospheric Chemistry and Physics*, 11(24):13001–13027.

Perez, C., Nickovic, S., Baldasano, J. M., Sicard, M., Rocadenbosch, F., and Cachorro, V. E. (2006a). A long Saharan dust event over the western Mediterranean: Lidar, Sun photome-

ter observations, and regional dust modeling. *Journal of Geophysical Research-Atmospheres*, 111(D15).

Perez, C., Nickovic, S., Pejanovic, G., Baldasano, J. M., and Oezsoy, E. (2006b). Interactive dust-radiation modeling: A step to improve weather forecasts. *Journal of Geophysical Research-Atmospheres*, 111(D16).

Pey, J., Querol, X., Alastuey, A., Forastiere, F., and Stafoggia, M. (2013). African dust outbreaks over the Mediterranean Basin during 2001-2011: PM10 concentrations, phenomenology and trends, and its relation with synoptic and mesoscale meteorology. *Atmospheric Chemistry and Physics*, 13(3):1395–1410.

Pio, C., Cardoso, J., Cerqueira, M., Calvo, A., Nunes, T., Alves, C., Custódio, D., Almeida, S., and Almeida-Silva, M. (2014). Seasonal variability of aerosol concentration and size distribution in Cape Verde using a continuous aerosol optical spectrometer. *Frontiers in Atmospheric Science*, 2.

Pleim, J. E. (2007). A Combined Local and Nonlocal Closure Model for the Atmospheric Boundary Layer. Part I: Model Description and Testing. *Journal of Applied Meteorology and Climatology*, 46:1383–1395.

Posfai, M., Axisa, D., Tompa, E., Freney, E., Bruintjes, R., and Buseck, P. R. (2013). Interactions of mineral dust with pollution and clouds: An individual-particle TEM study of atmospheric aerosol from Saudi Arabia. *Atmospheric Research*, 122:347–361.

Prospero, J., Ginoux, P., Torres, O., Nicholson, S., and Gill, T. (2002). Environmental characterization of global sources of atmospheric soil dust identified with the Nimbus 7 Total Ozone Mapping Spectrometer (TOMS) absorbing aerosol product. *Reviews of Geophysics*, 40(1).

Prospero, J. M., Collard, F.-X., Molinié, J., and Jeannot, A. (2014). Characterizing the annual cycle of African dust transport to the Caribbean Basin and South America and its impact on the environment and air quality. *Global Biogeochemical Cycles*, 28(7):757–773. 2013GB004802.

Putaud, J.-P., Dingenen, R. V., Alastuey, A., Bauer, H., Birmili, W., Cyrys, J., Flentje, H., Fuzzi, S., Gehrig, R., Hansson, H., Harrison, R., Herrmann, H., Hitzenberger, R., Hüglin, C., Jones, A., Kasper-Giebl, A., Kiss, G., Kousa, A., Kuhlbusch, T., Löschau, G., Maenhaut, W., Molnar, A., Moreno, T., Pekkanen, J., Perrino, C., Pitz, M., Puxbaum, H., Querol, X., Rodriguez, S., Salma, I., Schwarz, J., Smolik, J., Schneider, J., Spindler, G., ten Brink, H., Tursic, J., Viana, M., Wiedensohler, A., and Raes, F. (2010). A European aerosol phenomenology – 3: Physical and chemical characteristics of particulate matter from 60 rural, urban, and kerbside sites across Europe. *Atmospheric Environment*, 44(10):1308–1320.

Querol, X., Pey, J., Pandolfi, M., Alastuey, A., Cusack, M., Perez, N., Moreno, T., Viana, M., Mihalopoulos, N., Kallos, G., and Kleanthous, S. (2009). African dust contributions to mean ambient PM10 mass-levels across the Mediterranean Basin. *Atmospheric Environment*, 43(28):4266–4277.

Rodriguez, S., Alastuey, A., Alonso-Perez, S., Querol, X., Cuevas, E., Abreu-Afonso, J., Viana, M., Perez, N., Pandolfi, M., and de la Rosa, J. (2011). Transport of desert dust mixed with North African industrial pollutants in the subtropical Saharan Air Layer. *Atmospheric Chemistry and Physics*, 11(13):6663–6685.

Rodriguez, S., Alastuey, A., and Querol, X. (2012). A review of methods for long term in situ characterization of aerosol dust. *Aeolian Research*, 6:55–74.

Rodriguez, S., Querol, X., Alastuey, A., Kallos, G., and Kakaliagou, O. (2001). Saharan dust contributions to PM10 and TSP levels in Southern and Eastern Spain. *Atmospheric Environment*, 35(14):2433–2447.

Rodríguez, S., Querol, X., Alastuey, A., Viana, M.-M., and Mantilla, E. (2003). Events affecting levels and seasonal evolution of airborne particulate matter concentrations in the western mediterranean. *Environmental Science & Technology*, 37(2):216–222. PMID: 12564890.

Ropkins, K. and Carslaw, D. C. (2012). openair - Data Analysis Tools for the Air Quality Community. *R Journal*, 4(1):20–29.

Salvador, P., Alonso-Perez, S., Pey, J., Artinano, B., de Bustos, J. J., Alastuey, A., and Querol, X. (2014). African dust outbreaks over the western Mediterranean Basin: 11-year characterization of atmospheric circulation patterns and dust source areas. *Atmospheric Chemistry and Physics*, 14(13):6759–6775.

Salvador, P., Artinano, B., Molero, F., Viana, M., Pey, J., Alastuey, A., and Querol, X. (2013). African dust contribution to ambient aerosol levels across central Spain: Characterization of long-range transport episodes of desert dust. *Atmospheric Research*, 127:117–129.

Schepanski, K., Tegen, I., and Macke, A. (2009). Saharan dust transport and deposition towards the tropical northern Atlantic. *Atmospheric Chemistry and Physics*, 9(4):1173–1189.

Schepanski, K., Tegen, I., and Macke, A. (2012). Comparison of satellite based observations of Saharan dust source areas. *Remote Sensing of Environment*, 123:90–97.

Schladitz, A., Mueller, T., Nowak, A., Kandler, K., Lieke, K., Massling, A., and Wiedensohler, A. (2011). In situ aerosol characterization at Cape Verde Part 1: Particle number size distributions, hygroscopic growth and state of mixing of the marine and Saharan dust aerosol. *Tellus Series B-Chemical and Physical Meteorology*, 63(4, SI):531–548.

Schmechtig, C., Marticorena, B., Chatenet, B., Bergametti, G., Rajot, J. L., and Coman, A. (2011). Simulation of the mineral dust content over Western Africa from the event to the annual scale with the CHIMERE-DUST model. *Atmospheric Chemistry and Physics*, 11(14):7185–7207.

Schulz, M., Balkanski, Y. J., Guelle, W., and Dulac, F. (1998). Role of aerosol size distribution and source location in a three-dimensional simulation of a saharan dust episode tested against satellite-derived optical thickness. *Journal of Geophysical Research: Atmospheres*, 103(D9):10579–10592.

Seinfeld, J. and Pandis, S. (1998). *Atmospheric Chemistry and Physics: From Air Pollution to Climate Change*.

Shao, Y. (2001). A model for mineral dust emission. *Journal of Geophysical Research: Atmospheres*, 106(D17):20239–20254.

Shao, Y. (2004). Simplification of a dust emission scheme and comparison with data. *Journal of Geophysical Research: Atmospheres*, 109(D10):n/a–n/a. D10202.

Shao, Y., Nickling, W., Bergametti, G., Butler, H., Chappell, A., Findlater, P., Gillies, J., Ishizuka, M., Klose, M., Kok, J. F., Leys, J., Lu, H., Marticorena, B., McTainsh, G., McKenna-Neuman, C., Okin, G. S., Strong, C., and Webb, N. (2015). A tribute to Michael R. Raupach for contributions to aeolian fluid dynamics. *Aeolian Research*, 19(A):37–54.

Shao, Y. and Raupach, M. (1993). Effect of saltation bombardment on the entrainment of dust by wind. *Journal of Geophysical Research-Atmospheres*, 98(D7):12719–12726.

Shao, Y., Raupach, M. R., and Findlater, P. A. (1993). Effect of saltation bombardment on the entrainment of dust by wind. *Journal of Geophysical Research: Atmospheres*, 98(D7):12719–12726.

Skamarock, W. C., Klemp, J. B., Dudhia, J., Gill, D. O., Barker, M., Duda, K. G., Huang, X. Y., Wang, W., and Powers, J. G. (2008). A description of the advanced research WRF version 3. Technical report, National Center for Atmospheric Research.

Slezakova, K., Pereira, M. C., Reis, M. A., and Alvim-Ferraz, M. C. (2007). Influence of traffic emissions on the composition of atmospheric particles of different sizes – Part 1: concentrations and elemental characterization. *Journal of Atmospheric Chemistry*, 58(1):55–68.

Smirnov, A., Holben, B., Eck, T., Dubovik, O., and Slutsker, I. (2000). Cloud-screening and quality control algorithms for the AERONET database. *Remote Sensing of Environment*, 73(3):337–349.

Solazzo, E., Bianconi, R., Vautard, R., Appel, K. W., Moran, M. D., Hogrefe, C., Bessagnet, B., Brandt, J., Christensen, J. H., Chemel, C., Coll, I., van der Gon, H. D., Ferreira, J., Forkel, R., Francis, X. V., Grell, G., Grossi, P., Hansen, A. B., Jeričević, A., Kraljević, L., Miranda, A. I., Nopmongcol, U., Pirovano, G., Prank, M., Riccio, A., Sartelet, K. N., Schaap, M., Silver, J. D., Sokhi, R. S., Vira, J., Werhahn, J., Wolke, R., Yarwood, G., Zhang, J., Rao, S., and Galmarini, S. (2012). Model evaluation and ensemble modelling of surface-level ozone in Europe and North America in the context of AQMEII. *Atmospheric Environment*, 53(Supplement C):60 – 74. AQMEII: An International Initiative for the Evaluation of Regional-Scale Air Quality Models - Phase 1.

Song, Y., Lü, D., Li, Q., Bian, J., Wu, X., and Li, D. (2016). The impact of cut-off lows on ozone in the upper troposphere and lower stratosphere over Changchun from ozonesonde observations. *Advances in Atmospheric Sciences*, 33(2):135–150.

Spada, M., Jorba, O., Garcia-Pando, C. P., Janjic, Z., and Baldasano, J. M. (2013). Modeling and evaluation of the global sea-salt aerosol distribution: sensitivity to emission schemes and resolution effects at coastal/orographic sites. *Atmospheric Chemistry and Physics*, 13(23):11735–11755.

Stafoggia, M., Zauli-Sajani, S., Pey, J., Samoli, E., Alessandrini, E., Basagana, X., Cernigliaro, A., Chiusolo, M., Demaria, M., Diaz, J., Faustini, A., Katsouyanni, K., Kelessis, A. G., Linares, C., Marchesi, S., Medina, S., Pandolfi, P., Perez, N., Querol, X., Randi, G., Ranzi, A., Tobias, A., Forastiere, F., Alessandrini, E., Angelini, P., Berti, G., Bisanti, L., Cadum, E., Catrambone, M., Chiusolo, M., Davoli, M., de' Donato, F., Demaria, M., Gandini, M., Grosa, M., Faustini, A., Ferrari, S., Forastiere, F., Pandolfi, P., Pelosini, R., Perrino, C., Pietrodangelo, A., Pizzi, L., Poluzzi, V., Priod, G., Randi, G., Ranzi, A., Rowinski, M., Scarinzi, C., Stafoggia, M., Stivanello, E., Zauli-Sajani, S., Dimakopoulou, K., Elefteriadis, K., Katsouyanni, K., Kelessis, A., Maggos, T., Michalopoulos, N., Pateraki, S., Petrakakis, M., Rodopoulou, S., Samoli, E.,

Sypsa, V., Agis, D., Alguacil, J., Artinano, B., Barrera-Gomez, J., Basagana, X., de la Rosa, J., Diaz, J., Fernandez, R., Jacquemin, B., Karanasiou, A., Linares, C., Ostro, B., Perez, N., Pey, J., Querol, X., Salvador, P., Sanchez, A. M., Sunyer, J., Tobias, A., Bidondo, M., Declercq, C., Le Tertre, A., Lozano, P., Medina, S., Pascal, L., Pascal, M., and Grp, M.-P. S. (2016). Desert Dust Outbreaks in Southern Europe: Contribution to Daily PM10 Concentrations and Short-Term Associations with Mortality and Hospital Admissions. *Environmental Health Perspectives*, 124(4):413–419.

Szopa, S., Foret, G., Menut, L., and Cozic, A. (2009). Impact of large scale circulation on european summer surface ozone and consequences for modelling forecast. *Atmospheric Environment*, 43(6):1189 – 1195.

Tanre, D., Haywood, J., Pelon, J., Leon, J., Chatenet, B., Formenti, P., Francis, P., Goloub, P., Highwood, E., and Myhre, G. (2003). Measurement and modeling of the Saharan dust radiative impact: Overview of the Saharan Dust Experiment (SHADE). *Journal of Geophysical Research-Atmospheres*, 108(D18).

Taylor, K. (2001). Summarizing multiple aspects of model performance in a single diagram. *Journal of Geophysical Research-Atmospheres*, 106(D7):7183–7192.

Tchepel, O., Ferreira, J., Fernandes, A. P., Basart, S., Baldasano, J. M., and Borrego, C. (2013). Analysis of long-range transport of aerosols for Portugal using 3D chemical transport model and satellite measurements. *Atmospheric Environment*, 64:229–241.

Tegen, I., Harrison, S., Kohfeld, K., Prentice, I., Coe, M., and Heimann, M. (2002). Impact of vegetation and preferential source areas on global dust aerosol: Results from a model study. *Journal of Geophysical Research-Atmospheres*, 107(D21).

Tegen, I. and Lacis, A. (1996). Modeling of particle size distribution and its influence on the radiative properties of mineral dust aerosol. *Journal of Geophysical Research-Atmospheres*, 101(D14):19237–19244. International Specialty Conference on Aerosols and Atmospheric Optics - Radiative Balance and Visual Air Quality, SNOWBIRD, UT, SEP 26-30, 1994.

Todd, M. C., Karam, D. B., Cavazos, C., Bouet, C., Heinold, B., Baldasano, J. M., Cautenet, G., Koren, I., Perez, C., Solmon, F., Tegen, I., Tulet, P., Washington, R., and Zakey, A. (2008). Quantifying uncertainty in estimates of mineral dust flux: An intercomparison of model performance over the Bodele Depression, northern Chad. *Journal of Geophysical Research-Atmospheres*, 113.

Tsamalis, C., Chedin, A., Pelon, J., and Capelle, V. (2013). The seasonal vertical distribution of the Saharan Air Layer and its modulation by the wind. *Atmospheric Chemistry and Physics*, 13(22):11235–11257.

Valavanidis, A., Fiotakis, K., and Vlachogianni, T. (2008). Airborne particulate matter and human health: Toxicological assessment and importance of size and composition of particles for oxidative damage and carcinogenic mechanisms. *Journal of Environmental Science and Health Part C*, 26(4):339–362.

Valverde, V., Pay, M. T., and Baldasano, J. M. (2015). Circulation-type classification derived on a climatic basis to study air quality dynamics over the Iberian Peninsula. *International Journal of Climatology*, 35(10):2877–2897.

van Loon, M., Vautard, R., Schaap, M., Bergström, R., Bessagnet, B., Brandt, J., Builtjes, P., Christensen, J., Cuvelier, C., Graff, A., Jonson, J., Krol, M., Langner, J., Roberts, P., Rouil, L., Stern, R., Tarrasón, L., Thunis, P., Vignati, E., White, L., and Wind, P. (2007). Evaluation of long-term ozone simulations from seven regional air quality models and their ensemble. *Atmospheric Environment*, 41(10):2083 – 2097.

Vautard, R., Builtjes, P., Thunis, P., Cuvelier, C., Bedogni, M., Bessagnet, B., Honoré, C., Moussiopoulos, N., Pirovano, G., Schaap, M., Stern, R., Tarrason, L., and Wind, P. (2007). Evaluation and intercomparison of Ozone and PM10 simulations by several chemistry transport models over four European cities within the CityDelta project. *Atmospheric Environment*, 41(1):173 – 188.

Viana, M., Salvador, P., Artíñano, B., Querol, X., Alastuey, A., Pey, J., Latz, A. J., Cabañas, M., Moreno, T., García Dos Santos, S., Herce, M. D., Diez Hernández, P., Romero García, D., and Fernández-Patier, R. (2010). Assessing the performance of methods to detect and quantify african dust in airborne particulates. *Environmental Science & Technology*, 44(23):8814–8820.

Vicente, E. D., Duarte, M. A., Calvo, A. I., Nunes, T. F., Tarelho, L., and Alves, C. A. (2015). Emission of carbon monoxide, total hydrocarbons and particulate matter during wood combustion in a stove operating under distinct conditions. *Fuel Processing Technology*, 131:182–192.

Wagener, S., Langner, M., Hansen, U., Moriske, H.-J., and Endlicher, W. R. (2012). Spatial and seasonal variations of biogenic tracer compounds in ambient PM10 and PM1 samples in Berlin, Germany. *Atmospheric Environment*, 47:33–42.

Weinzierl, B., Sauer, D., Esselborn, M., Petzold, A., Veira, A., Rose, M., Mund, S., Wirth, M., Ansmann, A., Tesche, M., Gross, S., and Freudenthaler, V. (2011). Microphysical and optical properties of dust and tropical biomass burning aerosol layers in the Cape Verde region-an overview of the airborne in situ and lidar measurements during SAMUM-2. *Tellus Series B-Chemical and Physical Meteorology*, 63(4, SI):589–618.

White, B. (1979). Soil transport by winds on Mars. *Journal of Geophysical Research*, 84(NB9):4643–4651.

WHO-OCDE (2015). Economic cost of the health impact of air pollution in Europe: Clean air, health and wealth. Copenhagen: WHO Regional Office for Europe.

Willmott, C. J., Robeson, S. M., and Matsuura, K. (2012). A refined index of model performance. *International Journal of Climatology*, 32(13):2088–2094.

Xi, X. and Sokolik, I. N. (2015). Seasonal dynamics of threshold friction velocity and dust emission in Central Asia. *Journal of Geophysical Research: Atmospheres*, 120(4):1536–1564. 2014JD022471.

Yin, Y., Wurzler, S., Levin, Z., and Reisin, T. (2002). Interactions of mineral dust particles and clouds: Effects on precipitation and cloud optical properties. *Journal of Geophysical Research-Atmospheres*, 107(D23).

Zender, C. S., Bian, H., and Newman, D. (2003). Mineral dust entrainment and deposition (dead) model: Description and 1990s dust climatology. *Journal of Geophysical Research: Atmospheres*, 108(D14). 4416.

Zhang, L., Gong, S., Padro, J., and Barrie, L. (2001). A size-segregated particle dry deposition scheme for an atmospheric aerosol module. *Atmospheric Environment*, 35(3):549–560.

Zhang, L., Kok, J. F., Henze, D. K., Li, Q., and Zhao, C. (2013). Improving simulations of fine dust surface concentrations over the western United States by optimizing the particle size distribution. *Geophysical Research Letters*, 40(12):3270–3275.

Zhang, X., Zhao, L., Tong, D. Q., Wu, G., Dan, M., and Teng, B. (2016). A systematic review of global desert dust and associated human health effects. *Atmosphere*, 7(12).

Zyryanov, D., Foret, G., Eremenko, M., Beekmann, M., Cammas, J.-P., D'Isidoro, M., Elbern, H., Flemming, J., Friese, E., Kioutsioutkis, I., Maurizi, A., Melas, D., Meleux, F., Menut, L., Moinat, P., Peuch, V.-H., Poupkou, A., Razinger, M., Schultz, M., Stein, O., Suttie, A. M., Valdebenito, A., Zerefos, C., Dufour, G., Bergametti, G., and Flaud, J.-M. (2012). 3-D evaluation of tropospheric ozone simulations by an ensemble of regional Chemistry Transport Model. *Atmospheric Chemistry and Physics*, 12(7):3219–3240.